

**PROCESS AND QUALITY CHARACTERIZATION FOR
ULTRASONIC WELDING OF LITHIUM-ION BATTERIES**

by

Seungjae Lee

A dissertation submitted in partial fulfillment
of the requirements for the degree of
Doctor of Philosophy
(Mechanical Engineering)
in the University of Michigan
2013

Doctoral Committee:

Professor S. Jack Hu, Co-Chair
Professor Elijah Kannatey-Asibu Jr., Co-Chair
Professor John Edmond Allison
Wayne W. Cai, General Motors
Assistant Research Scientist Tae Hyung Kim

© Seungjae Lee 2013

Dedicated to my family
for their love, guidance, and support

ACKNOWLEDGEMENTS

I would like to express my sincere thanks to my advisors, committee members, colleagues, family and many others for their guidance, help and support. Without them, I would never have been able to finish this dissertation.

First and foremost, my deepest gratitude goes to my advisor, Professor S. Jack Hu for his countless advices and patient encouragement. He shared with me his brilliant insight and great vision on my research. He showed me an example of how to be a good researcher but at the same time a great leader and personnel. I have been amazingly fortunate to have an advisor who could provide me such a wonderful guidance to this long journey.

My deepest thank also goes to my co-advisor Professor Elijah Kannatey-Asibu Jr. for his invaluable comments and guidance on my thesis. He shared with me his vast knowledge and experience on my research area and provided me tremendous help to finish my dissertation thesis.

I would like to extend my sincere gratitude to the committee members including my, Professor John Allison, Dr. Tae Kim, and Dr. Wayne Cai for their support, guidance, and invaluable comments during my study. I also want to thank Dr. Cai and General Motors for the financial support and internship opportunities.

I thank all the Hu Lab members as well as many other friends and colleagues that I have worked with for their unconditional support and friendship. It has been a great pleasure to work with you all.

More importantly, none of this would have been possible without the love and support from my family. My parents and parents-in-law have been a constant source of love, concern, support and strength all these years. I want to express my deepest thanks to all my family members in Korea and the United States for all the love and support they have given me. Finally, I would like to dedicate this thesis to my lovely wife, Juyoung, and my precious daughter, Olivia, who mean everything to me.

TABLE OF CONTENTS

DEDICATION	ii
ACKNOWLEDGEMENTS.....	iii
LIST OF FIGURES	viii
LIST OF TABLES.....	xiv
ABSTRACT	xv
CHAPTER 1 INTRODUCTION	1
1.1 Background	1
1.2 Statement of Problem	6
1.3 Research Objectives	7
1.4 Organization of Dissertation	8
References.....	10
CHAPTER 2 CHARACTERIZATION OF JOINT QUALITY IN ULTRASONIC WELDING OF BATTERY TABS	15
Abstract.....	15
2.1 Introduction	16
2.2 Materials and Experiments.....	18
2.2.1 Experiments.....	20
2.2.2 Weld performance testing	21
2.2.3 Sample preparation/microscopy/hardness testing	21
2.3 Definition of Attributes and Weld Characterization	22
2.3.1 Definition of weld attributes.....	22
2.3.2 Characterization of ultrasonic welds using weld attributes.....	24

2.4 Correlation Between Weld Attributes and Quality	36
2.4.1 Bond density	36
2.4.2 Post-weld thickness	38
2.4.3 Thermo-mechanically affected zone (TMAZ) and weld nugget.....	39
2.4.4 Surface cracks.....	47
2.4.5 Summary of correlation between weld attributes and quality	50
2.5 Conclusions	51
Acknowledgement	52
References.....	53

CHAPTER 3 CHARACTERIZATION OF ULTRASONIC METAL WELDING BY CORRELATING ONLINE SENSOR SIGNALS WITH WELD ATTRIBUTES	56
Abstract	56
3.1 Introduction	57
3.2 Weld Formation Mechanism in Ultrasonic Metal Welding	60
3.3 Sensor Signals from the Ultrasonic Welding Process	62
3.3.1 Experiment	62
3.3.2 Sensor signals	65
3.3.3 Signal variation under process disturbance	68
3.4 Relationship Between Weld Attributes and Signal Features.....	72
3.4.1 Features in sensor signals	72
3.4.2 Effect of welding parameters on signal features	75
3.4.3 Relationship between weld attributes and signal features.....	76
3.5 Conclusions	80
References.....	82

CHAPTER 4 ANALYSIS OF WELD FORMATION IN MULTILAYER ULTRASONIC METAL WELDING USING HIGH-SPEED IMAGES..	85
Abstract	85
4.1 Introduction	86
4.2 Experiment	89

4.2.1 Ultrasonic welding process	89
4.2.2 High speed imaging	89
4.2.3 Multilayer welding experiment	91
4.2.4 Post-weld performance testing/ microscopy/ bond density measurement	92
4.3 Results and Discussion	93
4.3.1 Observation of vibration development in multiple layers	93
4.3.2 Weld formation mechanism in multilayer welding	96
4.3.3 Post-weld microscopy	100
4.3.4 Effect of weld tool geometry on bond density and joint strength	102
4.4 Conclusions	105
References	107
CHAPTER 5 CONCLUSIONS AND FUTURE WORK	110
5.1 Conclusions	110
5.2 Future Work	114
References	115

LIST OF FIGURES

Figure 1.1	Hierarchy of joining processes in battery pack manufacturing [Lee 2010]... 2
Figure 1.2	Ultrasonic metal welding 5
Figure 2.1	Ultrasonic welding configuration: (a) an example of battery tab joining; (b) dimension and configuration of weld coupons; and (c) cross-section image (AA')..... 19
Figure 2.2	Weld performance testing: (a) U-tensile test configuration; (b) maximum U-tensile load plotted against welding time for three different clamping pressures..... 20
Figure 2.3	Optical images of Cu and Ni-plated Cu weld cross-sections produced with a pressure of 50psi, with increasing welding times (0.2s, 0.6s, and 1.0s) 25
Figure 2.4	Knurl pattern of horn (left) and its dimension (right) 26
Figure 2.5	Optical images of the formation process of micro-bonds and interfacial waves along the bonding line..... 27
Figure 2.6	Convolutd bonding line in the weld samples produced in 1.0s weld time. 28
Figure 2.7	Optical images of Cu and Ni-plated Cu joints produced in 0.4s weld time: the layer of deformed material (a) overflowing onto the edge of horn edge (b) starting to flow along the inclined plane..... 29

Figure 2.8	Material flow during the welding process: (a) a LVDT signal for 1.0sec process time; (b) optical images of valley areas of the horn knurl pattern for different welding time (a: 0.2s, b: 0.4s, c: 0.6s).....	30
Figure 2.9	Optical images of Cu and Ni-plated Cu joints with increasing welding time: (a) as-received condition (b) 0.2s; (c) 0.4s; (d) 0.6s; (e) 0.8s; (f) 1.0s	32
Figure 2.10	Hardness profile of weld samples for different welding time. The hardness is averaged over the peaks of the horn (dots in the cross-section image)....	33
Figure 2.11	Hardness variation in horizontal locations: (a) horizontal hardness profile of the weld cross-sections; (b) Optical images for 0.4s and 1.0s weld time	34
Figure 2.12	Hardness variation in vertical locations: (a) vertical hardness profile of the weld cross-sections; (b) Optical images at the valley area of the horn for 0.4s and 1.0s weld time.....	35
Figure 2.13	Optical images of ultrasonically welded joints made in different weld qualities (i.e., ‘under’, ‘good’, and ‘over’ weld).....	37
Figure 2.14	Horn height obtained from LVDT sensor (upper); percentile ratio of indentation measured from optical cross-section images (lower).....	38
Figure 2.15	Hardness distribution of the weld samples for different weld time: (a) a schematic diagram of ultrasonically welded joint; (b) hardness profile of the weld interface; (c) hardness profile outside of weld zone	41

Figure 2.16	Weld region classification: (a) a schematic diagram of weld region classification; (b) optical micrograph of an ultrasonic weld produced in 0.6s welding time, giving an overview of classified weld regions.....	44
Figure 2.17	Optical micrograph of an ultrasonic weld produced in 1.0s welding time with classified weld regions.....	45
Figure 2.18	Classified weld regions associated with failure types: (a) a schematic diagram indicating dimension of each weld region (TMAZ and WN); (b) half TMAZ size and half WN size over weld time, with failed weldment images after U-tensile test.....	47
Figure 2.19	SEM images of deformed surfaces around the weld zone from the ‘over’ weld: (a) a front view image (vibration direction: out-and-in-plane); (b) ‘island’ features; (c) fatigue striation marks; (d) another front view image of the right hand side of image-(a); (e) crack propagations; (f) micro-cracks .	49
Figure 2.20	Correlation of weld performance with bond density and post-weld thickness	50
Figure 3.1	Ultrasonic metal welding system and sensor signal acquisition	57
Figure 3.2	Optical micrographs with two main bonding mechanisms for ultrasonic metal welds: (a) metallurgical adhesion; and (b) mechanical interlocking [Lee <i>et al.</i> 2013].....	61

Figure 3.3	Influence of weld time on (a) weld strength obtained from U-tensile test; (b) bond density; and (c) post-weld thickness	63
Figure 3.4	Power signal variation over time: (a) power profile for a single welding cycle; and (b) continuous cross-section images at the weld interface during welding cycle	67
Figure 3.5	LVDT signal: (a) profile of horn displacement; (b) cross-section images at the top of metal surface illustrating material filling behavior that corresponds to the displacements shown in (a).....	68
Figure 3.6	Variation of (a) power signal and (b) displacement signal for different levels of surface contamination.....	70
Figure 3.7	Optical micrographs showing weld line formation with welding time of (a) 0.1s, (b) 0.2s, (c) 0.3s, and (d) 0.4s.....	71
Figure 3.8	Optical micrographs at the weld interface for three levels of surface contamination: (a) level 0 (clean); (b) level 1; and (c) level 2.....	72
Figure 3.9	Features in power and displacement signals	73
Figure 3.10	Relationship between weld performance and signal features: (a) E_{total} ; (b) E_{mid} ; (c) D_{total} ; and (d) D_{mid}	74
Figure 3.11	Effect of welding time on: (a) E_{total} ; and (b) D_{total}	76
Figure 3.12	Relationship between weld attributes and power signal features: (a) BD vs. E_{total} ; (b) PWT vs. E_{total} ; (c) BD vs. E_{mid} ; and (c) PWT vs. E_{mid}	77

Figure 3.13	Relationship between weld attributes and displacement signal features: (a) BD vs. D_{total} ; (b) PWT vs. D_{total} ; (c) BD vs. D_{mid} ; and (c) PWT vs. D_{mid}	78
Figure 3.14	Relationship between signal features: (a) E_{mid} vs. D_{mid} ; (b) E_{total} vs. D_{total} ..	79
Figure 4.1	Ultrasonic metal welding system	89
Figure 4.2	High-speed camera setup: (a) entire view of setup; (b) focused view on welding part; and (c) workpiece in PC screen view	90
Figure 4.3	Schematic of high-speed camera setup: (a) workpiece stack-up aligned with horn (side view); and (b) displacement measurement of metal layer (front view)	91
Figure 4.4	Two anvil types and their knurl dimensions	92
Figure 4.5	T-peel test for multi-joint welds	93
Figure 4.6	Example of displacement variation in one weld cycle (5×10^{-5} second): (a) consecutive high-speed images showing single vibration cycle of a metal layer; (b) an illustration of displacement curve measured from (a).....	94
Figure 4.7	Development of vibration cycles of multiple layers with fine anvil: (a) 0.005s; (b) 0.020s; (c) 0.040s; (d) 0.060s; (e) 0.080s; and (f) 0.100s weld time	95
Figure 4.8	Progress of vibration amplitude of horn and four metal layers during initial stages (0 ~ 0.1s) of welding process when using (a) fine anvil; and (b) coarse anvil	97

Figure 4.9	Progress of vibration amplitude of horn and four metal layers during the entire welding process when using (a) fine anvil; and (b) coarse anvil.....	98
Figure 4.10	Progress of relative displacement between metal layers during initial stages (0 ~ 0.1s) of welding process when using (a) fine anvil; and (b) coarse anvil	99
Figure 4.11	Progress of vibration amplitude of the 4 th layer (anvil side) during the entire welding process with different anvil types	100
Figure 4.12	Micrographs of cross-sectioned weld samples produced with a fine anvil type for: (a) 0.2s, (b) 0.3s, (c) 0.4s, and (d) 0.5s.....	101
Figure 4.13	Micrographs of cross-sectioned weld samples produced with a coarse anvil for: (a) 0.2s, (b) 0.3s, (c) 0.4s, and (d) 0.5s.....	102
Figure 4.14	Bond density development at multiple weld interfaces for different anvil types	103
Figure 4.15	Mechanical performance of multiple joints (three weld interfaces) obtained by T-peel test for: (a) fine anvil type; and (b) coarse anvil type.....	104

LIST OF TABLES

Table 1.1	Summary of battery joining technologies [Lee 2010]	3
Table 2.1	Factors and levels for experimental design.....	20
Table 2.2	Definitions of ultrasonic weld attributes and schematic diagrams of attribute measurement	24
Table 3.1	Factors and levels for experimental design.....	65
Table 4.1	Factors and levels for experimental design.....	92

ABSTRACT

PROCESS AND QUALITY CHARACTERIZATION FOR ULTRASONIC WELDING OF LITHIUM-ION BATTERIES

by

Seungjae (Shawn) Lee

Chairs: S. Jack Hu and Elijah Kannatey-Asibu Jr.

Lithium-ion batteries have received a great deal of attention in the electric or hybrid-electric vehicle industry due to the advantage of providing the highest energy density compared with other available battery systems. Manufacturing of lithium-ion battery packs demands a significant amount of joining, such as welding, to fulfill the desired power and capacity requirements. However, conventional fusion welding processes, such as resistance spot welding and laser welding, face difficulties in joining multiple thin sheets of highly conductive, dissimilar materials. Ultrasonic metal welding overcomes such difficulties by using its inherent solid-state process characteristics. Despite a considerable amount of past research on ultrasonic metal welding, the fundamental mechanisms behind this process are still uncertain. Moreover, there is a lack of scientific quality guidelines for implementing ultrasonic welding in volume production. This dissertation develops methods for comprehensive characterization of the process and quality in ultrasonic welding of multiple thin layers of battery materials for high power lithium-ion battery packs.

Three research topics are addressed in this dissertation:

1. *Characterization of joint quality in ultrasonic welding of battery tabs:* Several physical weld attributes are identified by experimentally characterizing the weld formation over time using copper-to-nickel plated copper welding as an example. The weld attributes are then correlated to weld performance by examining the cross-sectioned samples of different weld quality using optical microscopy, scanning electronic microscopy, and hardness measurements.
2. *Characterization of ultrasonic metal welding by correlating online sensor signals with weld attributes:* Online process monitoring using sensors is a key enabler of securing product quality and process stability in manufacturing. To develop a robust and reliable monitoring system for ultrasonic welding, this research establishes an in-depth characterization of the sensor signals and their relationship to the welding process and quality. Selected online features are correlated to weld attributes in order to understand the physics behind the weld formation under abnormal process conditions.
3. *Analysis of weld formation in multilayer ultrasonic metal welding using high-speed images:* This research establishes real-time phenomenological observation on multilayer ultrasonic welding by analyzing the vibration behaviors of metal layers. Such behaviors are characterized by a direct measurement of the lateral displacement of each metal layer using high-speed images.

This dissertation provides new knowledge and insights for enhancing the process stability and quality in ultrasonic metal welding in lithium-ion battery pack manufacturing.

CHAPTER 1

INTRODUCTION

1.1 BACKGROUND

Re-chargeable batteries are used in all places of our daily lives and are considered a key technology for renewable, sustainable, and portable energy applications. Portable electronic devices, such as mobile phones, notebooks, and GPS, rely on batteries for their power supply.

Electrification of automobiles requires new developments in high energy/power density batteries. The performance of battery electric vehicles depends on the power and energy capacity of battery packs. Of the different battery technologies, the lithium-ion battery in particular has received great attention since it provides the highest energy density of all available systems [Fuller *et al.* 1994]. Hence it is the one critical technology that may determine the auto industry's future in the next several decades.

In current automotive lithium-ion battery manufacturing, different sizes and shapes of cells are fabricated and are subsequently assembled into packs of different configurations [Matsuoka *et al.* 2002; Kawakatsu *et al.* 2006; Buck *et al.* 2008]. Figure 1.1 describes the hierarchy of battery assembly. An automotive battery pack typically consists of a large number of battery cells, sometimes several hundreds, even thousands, to meet desired power and capacity needs. Each battery cell contains a group of flat-

wound or cut-and-stacked positive/negative electrodes and separators, with electrode leads (i.e., tabs) attached, in a laminate pouch [Dhameja 2002]. Several cells are usually joined together through battery tabs and bus-bars (i.e., interconnecting units) to form a module, and there are tens of modules in a battery pack [Lee *et al.* 2010]. As a result, a significant amount of joining, such as welding, is needed to deliver the desired electricity in a battery pack. It is not easy to join such a large number of battery cells because of the difficulty of welding multiple thin layers of highly conductive and dissimilar materials with high reliability. In addition, automobile batteries are exposed to harsh driving environments, such as vibration, severe temperature, and the occasional crash - which can affect the battery performance and safety. Furthermore, hundreds of thousands of battery packs will be produced annually for automotive volume production. As such, batteries must be assembled using robust joining processes and the development of effective joining technologies for battery manufacturing is essential for auto manufacturers.

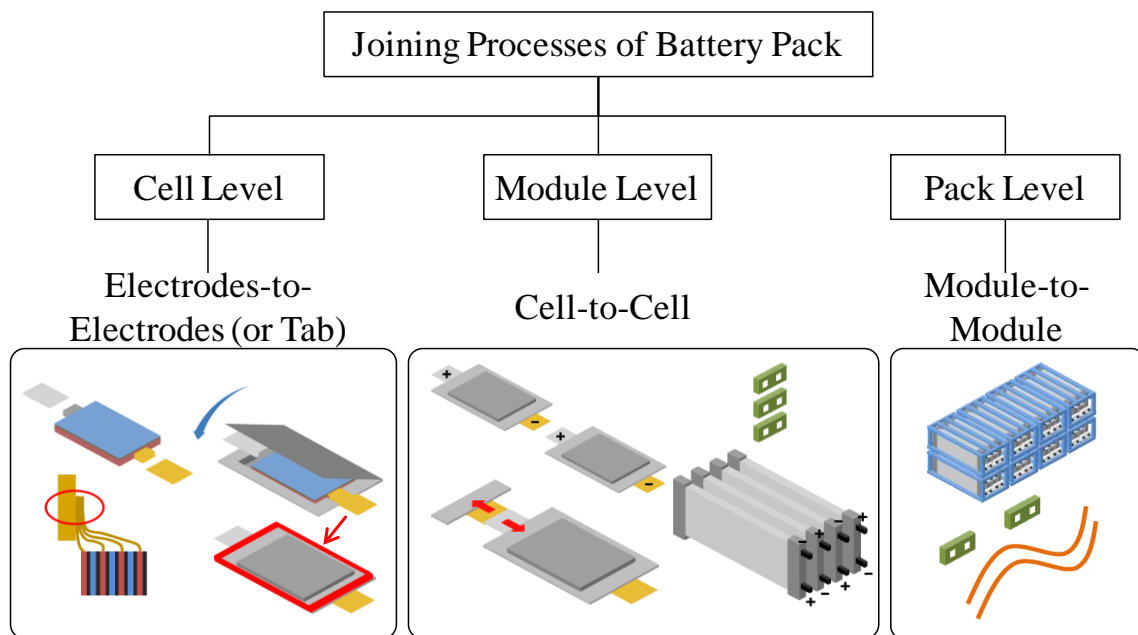


Figure 1.1 Hierarchy of joining processes in battery pack manufacturing [Lee 2010]

Several joining methods, including different welding techniques such as resistance welding, laser welding, and ultrasonic welding, have been used to connect battery cells. The advantages and disadvantages of these joining technologies are summarized in Table 1.1.

Table 1.1 Summary of battery joining technologies [Lee 2010]

Joining methods	Advantages	Disadvantages
Resistance welding	<ul style="list-style-type: none"> •Low cost •Efficient and fully automated •No filler metals or gases •Existing technology for weld quality control 	<ul style="list-style-type: none"> •Difficult for highly conductive materials •Difficult to produce large nuggets •Electrode sticking/ wear •Possible expulsions
Laser welding	<ul style="list-style-type: none"> •Non-contact process •Less thermal input – less distortion •Very high precision welding •High speed 	<ul style="list-style-type: none"> •Hard to produce a large joint area •Needs good joint fit-up •Material reflectivity •Need of shielding gas •High initial cost
Ultrasonic welding	<ul style="list-style-type: none"> •Solid state process •Good for highly conductive materials •Good for dissimilar materials •Good for thin sheets or wires •Good for multi-layered sheets •Gauge ratio insensitive •No filler metals or gases 	<ul style="list-style-type: none"> •Restricted to lap joints •Joint thickness limitation (< 3mm) •Challenging with high strength, hardness materials •Sensitive to surface conditions •Possible audible noise

Resistance welding, as one of the oldest welding processes in use, relies on the electrical resistance at the metal interface to cause localized heating and fusion of materials [Zhang and Senkara 2011]. The resistance welding process has been widely applied to the automotive, electronics, and heavy industries because it is very fast and easily automated. However, resistance welding has many challenges when applied to

battery welding. First, typical materials for battery electrodes and tabs are pure aluminum or copper, which are difficult to weld by resistance welding due to their high thermal/electrical conductivities and dissimilar material properties [Ekern and Czanderna 1977; Sun and Dong 2000; Fukumoto *et al.* 2003]. In addition, because of the thicknesses of target materials, it is very challenging to produce large-sized welds which are desirable for batteries in order to reduce the electrical resistance of the joints and the heat generated when a large amount of current flows through the cells.

Laser welding is a non-contact process that joins multiple pieces of metal through the use of a laser [Sun and Ion 1995]. The weld is formed as the intense laser beam rapidly heats the material, typically in milli-seconds [Shannon 2004]. The welding process using a low power pulsed Nd:YAG laser offers the advantage of low heat input to the specimen [Frewin and Scott 1999] and the ability of multilayer joining [Kelly and Kampe 2004]. However, a poor metallurgical affinity between dissimilar materials limits the laser welding process and leads to a large number of weld defects, such as brittle phases, and crack sensitivity [Esser *et al.* 2004].

Ultrasonic metal welding, as illustrated in Figure 1.2, uses the oscillating shears generated by a high frequency ultrasonic energy to create a solid-state bond between metals [Zhang and Li 2009]. This process overcomes the difficulties of multiple sheets of dissimilar materials by using its inherent advantages derived from the solid-state process characteristics [Lee *et al.* 2012; Lee *et al.* 2013]. In addition, unlike resistance welding and laser welding, the temperature in the ultrasonic welding process does not exceed the melting point of the metal workpiece, eliminating undesirable compounds, phases, and metallurgical defects that commonly exist in most other fusion welds [Annoni and

Carboni 2011; Kim *et al.* 2011]. Thus, of the different joining options, ultrasonic metal welding is believed to be most suitable for battery joining.

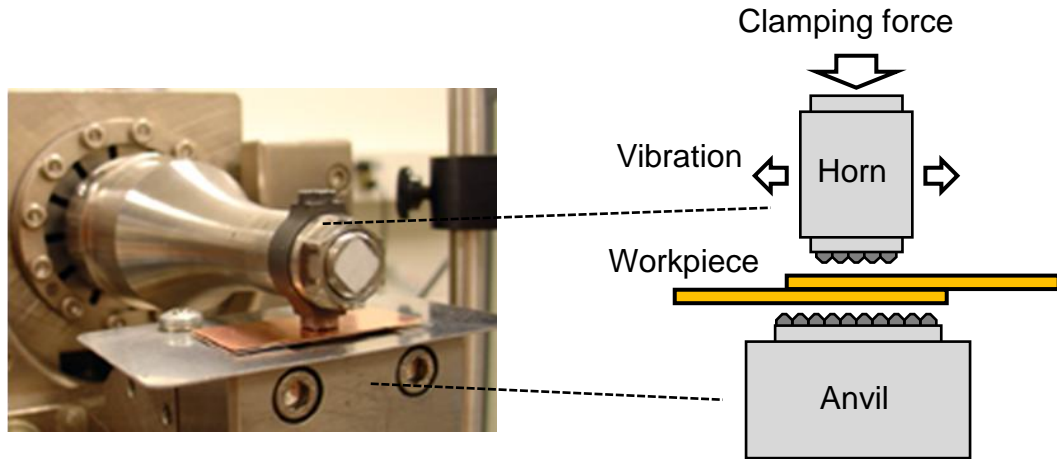


Figure 1.2 Ultrasonic metal welding

A considerable amount of research has been carried out on the ultrasonic welding of wires for microelectronic packaging in the semiconductor industry [Harman and Albers 1977; Krzanowski 1990; Jeng and Horng 2001; Li *et al.* 2008] or on ultrasonic consolidation for metal foil fabrication in additive manufacturing [Gao and Doumanidis 2002; Kong *et al.* 2003; 2004; 2005; Ram *et al.* 2006; 2007; Yang *et al.* 2010]. However, the ultrasonic welding of batteries in automotive applications is still in the early stage and only limited research has been done in this area. Lee *et al.* [2012] investigated the temperature distribution within multi-stacked battery tabs using finite element analysis. Li and his team [Li *et al.* 2013; Zhao *et al.* 2013] presented a methodology of using thin-film thermocouples to study the heat flux in the ultrasonic welding of battery tabs. Kang *et al.* [2012; 2013] investigated the effect of structural vibration that is generated from the ultrasonic welding process on weld quality in the multilayer battery tab configuration.

However, most research has focused on characterizing different aspects of the weld process, and there is still a lack of standard quality definitions in ultrasonic metal welding.

1.2 STATEMENT OF PROBLEM

Weld quality is usually defined by its performance, and the performance is associated with physical attributes [Zhou 2001]. For example, in resistance spot welding, the weld quality is identified by several weld attributes such as nugget diameter [Pouranvari *et al.* 2007; Pouranvari and Marashi 2010], size of heat affected zone (HAZ) or sheet penetration [Zhou *et al.* 2003], and defects [Jenney and O'Brien 2001]. However, the quality of an ultrasonic metal weld has not yet been systematically defined for high power battery packs despite the increasing need in quality evaluation for a vast amount of battery joints. Due to a lack of quality guidelines for the ultrasonic metal welds, it is difficult to have a robust and reliable battery joining system.

Online process monitoring has been widely used for ensuring weld quality [Sun *et al.* 1999; Li *et al.* 2000; Ling *et al.* 2006; Wu *et al.* 2007; Ling *et al.* 2010]. Sensor signals are collected for weld process monitoring and critical online features are related to product and process quality [Shao *et al.* 2013]. However, there is a lack of understanding about the relationship between the features and the ultrasonic welding process since it is newly adopted for battery joining and the physics behind the process remain uncertain. Even without expert knowledge of the process, developing a reliable monitoring algorithm can be still achieved by systematic feature selection, but selected features may not perform well when new abnormal process conditions are encountered.

One of the biggest challenges in automotive battery manufacturing is to achieve consistent weld quality among multiple layers of dissimilar materials. Although ultrasonic welding provides relatively good weldability for multilayers of dissimilar metals compared to conventional fusion welding techniques [Lee *et al.* 2010], there still exists inconsistency of quality due to a lack of knowledge on the weld formation through the multiple interfaces. Based upon a literature review [Elangovan *et al.* 2009; Zhang and Li 2009; Lee *et al.* 2012; Li *et al.* 2013], no real-time phenomenological observation on the welding process has yet been carried out.

1.3 RESEARCH OBJECTIVES

The objective of this research is to establish an in-depth understanding of the weld formation mechanisms in ultrasonic metal welding, develop scientific definitions for ultrasonic weld quality, and, ultimately, achieve a robust ultrasonic welding process for high quality battery joining. The specific tasks are:

- 1) to identify critical weld attributes that determine the quality of ultrasonic metal welds, and establish the quantitative relationships to link weld attributes and mechanical performance obtained by tensile testing;
- 2) to investigate the fundamental physics behind the ultrasonic welding process by examining sensor signals and their variations under abnormal process conditions, and predict joint quality by correlating key online features to weld attributes;

- 3) to investigate the weld development in multilayer ultrasonic welding and the effect of weld tools on propagation mechanisms by analyzing the vibration behaviors of metal layers using high-speed images.

The fulfillment of the objectives will provide a comprehensive understanding of the effects of process variables on the weld formation and weld quality in the ultrasonic metal welding of multiple thin sheets. The results from this dissertation will lead to an improved joining process for lithium-ion batteries. Furthermore, they will provide insights for in-line process monitoring/control and optimum tool design to enhance the joint quality and reduce cost.

1.4 ORGANIZATION OF DISSERTATION

This dissertation is presented in a multiple manuscript format. Chapters 2, 3 and 4 are written as individual research papers that are partially revised for this dissertation and include abstracts, main body sections and references.

Chapter 2 investigates the weld formation mechanisms and material behaviors in the ultrasonic welding of pure copper and nickel-plated copper. Several key weld attributes that determine the weld quality are defined and quantified by cross-sectioned weld samples using microscopy and hardness measurements. The effect of process variables on the weld attributes is examined, and the relationship between the weld attributes and mechanical strength is investigated. Critical weld regions are classified in the ultrasonic metal weld, and their changes in size are shown in the weld samples produced with different levels of quality.

Chapter 3 presents the characterization of ultrasonic metal welds using two sensor signals: weld power and horn displacement. Signal variations under abnormal process conditions are thoroughly examined in order to understand the physics behind the ultrasonic welding process. Based on these understandings, several online features are identified from the sensor signals and correlated to weld attributes that impact the weld quality. The feasibility of selected online features for process monitoring is also discussed.

Chapter 4 investigates the weld development in the ultrasonic welding of multilayered nickel-plated copper sheets using high-speed images. The vibration behaviors of the workpieces are characterized by measuring the lateral displacement of each metal layer from the digitally recorded images. The propagation mechanism in weld formation through multiple interfaces is presented by analyzing the relative displacement between the mating metal layers. A series of optical micrographs and bond density measurements were carried out to verify the high-speed imaging results. The effect of knurl geometry of the weld tools on the weld formation mechanism is identified by separate welding experiments using two different tool designs. This chapter also provides insights on tool wear that results from the extensive amount of slippage during the ultrasonic welding process.

Chapter 5 summarizes the findings and the original contributions of the dissertation. Several topics are also proposed for future work.

REFERENCES

- Annoni, M. and Carboni, M. (2011). "Ultrasonic Metal Welding of AA 6022-T4 Lap Joints: Part I-Technological Characterisation and Static Mechanical Behaviour." *Science and Technology of Welding & Joining* 16(2): 107-115.
- Buck, D. S., Fattig, R. N. and Silk, B. J. (2008). Battery Pack with Integral Cooling and Bussing Devices. USA, Enerdel.
- Dhameja, S. (2002). Electric Vehicle Battery Systems, Newnes.
- Ekern, R. and Czanderna, A. W. (1977). "Resistance Welding of Metals with High Electrical and Thermal Conductivity." *Review of scientific instruments* 48(6): 708-708.
- Elangovan, S., Semeer, S. and Prakasan, K. (2009). "Temperature and Stress Distribution in Ultrasonic Metal Welding—an Fea-Based Study." *journal of materials processing technology* 209(3): 1143-1150.
- Esser, G., Mys, I. and Schmidt, M. H. (2004). "Laser Micro Welding of Copper and Aluminium Using Filler Materials." *Fifth International Symposium on Laser Precision Microfabrication*: 337-342.
- Frewin, M. and Scott, D. (1999). "Finite Element Model of Pulsed Laser Welding." *WELDING JOURNAL-NEW YORK*- 78: 15-s.
- Fukumoto, S., Lum, I., Biro, E., Boomer, D. and Zhou, Y. (2003). "Effects of Electrode Degradation on Electrode Life in Resistance Spot Welding of Aluminum Alloy 5182." *Welding Journal-New york* 82(11): 307.
- Fuller, T. F., Doyle, M. and Newman, J. (1994). "Simulation and Optimization of the Dual Lithium Ion Insertion Cell." *Journal of The Electrochemical Society* 141(1): 1-10.
- Gao, Y. and Doumanidis, C. (2002). "Mechanical Analysis of Ultrasonic Bonding for Rapid Prototyping." *Journal of Manufacturing Science and Engineering* 124(2): 426-434.
- Harman, G. and Albers, J. (1977). "The Ultrasonic Welding Mechanism as Applied to Aluminum-and Gold-Wire Bonding in Microelectronics." *Parts, Hybrids, and Packaging, IEEE Transactions on* 13(4): 406-412.

- Jeng, Y. R. and Horng, J. H. (2001). "A Microcontact Approach for Ultrasonic Wire Bonding in Microelectronics." *Journal of tribology* 123: 725.
- Jenney, C. L. and O'Brien, A. (2001). *Welding Handbook*, American Welding Society.
- Kang, B. S., Cai, W. and Tan, C. A. (2012). "Vibrational Energy Loss Analysis of Battery Bus-Bar in Ultrasonic Welding." *submitted to International Journal of Mechanical Sciences*.
- Kang, B. S., Cai, W. and Tan, C. A. (2013). "Dynamic Response of Battery Tabs under Ultrasonic Welding." *accepted by Journal of Manufacturing Science & Engineering*.
- Kawakatsu, T., Fukuoka, T., Tsutsui, K., Katsumata, I. and Hattori, Y. (2006). Nickel-Metal Hydride Battery for Hybrid Electric Vehicles. *Matsushita Technical Journal*. 52.
- Kelly, S. and Kampe, S. (2004). "Microstructural Evolution in Laser-Deposited Multilayer Ti-6Al-4V Builds: Part I. Microstructural Characterization." *Metallurgical and Materials Transactions A* 35(6): 1861-1867.
- Kim, T. H., Yum, J., Hu, S. J., Spicer, J. P. and Abell, J. A. (2011). "Process Robustness of Single Lap Ultrasonic Welding of Thin, Dissimilar Materials." *CIRP Annals - Manufacturing Technology* 60(1): 17-20.
- Kong, C., Soar, R. and Dickens, P. (2003). "Characterisation of Aluminium Alloy 6061 for the Ultrasonic Consolidation Process." *Materials Science and Engineering A* 363(1-2): 99-106.
- Kong, C., Soar, R. and Dickens, P. (2004). "Optimum Process Parameters for Ultrasonic Consolidation of 3003 Aluminium." *Journal of Materials Processing Technology* 146(2): 181-187.
- Kong, C., Soar, R. and Dickens, P. M. (2005). "A Model for Weld Strength in Ultrasonically Consolidated Components." *Proceedings of the Institution of Mechanical Engineers, Part C: Journal of Mechanical Engineering Science* 219(1): 83-91.
- Krzanowski, J. E. (1990). "A Transmission Electron Microscopy Study of Ultrasonic Wire Bonding." *Components, Hybrids, and Manufacturing Technology, IEEE Transactions on* 13(1): 176-181.

- Lee, D., Kannatey-Asibu, E. and Cai, W. (2012). "Ultrasonic Welding Simulations for Multiple, Thin and Dissimilar Metals." *submitted to ASME International Symposium on Flexible Automation*.
- Lee, D. K., Kannatey-Asibu Jr., E. and Cai, W. (2012). "Ultrasonic Welding Simulations for Multiple, Thin and Dissimilar Metals." *ASME International Symposium on Flexible Automation, St. Louis*.
- Lee, S. S., Kim, T. H., Hu, S. J., Cai, W. and Abell, J. A. (2010). "Joining Technologies for Automotive Lithium-Ion Battery Manufacturing: A Review." *ASME Conference Proceedings* 2010(49460): 541-549.
- Lee, S. S., Kim, T. H., Hu, S. J., Cai, W., Abell, J. A. and Li, J. (2013). "Characterization of Joint Quality in Ultrasonic Welding of Battery Tabs." *Journal of Manufacturing Science and Engineering* 135(2): 021004.
- Li, H., Choi, H., Zhao, J., Li, X. C., Cai, W. and Abell, J. A. (2013). "Transient Temperature and Heat Flux Measurement in Ultrasonic Joining of Battery Tabs Using Thin-Film Micro Sensors." *accepted by Journal of Manufacturing Science and Engineering*.
- Li, J., Han, L. and Zhong, J. (2008). "Short Circuit Diffusion of Ultrasonic Bonding Interfaces in Microelectronic Packaging." *Surface and Interface Analysis* 40(5): 953-957.
- Li, W., Hu, S. J. and Ni, J. (2000). "On-Line Quality Estimation in Resistance Spot Welding." *Journal of manufacturing science and engineering* 122(3): 511-512.
- Ling, S.-F., Wan, L.-X., Wong, Y.-R. and Li, D.-N. (2010). "Input Electrical Impedance as Quality Monitoring Signature for Characterizing Resistance Spot Welding." *NDT & E International* 43(3): 200-205.
- Ling, S., Luan, J., Li, X. and Yong Ang, W. L. (2006). "Input Electrical Impedance as Signature for Nondestructive Evaluation of Weld Quality During Ultrasonic Welding of Plastics." *NDT & E International* 39(1): 13-18.
- Matsuoka, T., Matsumoto, K., Takedomi, H. and Hasegawa, O. (2002). Charging Element Device and Holding Structure Therefor, Honda Giken Kogyo Kabushiki Kaisha.
- Pouranvari, M., Asgari, H. R., Mosavizadch, S. M., Marashi, P. H. and Goodarzi, M. (2007). "Effect of Weld Nugget Size on Overload Failure Mode of Resistance Spot Welds." *Science and Technology of Welding & Joining* 12(3): 217-225.

- Pouranvari, M. and Marashi, S. (2010). "Factors Affecting Mechanical Properties of Resistance Spot Welds." *Materials Science and Technology* 26(9): 1137-1144.
- Ram, G. D. J., Robinson, C., Yang, Y. and Stucker, B. (2007). "Use of Ultrasonic Consolidation for Fabrication of Multi-Material Structures." *Rapid Prototyping Journal* 13(4): 226-235.
- Ram, G. D. J., Yang, Y. and Stucker, B. (2006). "Effect of Process Parameters on Bond Formation During Ultrasonic Consolidation of Aluminum Alloy 3003." *Journal of Manufacturing Systems* 25(3): 221-238.
- Shannon, G. J. (2004). Spot and Seam Welding Applications Using Nd:Yag Lasers, Unitek Miyachi Corporation.
- Shao, C., Paynabar, K., Kim, T. H., Jin, J. J., Hu, S. J., Spicer, J. P., Wang, H. and Abell, J. A. (2013). "Feature Selection for Manufacturing Process Monitoring Using Cross-Validation." *submitted to Journal of Manufacturing Systems*.
- Sun, A., Kannatey-Asibu, E. and Gartner, M. (1999). "Sensor Systems for Real-Time Monitoring of Laser Weld Quality." *Journal of Laser Applications* 11(4): 153-168.
- Sun, X. and Dong, P. (2000). "Analysis of Aluminum Resistance Spot Welding Processes Using Coupled Finite Element Procedures." *Welding Journal-New york* 79(8): 215.
- Sun, Z. and Ion, J. (1995). "Laser Welding of Dissimilar Metal Combinations." *Journal of Materials Science* 30(17): 4205-4214.
- Wu, C., Gao, J. and Hu, J. (2007). "Real-Time Sensing and Monitoring in Robotic Gas Metal Arc Welding." *Measurement science and technology* 18(1): 303.
- Yang, Y., Ram, G. D. J. and Stucker, B. E. (2010). "An Analytical Energy Model for Metal Foil Deposition in Ultrasonic Consolidation." *Rapid Prototyping Journal* 16(1): 20-28.
- Zhang, C. and Li, L. (2009). "A Coupled Thermal-Mechanical Analysis of Ultrasonic Bonding Mechanism." *Metallurgical and Materials Transactions B* 40(2): 196-207.
- Zhang, H. and Senkara, J. (2011). Resistance Welding: Fundamentals and Applications, CRC Press LLC.

Zhao, J., Li, H., Choi, H., Cai, W., Abell, J. A. and Li, X. (2013). "Insertable Thin Film Thermocouples for in Situ Transient Temperature Monitoring in Ultrasonic Metal Welding of Battery Tabs." *Journal of Manufacturing Processes* 15(1): 136-140.

Zhou, M. (2001). A Unified Approach to Assessing the Mechanical Performance of Resistance Spot Welds, University of Michigan.

Zhou, M., Zhang, H. and Hu, S. J. (2003). "Relationships between Quality and Attributes of Spot Welds." *Welding Journal (Miami, Fla)* 82(Compendex): 72S-77S.

CHAPTER 2

CHARACTERIZATION OF JOINT QUALITY IN ULTRASONIC WELDING OF BATTERY TABS*

ABSTRACT

Conventional fusion welding processes such as resistance spot welding and laser welding face difficulties in joining multiple sheets of highly conductive, dissimilar materials for automotive lithium ion battery manufacturing. Ultrasonic metal welding overcomes these difficulties by using its inherent advantages derived from its solid-state process characteristics. Although ultrasonic metal welding is well-suited for battery manufacturing, there is a lack of scientific quality guidelines for implementing ultrasonic welding in volume production. To establish such quality guidelines, this chapter identifies a number of critical weld attributes that determine the quality of welds by experimentally characterizing the weld formation over time using copper-to-copper welding as an example. Samples of different weld quality were cross-sectioned and characterized with optical microscopy, scanning electronic microscopy (SEM), and hardness measurements in order to identify the relationship between physical weld attributes and weld performance. The methodology provided in this chapter links process parameters to weld performance through physical weld attributes.

* The contents of this chapter have been published in *ASME Journal of Manufacturing Science and Engineering*, under "Characterization of Joint Quality in Ultrasonic Welding of Battery Tabs," April 2013, 135(2), p. 021004.

2.1 INTRODUCTION

Battery electric vehicles (BEVs) including electric, hybrid electric, and plug-in hybrid electric vehicles have received a great deal of attention in the automotive industry. The performance of these BEVs relies on the power and energy capacities of their batteries. Among the various battery technologies, lithium-ion batteries have the advantages of being compact and light weight for the same power requirement. To meet the desired power and capacity needs for BEVs, a lithium-ion battery pack is assembled from a large number of battery cells, sometimes several hundreds, even thousands depending on the cell configuration and pack size. Several cells are usually joined together to form a module with common bus-bars, and tens of modules are then assembled into a battery pack [Lee *et al.* 2010]. Therefore, a significant amount of battery joining is needed in battery pack manufacturing. However, battery joining is faced with several challenges [Lee *et al.* 2010]: joining of highly conductive materials such as copper, aluminum, and nickel; dissimilar and multi-layer materials with varying sheet thickness combinations; and large weld areas to decrease current density and to increase mechanical strength. In addition, reliable joints are required for batteries to stand for harsh environments such as vibration, severe weather, and humidity. Hence, it is essential to develop robust and reliable technologies for battery joining.

In this study, ultrasonic metal welding is applied to battery joining because of its advantages over other fusion welding methods such as resistance spot welding and laser welding. First, highly conductive materials with thin, dissimilar, and multi-layer sheets can be welded by ultrasonic metal welding. Second, ultrasonic metal welding does not generate a large amount of heat since high heat may damage the battery. Finally,

ultrasonically welded joints typically eliminate metallurgical defects that commonly exist in most other fusion welds, such as formation of intermetallic compounds, brittle phases, or porosities in the fused zone. Although ultrasonic metal welding is well-suited for battery manufacturing, scientific quality guidelines do not yet exist for volume production of batteries. Therefore, it is necessary to develop understanding of the mechanisms of weld formation and the resulting quality characteristics for battery joining.

A commonly accepted weld quality definition does not yet exist for ultrasonic welding, but methods have been established for other joining processes. The quality for spot welds is assessed by whether the performance of a weld meets the specific requirements or by the size of a weld nugget usually obtained from the peel test [Hu *et al.* 1996]. Although there are not as many quality guidelines as in spot welding, some research has been carried out to define the weld quality in ultrasonic metal welding. Kong *et al.* [2003; 2004] proposed the ‘linear weld density’, the proportion of bonded line to the entire weld along the weld interface, as a quantitative quality criterion for ultrasonic welds. Based on this linear weld density, Yang *et al.* [2010] developed an analytical energy model for metal foil deposition in ultrasonic consolidation and studied the effects of process parameters on weld quality. Hetrick *et al.* [2009] used several microstructural features of a weld cross section to characterize ultrasonic metal welding process in auto body fabrication. Bakavos and Prangnell [2010] performed a microstructural analysis on the mechanisms of weld formation in ultrasonic metal welding of aluminum alloys. Zhou *et al.* [2005; 2006] developed finite element models of the welded samples to predict performance based on two distinct failure modes: interfacial fracture and pull-out fracture of ultrasonic welds. Kim *et al.* [2011] attempted to develop a quality criterion for

ultrasonic metal welding of conductive materials such as copper and nickel plated copper by identifying failure modes in T-peel tests. Nevertheless, none of these studies has established an explicit relationship between physical weld attributes and weld performance, and scientific quality guidelines of ultrasonic welds are still lacking, particularly for battery applications. Physical weld attributes can be defined as any measurable characteristics of the weldment that may affect the weld performance, which refers here to the mechanical strength at the joint [Zhou *et al.* 2003]. Therefore, this chapter identifies a number of critical weld attributes that determine the quality of welds by experimentally characterizing the weld formation over time using copper-to-copper welding as an example and establishes a quality classification for ultrasonically welded joints. A microstructural classification method for the weld region is introduced to complete the weld quality characterization.

The remainder of this chapter is organized as follows: Section 2.2 describes the materials and experimental procedures; Section 2.3 defines the attributes in an ultrasonic metal weld, summarizes the microstructural observations on weld cross-sections. Section 2.4 discusses the relationship between weld attributes and quality.

2.2 MATERIALS AND EXPERIMENTS

To simulate the joining of battery tabs and bus-bars, as shown in Figure 2.1(a), 0.4mm C11000 copper sheets (Cu 99.9%) and nickel plated 1.0mm copper sheets of the same copper alloy (ASTM B689) were used for the welding experiments. Nickel coating, approximately of 3 μ m, was intended originally for corrosion resistance, but it also served as an indicator of surface separation between the two similar materials during the

microscopic analysis. For example, the bond density over the weld interface can be measured by 1) the interfacial area where the nickel layer is broken and two copper surfaces are fused together, and 2) the area where the nickel layer is distorted so that it leads to a mechanical interlocking between materials. It is difficult to determine these bonded regions between two copper surfaces without the nickel layer.

The experimental procedure is as follows:

- 1) Coupon sheets of Cu and Ni-plated Cu were ultrasonically welded at different levels of clamping pressure (40, 50, and 60psi) and welding time (0.2, 0.4, 0.6, 0.8, and 1.0s);
- 2) The produced weld samples were then subjected to U-tensile tests to identify the failure types and to evaluate the weld quality; and
- 3) The weld zones were characterized by optical microscopy (Figure 2.1(c)), SEMs and microhardness tests.

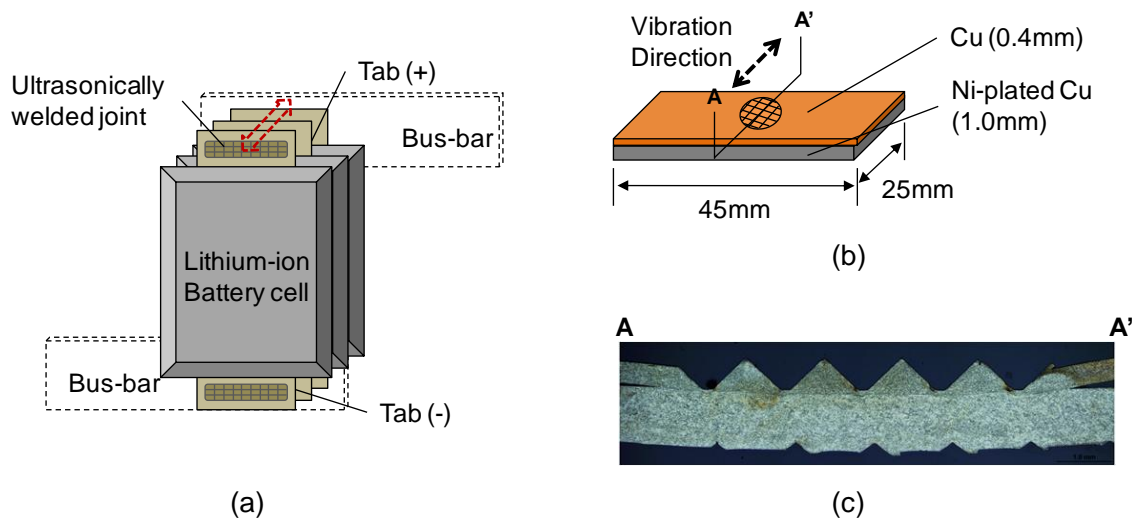


Figure 2.1 Ultrasonic welding configuration: (a) an example of battery tab joining; (b) dimension and configuration of weld coupons; and (c) cross-section image (AA')

2.2.1 Experiments

Test coupons, 25mm wide and 45mm long, with complete overlap (Figure 2.1(b)), were welded by an AmTech Ultraweld®L-20 high power welder with a vibration frequency of 20kHz and a vibration direction along the shorter side of the coupon. The dimensions and configurations of weld samples were designed to allow the U-tensile test, as illustrated in Figure 2.2(a). According to the screening tests performed prior to this study, the clamping pressure and welding time were selected as input variables while the vibration amplitude was kept constant at 30 μ m throughout the experiment, as detailed in Table 2.1. Using a full factorial design, 15 test conditions in total and 10 replicates at each condition were conducted.

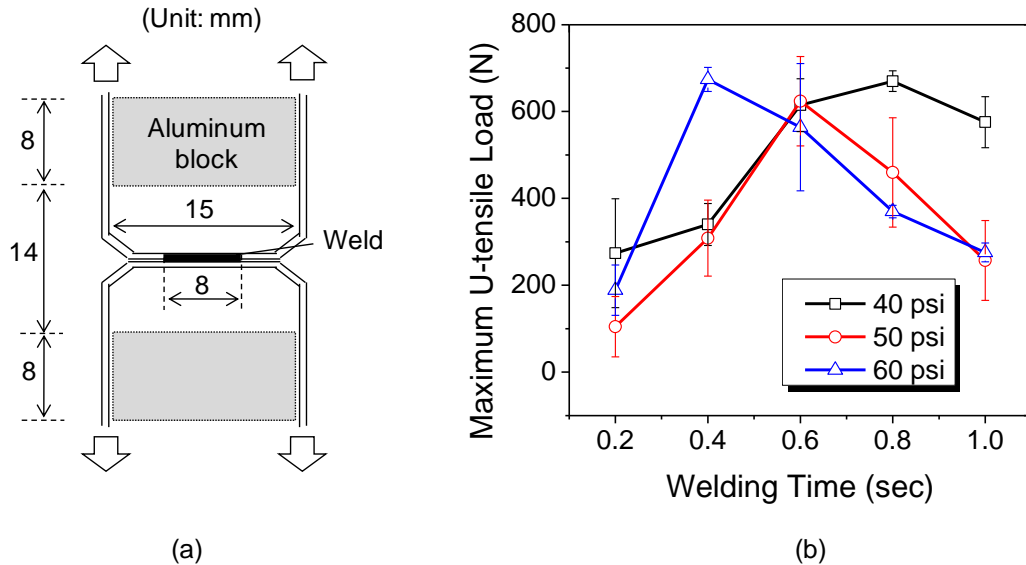


Figure 2.2 Weld performance testing: (a) U-tensile test configuration; (b) maximum U-tensile load plotted against welding time for three different clamping pressures

Table 2.1 Factors and levels for experimental design

Factor	Factor name	Level
P	Clamping pressure (psi)	40, 50, 60
T	Welding time (sec)	0.2, 0.4, 0.6, 0.8, 1.0

2.2.2 Weld performance testing

In order to evaluate the mechanical strength, welded samples were subjected to U-tensile tests performed using an *Instron* testing machine with a 5kN load cell. A pulling speed of 20 mm/min was selected to minimize unnecessary dynamic effects for weld failure. The peak load during the test was recorded as a measure of weld performance. After the weld had failed, photo images were taken and examined to record different failure types.

Figure 2.2(b) shows the maximum U-tensile load against welding time for three different clamping pressures. The load at each clamping pressure increases as welding time increases, and begins to decrease beyond a critical welding time due to material thinning and crack formations. For 40psi of clamping pressure, the maximum U-tensile load is achieved at 0.8 sec of weld time, and this optimum welding time decreases with higher clamping pressures: 0.6 sec for 50psi and 0.4 sec for 60psi, respectively.

2.2.3 Sample preparation/microscopy/hardness testing

To identify weld attributes, SEM and metallurgical examination were conducted. The weld samples were sectioned across their center, parallel to the direction of welding vibration, by a low speed diamond wheel saw without creating any residual stresses. The cross-sectioned specimens were then cold-mounted in epoxy, carefully ground until the plane of the maximum horn indentation depth was reached. Then they were polished down to 1 μ m diamond, and further polished to 0.25 μ m colloidal silica. Following etching using ammonium hydroxide mixed with dilute hydrogen peroxide, optical images were obtained from a fluorescent microscope (Olympus BX51 W/DP71) to provide metallographs of the samples. More detailed microstructural analysis was performed with

a SEM with a Philips XL30 FEG-SEM at 30kV to characterize the circumferential defect of the weld. Finally, to identify the mechanical property change within the weld zone, microhardness was measured by using a Vickers microhardness tester (Clark, CM-400AT) with an indentation load of 25g for 15 seconds.

2.3 DEFINITION OF ATTRIBUTES AND WELD CHARACTERIZATION

In this section, critical weld attributes that impact on the weld performance are defined first. Then, the ultrasonically welded joints of Cu and Ni-plated Cu are characterized using microstructural images and hardness distribution. The bond mechanisms for these particular materials and the metallurgical characteristics, such as material flow in the metal surface of the top sheet and hardening/softening during the weld development, are discussed as those are associated with the formation of weld attributes.

2.3.1 Definition of weld attributes

Weld strength can be determined by the physical attributes of the weldment [Zhou *et al.* 2003]. Several weld attributes of ultrasonically welded joints are defined in Table 2.2. Each weld attribute was quantitatively measured or qualitatively estimated by using the cross-section images and microhardness profiles in the weld zone.

- *Bond density*: the relative bond density for different welding time is estimated by distinguishing bonded and unbonded regions at the weld interface and measuring

the proportion of bonded portion projected onto the horizontal line to the entire horn width, as described in Table 2.2(a).

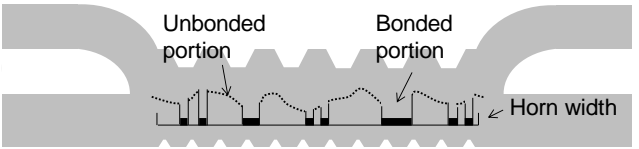
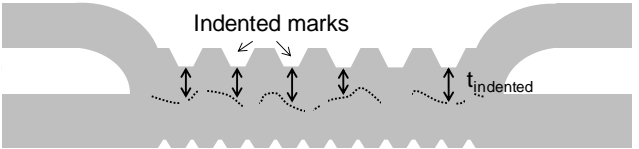
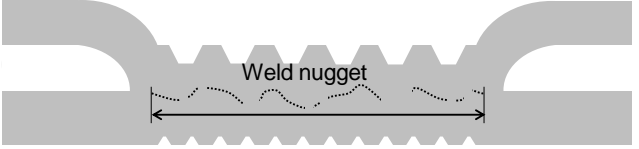
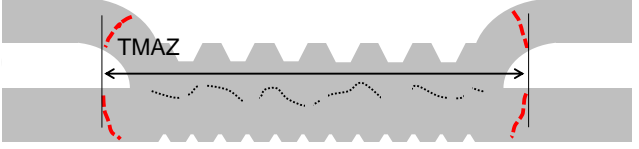
- *Post-weld thickness*: the post-weld thickness is the thickness of the indented material by the horn's pressing force. The indented thickness of the upper sheet for each weld sample produced in different welding time is measured from the microscope and averaged over the whole bonding line, and then the deformed material thickness is calculated as,

$$\text{post weld thickness (\%)} = \frac{t_{\text{indented}}}{t_{\text{original}}} \times 100 \quad (1)$$

where t_{indented} is the minimum distance from indented surface to weld interface and t_{original} is the original unwelded thickness, which is a constant value. Table 2.2(b) provides a schematic explanation of the post-weld thickness.

- *Weld nugget size*: the weld nugget size is measured using the cross-section length where the actual ultrasonic weld is formed. A schematic diagram of this weld nugget size is described in Table 2.2(c). This attribute is one of the most decisive factors that determine the failure types in the U-tensile test.
- *Thermo-mechanically affected zone*: the size of thermo-mechanically affected zone (TMAZ), as illustrated in Table 2.2(d), is the width of the entire area influenced by both plastic deformation and heat. Both weld nugget and TMAZ size are indirectly measured from the hardness profile where the mechanical property change in the weld zone was reflected. Detailed weld region classification will be discussed in the later section (2.4.3).

Table 2.2 Definitions of ultrasonic weld attributes and schematic diagrams of attribute measurement

Attribute	Definition	Schematic diagram
(a) Bond density	The proportion of projected bonded region to entire weld interface	
(b) Post-weld thickness	The average thickness of the top material after weld	
(c) Weld nugget size	The entire width of ultrasonically bonded area under horn	
(d) TMAZ size	The entire width of thermo-mechanically affected zone outside the weld nugget	

2.3.2 Characterization of ultrasonic welds using weld attributes

To understand the relationship between physical weld attributes and weld performances, multiple weld samples of different weld quality were cross-sectioned and characterized with optical microscopy, SEMs, and hardness measurements. The cross-section samples were selected from the weld samples produced in 50psi clamping pressure with increasing weld time (0.2s~1.0s) since they revealed various failure types within the entire range of weld time. Observations from the selected samples are shown in Figure 2.3. Gaps along the weld interface are clearly visible due to the lack of bonding (0.2s weld time). As weld time increases, these gaps become less distinct since materials are now in intimate contact. The imprints from the horn (Figure 2.4) and the anvil,

however, become intense for the 1.0s case, and the outer edges of top sheet are thinned due to excessive welding energy input. Detailed joint characteristics including the bond mechanism, material flow, and hardening and softening behaviors are discussed in this section. The formation process of each weld attribute as defined in Section 2.3.1 has a deep affinity with those joint characteristics. For example, the bond density is measured by identifying the bonded region, which is based on the bond mechanisms discussed in this section. The formation process of indentation in the weld zone is closely related to the material flow occurred on the metal surface. Lastly, the rationale behind the weld region classification such as WN or TMAZ grounds on the hardness change resulted from such phenomenon as work hardening and softening happened during the welding process.

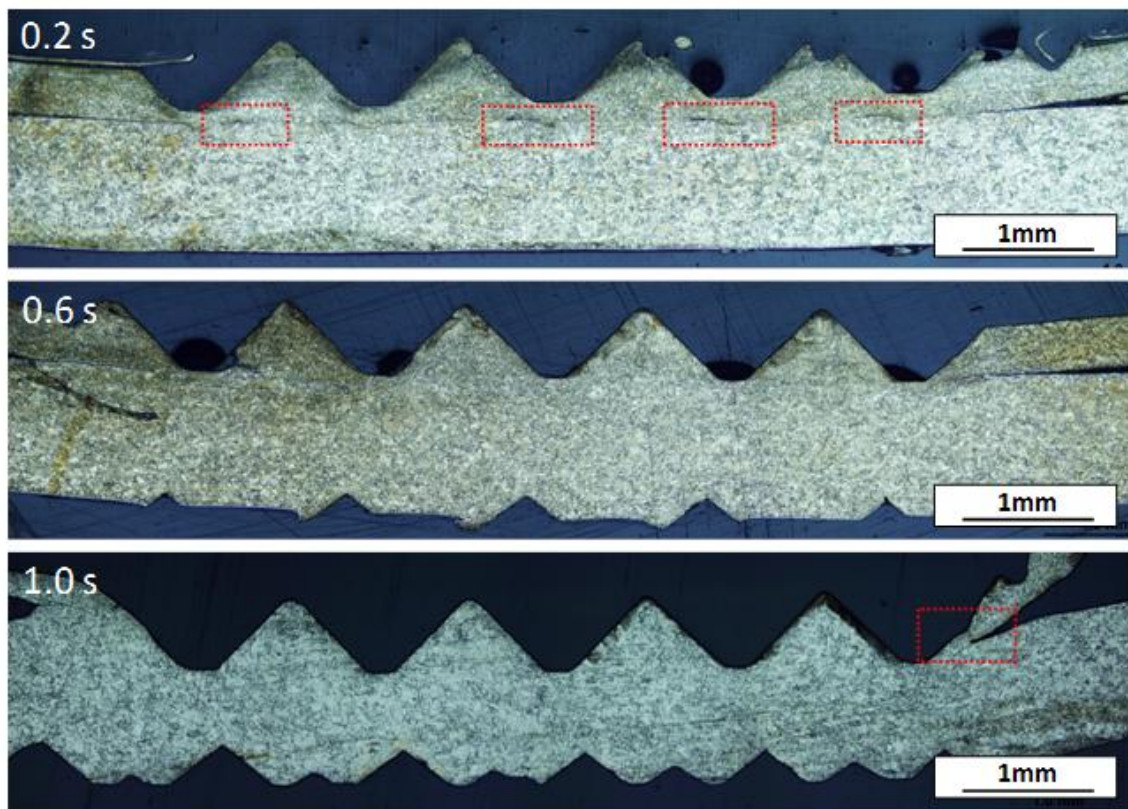


Figure 2.3 Optical images of Cu and Ni-plated Cu weld cross-sections produced with a pressure of 50psi, with increasing welding times (0.2s, 0.6s, and 1.0s)

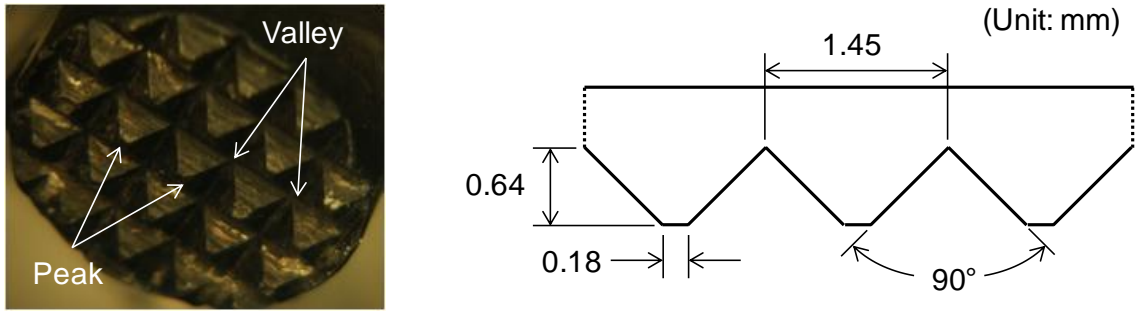


Figure 2.4 Knurl pattern of horn (left) and its dimension (right)

Bond mechanism

There are several theories of weld formation in ultrasonic metal welding, which include metallurgical adhesion derived from a significant amount of plastic deformation [Kong *et al.* 2003; Ram *et al.* 2007; Zhang and Li 2009], diffusion across the weld interface [Ji *et al.* 2005; Cheng and Li 2007; Li *et al.* 2008], local melting [Kreye 1977; Gunduz *et al.* 2005], and mechanical interlocking [Joshi 1971]. Among these theories, metallurgical adhesion and mechanical interlocking are observed in this cross-sectioning analysis. Diffusion bonding is excluded in this study because the diffusion between materials of the same kind, copper-to-copper in this study, is hardly observable in the microscopic analysis. The microstructures of the weld specimen produced in 0.4s of welding time are shown in Figure 2.5, which describes the formation process of bonding lines between two metal surfaces. Three different stages during the formation process are identified along the weld interface in the same cross-section sample: 1) micro-bond development, 2) curvy bonding line initiation, and 3) completion of interfacial wave formation. In Figure 2.5, the local micro-bonds are developed through the broken Ni layer, and by continuing shear oscillations around the micro-bonds, the bonding line forms into a twisted, rolled shape, so called “interfacial waves”. This compound

phenomenon agrees with the previous study [Bakavos and Prangnell 2010]. Hence, the bonding strength of ultrasonically welded joints is a result of a synergistic effect of 1) metallurgical adhesion (micro-bonds) and 2) mechanical interlocking (interfacial waves).

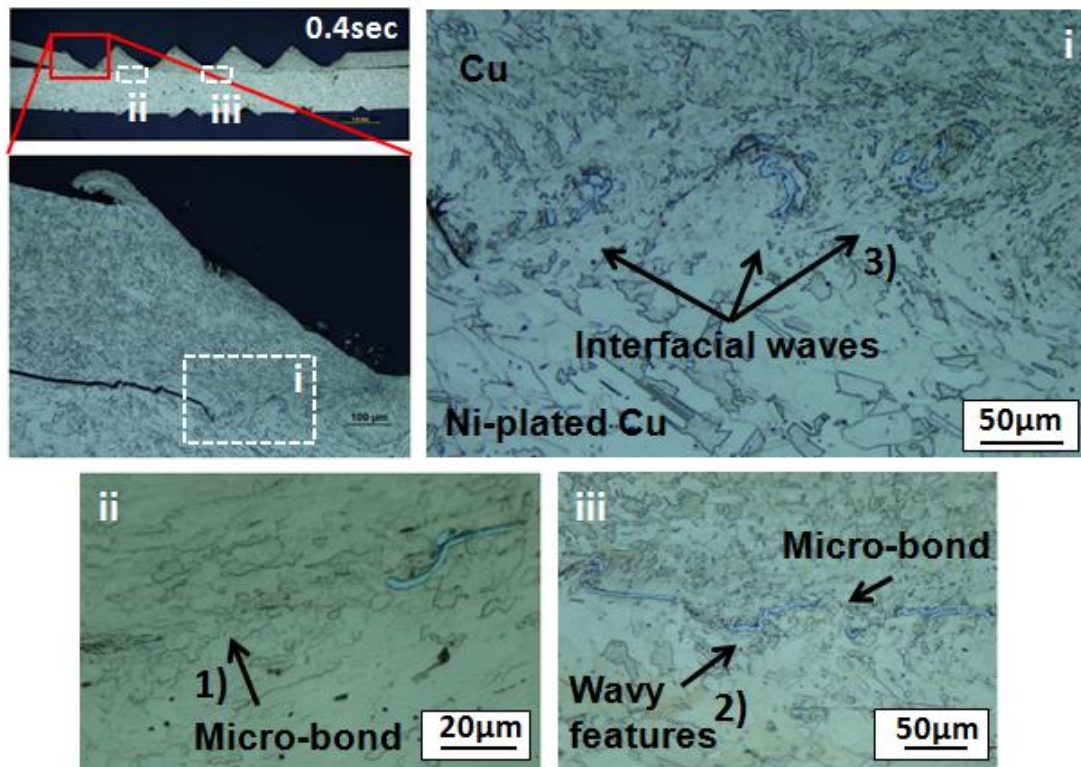


Figure 2.5 Optical images of the formation process of micro-bonds and interfacial waves along the bonding line

Figure 2.6 shows a special case of bonding line appearances when the weld time or the energy input exceeds its optimum range within which good weld quality is achieved. The cross-section image exhibits an extremely convoluted bonding line, which appears to be different from typical bonding lines with good weld quality. This macroscopic convolution of the bonding line is caused by the similar process of interfacial waves formation, but in a much greater scale. In other words, as the locally bonded regions (used to be concentrated on the peaks of the horn teeth) grow over the entire weld interface, the bonding line of the highly softened materials experiences a

significant amount of deformation by the combined forces in shear and normal directions. Therefore, the forming mechanism of these convoluted bonding lines is summarized as 1) an expansion of bonding line through the entire interface; 2) macroscopic deformation of the bonding line by continuous vibrations and clamping forces from the horn; 3) the completion of a very complex-shaped bonding line.

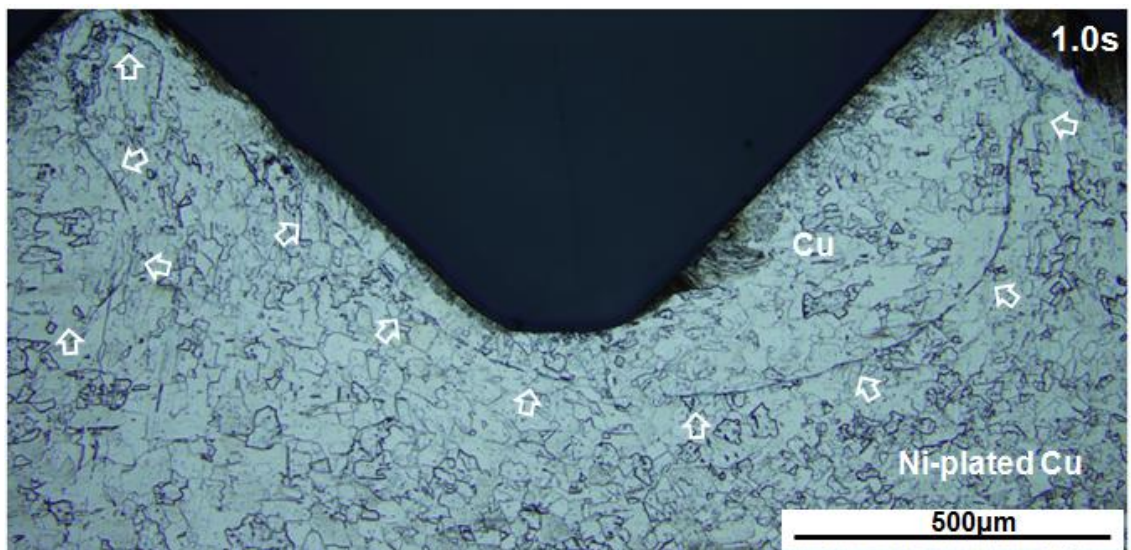


Figure 2.6 Convoluted bonding line in the weld samples produced in 1.0s weld time

Material flow

In an ultrasonic weld, there exist imprints by the knurl patterns of the horn and anvil, which was customized for the material type and thicknesses of the test coupons. By analyzing optical micrographs of the cross-sectioned weld samples, the deformation process of these imprints is as follows: 1) a shear force is exerted to the metal surface by friction as the horn starts to vibrate; 2) plastic deformation begins at the material surface around the peaks of the horn teeth and expands outwards from each teeth through a repetition of friction and sliding; 3) the indentation of the horn is intensified as the plastically deformed areas grow.

Figure 2.7(a) describes a layer of deformed material overflowing onto the edge of horn tip, while Figure 2.7(b) shows a captured image of the material flowing along the inclined surface. As such, the flows of material layers occur in local horn tooth areas throughout the entire knurl plane. It is seen that the regions close to the contact surface have elongated grains parallel to the slopes, and the regions where the materials actually flow have very fine grains due to high local strain (high magnification images of Figure 2.7(a-b)).

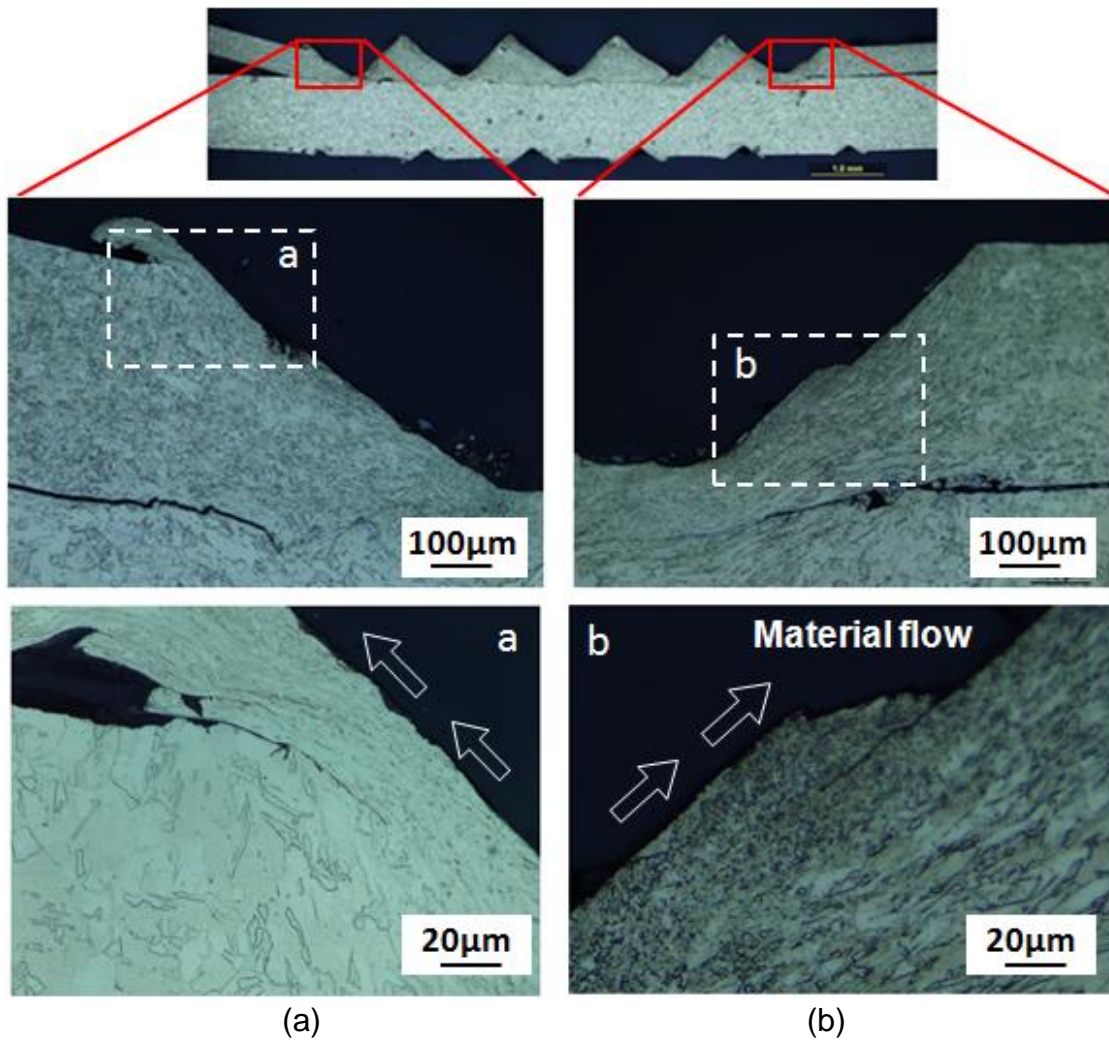


Figure 2.7 Optical images of Cu and Ni-plated Cu joints produced in 0.4s weld time: the layer of deformed material (a) overflowing onto the edge of horn edge (b) starting to flow along the inclined plane

As shown in Figure 2.8(a), the vertical position of the horn during the welding with 1.0sec process time and 50psi clamping pressure was obtained from a LVDT sensor equipped in the welder. The horn's position rapidly decreases at the beginning (0~0.2s), slows down in the middle (0.2~0.6s), and then decreases again after that (0.6~0.9s). This indentation rate is related to how the knurl imprint is formed during the welding process. The initial fast indentation is resulted from the fact that there exists enough space (i.e., horn valleys) for the deformed material layers to flow in. However, once this space is filled up, the material flow cannot extensively occur any longer, and the indentation slows down its rate. The filling process of the material is clearly shown in a series of optical images of the horn's valley area with increasing weld time (Figure 2.8(b)). Regaining the indentation rate after 0.6s is caused by intensified material softening due to an annealing effect, which will be further discussed.

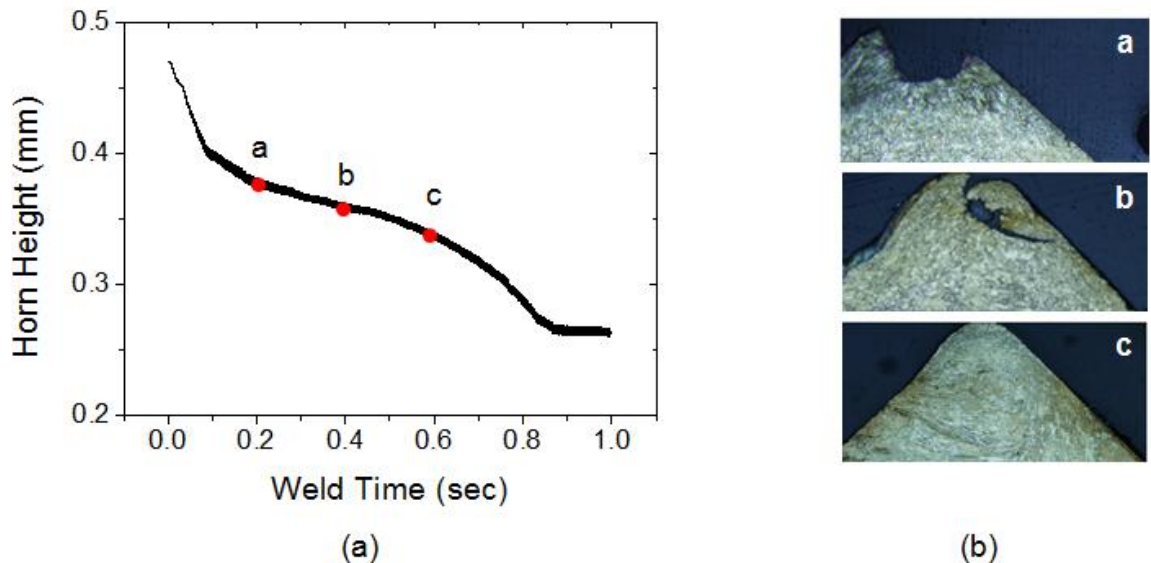


Figure 2.8 Material flow during the welding process: (a) a LVDT signal for 1.0sec process time; (b) optical images of valley areas of the horn knurl pattern for different welding time (a: 0.2s, b: 0.4s, c: 0.6s)

In conclusion, the process of material flow with extensive plastic deformation is one of the important characteristics in ultrasonic metal welding, because it improves gripping of the specimens so that more frictional work can be done at the weld interface. Nonetheless, an excessive material flow causes the material thinning, which negatively affects the weld quality.

Work hardening and softening

In this study, an extensive amount of microscopic analyses and microhardness measurements were performed to observe microstructural changes during the ultrasonic metal welding process. Figure 2.9 shows a series of optical cross-section images over time (0~1.0s), focused on the weld interface area. Figure 2.9(a) shows microstructures of the as-received materials for Cu and Ni-plated Cu. As ultrasonic excitation begins, the interface experiences the shear forces due to friction resulting in a significant amount of plastic deformation. Elongated grains along the bonding line are observed in the initial stage of the welding process (Figure 2.9(b-c)). As welding proceeds, the elongated grains disappear and new crystal structures are shown with uniform grain size and with similar lattice structure to the original undeformed grains (Figure 2.9(d)). This recrystallization process is due to the continuous ultrasonic power input into drastically deformed grains with elevated temperature. However, as welding continues beyond this point, the grain sizes in Figure 2.9(e-f) grow and the material softening is accelerated as a result of the continuous temperature rise. These microstructural changes are related to the mechanical performance of ultrasonically welded joints. The weld samples produced in short welding time (~0.4s), showing cold worked microstructures, failed at the interface during U-

tensile test. These “undeveloped” welds were classified as ‘under’ weld. The weld samples produced with 0.6s welding time were confirmed as ‘good’ weld in which recrystallization was identified. Finally, the samples produced with 0.8s or 1.0s welding time, showing their microstructures with enlarged grains, were assessed as ‘over’ weld quality.

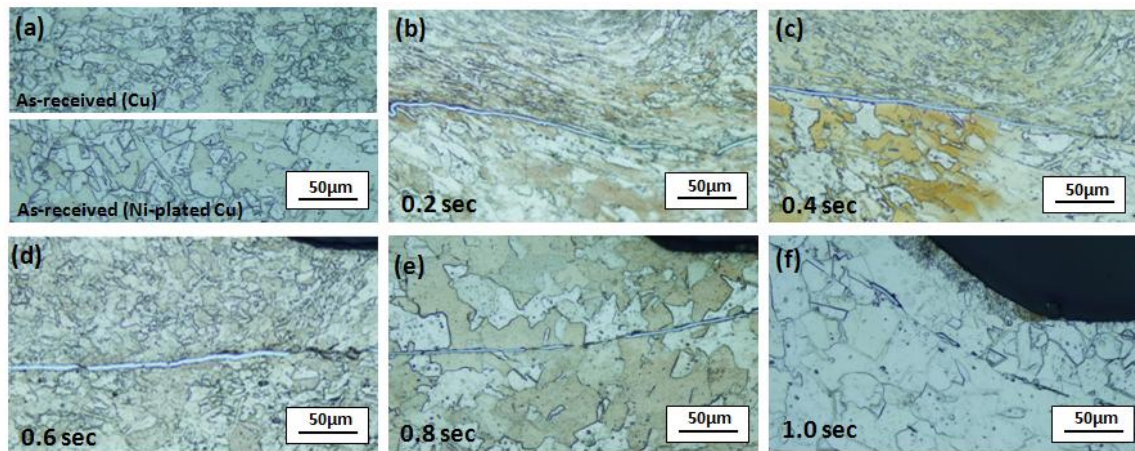


Figure 2.9 Optical images of Cu and Ni-plated Cu joints with increasing welding time: (a) as-received condition (b) 0.2s; (c) 0.4s; (d) 0.6s; (e) 0.8s; (f) 1.0s

Microhardness measurements were taken on the cross-sectional samples in order to verify the existences of hardening and softening during the weld process that were observed in the microstructures. The Vickers hardness profile measured at the peaks of the horn tip, where the highest strain rate is expected, is plotted against the welding time (Figure 2.10). The hardness of the initial welding stages shows almost over 40% increase from the as-received condition, which is caused by a large amount of cold working along the weld interface. Then, it is dramatically decreased as the welding time increases, and falls even below the original hardness. The results shown in the hardness profile together with the microscopic analysis in grain size demonstrate the plastic behaviors (i.e., work

hardening and softening) that any soft metals in the ultrasonic metal welding process can show.

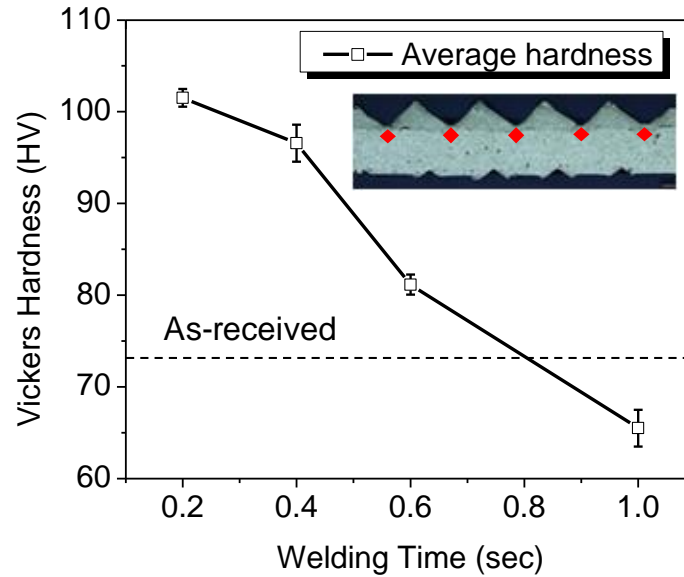


Figure 2.10 Hardness profile of weld samples for different welding time. The hardness is averaged over the peaks of the horn (dots in the cross-section image)

A) Hardness profile in horizontal locations:

Figure 2.11(a) shows the hardness variation along the bonding line, and the micrographs for 0.4s and 1.0s are represented in Figure 2.11(b). For short welding time (i.e., 0.2s or 0.4s), the hardness values of the regions below the peaks of the horn are higher than those below the valleys. This is because the plastic deformation begins at the centers of each peak and expands outwards as welding proceeds, so the valley areas of the weld interface are not as much work hardened as the peak areas are. However, as welding time increases, this local fluctuation in hardness value is diminished, and the overall hardness profile is lowered

simultaneously due to material softening. Micrographic evidences in Figure 2.11(b) substantiate the hardness result, by having more distorted grains in the peak area than the valley for shorter welding time (0.4s), and evenly grown grain size for higher welding time (1.0s).

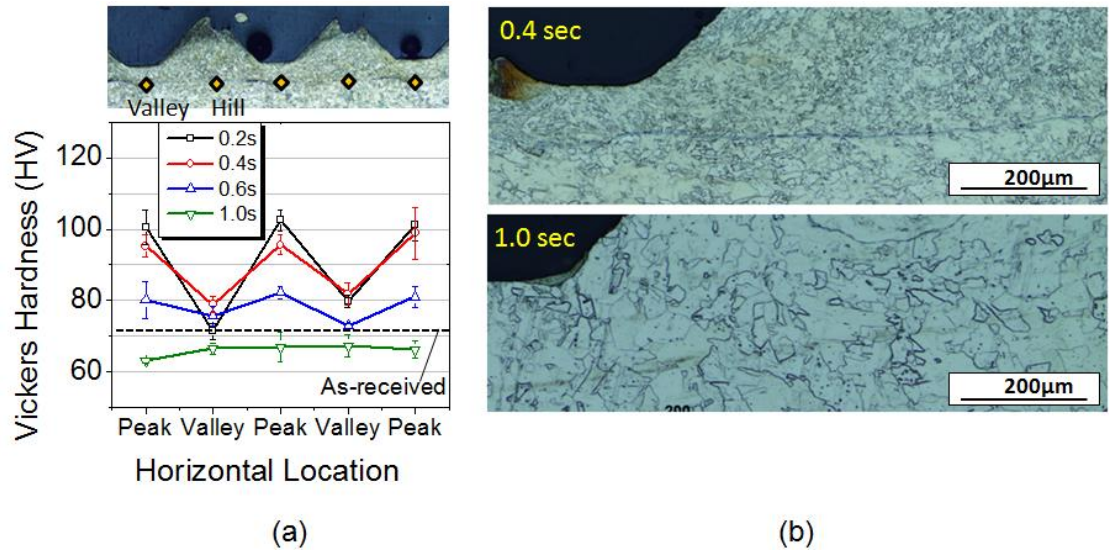


Figure 2.11 Hardness variation in horizontal locations: (a) horizontal hardness profile of the weld cross-sections; (b) Optical images for 0.4s and 1.0s weld time

B) Hardness profile in vertical locations:

In addition, the hardness profiles in the vertical direction were also measured in order to complete the entire two-dimensional hardness map of the weld cross-sections. The results shown in Figure 2.12(a) describe how the hardness changes over the vertical measurement locations below the valley area, and over the welding time. For shorter weld time (e.g., 0.2s), the hardness of the area close to the surface is much higher than that of the interface area, whereas this hardness difference with space is not so severe for longer weld time (e.g., 0.8 or 1.0s). This

is mainly because there is a tremendous amount of cold working at the surface of the valley area (i.e., material flow), as discussed in the previous section. As seen in the optical images in Figure 2.12(b), the grains of the weld specimen for 0.4s welding time are vertically elongated while the area close to interface does not seem affected by plastic deformation. In contrast, the microstructure of the weld specimen with 1.0s weld time does not show any differences in terms of grain size in vertical direction although the overall grain size is much increased than 0.4s.

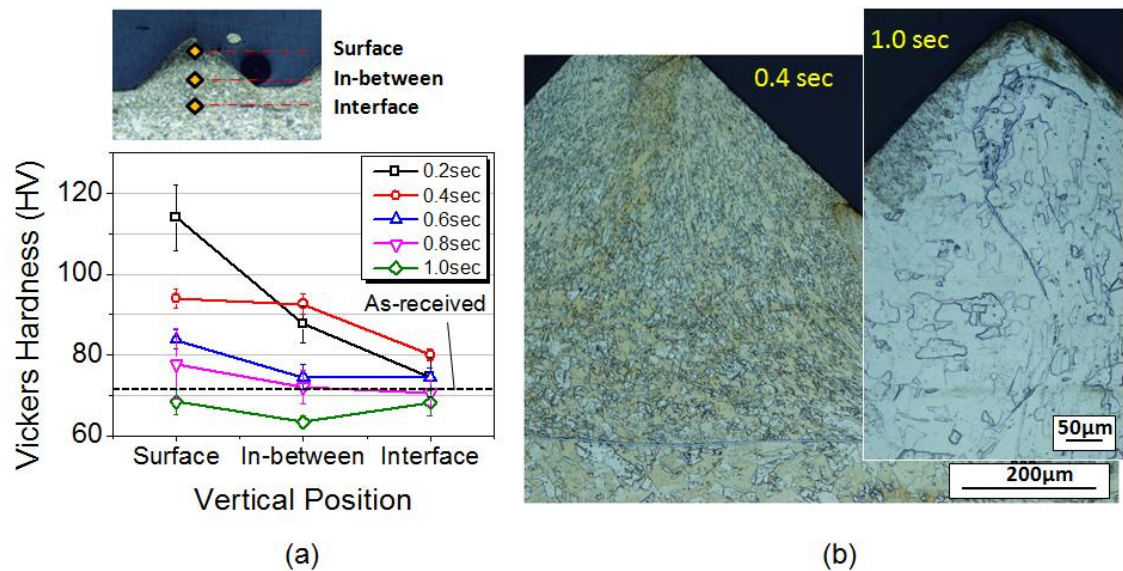


Figure 2.12 Hardness variation in vertical locations: (a) vertical hardness profile of the weld cross-sections; (b) Optical images at the valley area of the horn for 0.4s and 1.0s weld time

To summarize, the materials undergone high ultrasonic energy exhibit instant work hardening due to the cold working at the joint and then softening with the continuous temperature rise. This ultrasonic metal welding process resembles a cold work and subsequent annealing process (i.e., dynamic recrystallization), where the cold worked metals are recovered to the strain free stage through the recrystallization and grain growth with the application of heat.

2.4 CORRELATION BETWEEN WELD ATTRIBUTES AND QUALITY

In this section, weld quality is correlated to the joint characteristics (i.e., attributes). An ultrasonic metal weld with good weld quality should have dense interfacial bonds without having any severe symptoms of material thinning and surface cracks around the weld zone. Detailed discussions on each attribute including bond density, post-weld thickness, sizes of critical weld regions, and surface cracks are followed with microstructural analyses using optical images, SEMs, and microhardness measurements.

2.4.1 Bond density

Per previous discussion (Section 2.3.2), an ultrasonically welded joint of Cu and Ni-plated Cu is created along the interface by breakage of nickel layers followed by severe plastic deformation and metallurgical adhesion with partial aid of mechanical interlocking. Hence, the high density of bonded area through these mechanisms should be critical for higher weld performances.

There was an attempt to quantify the ultrasonic weld quality by directly measuring the percentage of contact points showing diffusion, so called 'linear weld density' [Kong *et al.* 2003; 2004]. This linear weld density is relatively easy to measure because the samples are produced by ultrasonic consolidation process where the bonding lines are almost straight. However, the quantification of bond density for ultrasonic spot welding applications is much difficult due to the complex shape of the bonding line (interfacial waves). Therefore, in this study, the relative bond density was qualitatively

estimated for different welding conditions through the microscopic examination of cross-sectioned weld samples.

In Figure 2.13, the microstructural images of the bonding line for different welding time, 0.2s (under), 0.6s (good), and 1.0s (over), are shown. Distinct gaps between the sheets, referred as unbonded regions, were found along the bonding line in the under weld specimens, whereas there were multiple regions of metallurgical bonds between clean copper surfaces, forming a unified grain structure, in good and even in over weld specimens. There were also very complicated appearances (i.e., mechanical interlocking) throughout the bonding line, which could give additional bonding strength to the joint. However, the densities of metallic bonds and interlocking in the over welds were much larger than those in the good welds, even though the U-tensile test showed the opposite result (i.e., higher weld performance in good welds). Therefore, the weld performance of ultrasonic metal welds is not a function of the bond density alone.

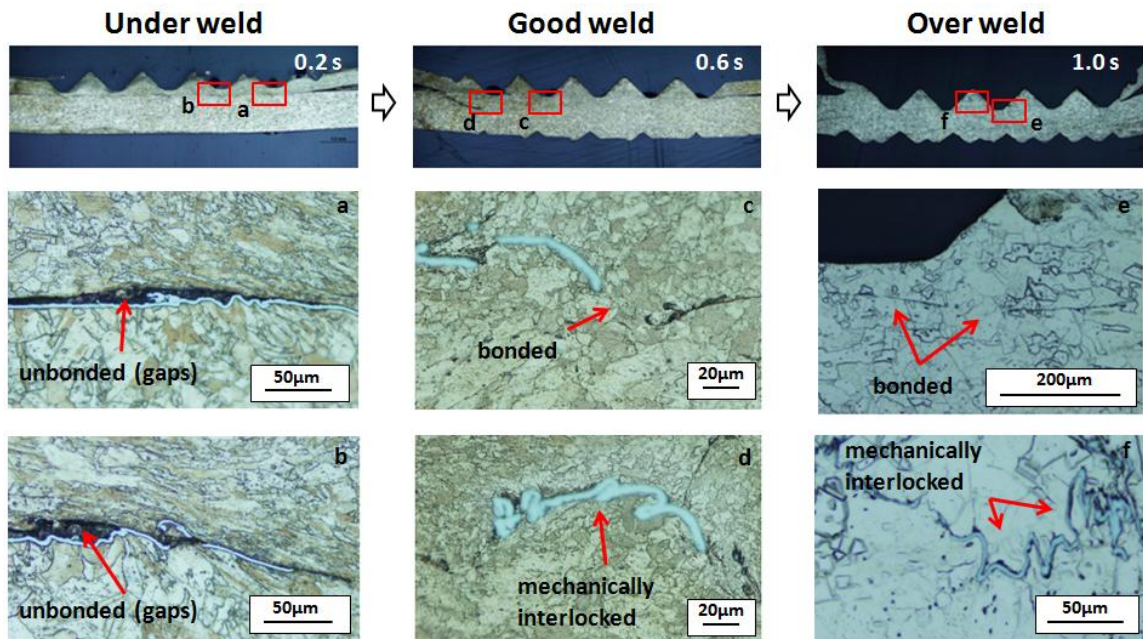


Figure 2.13 Optical images of ultrasonically welded joints made in different weld qualities (i.e., ‘under’, ‘good’, and ‘over’ weld)

2.4.2 Post-weld thickness

The post-weld thickness in the knurl imprints is another important attribute that can affect the weld performance of the ultrasonic metal weld. The percentile thickness of post-weld samples, as defined in Section 2.3.1, is plotted against the welding time in Figure 2.14.

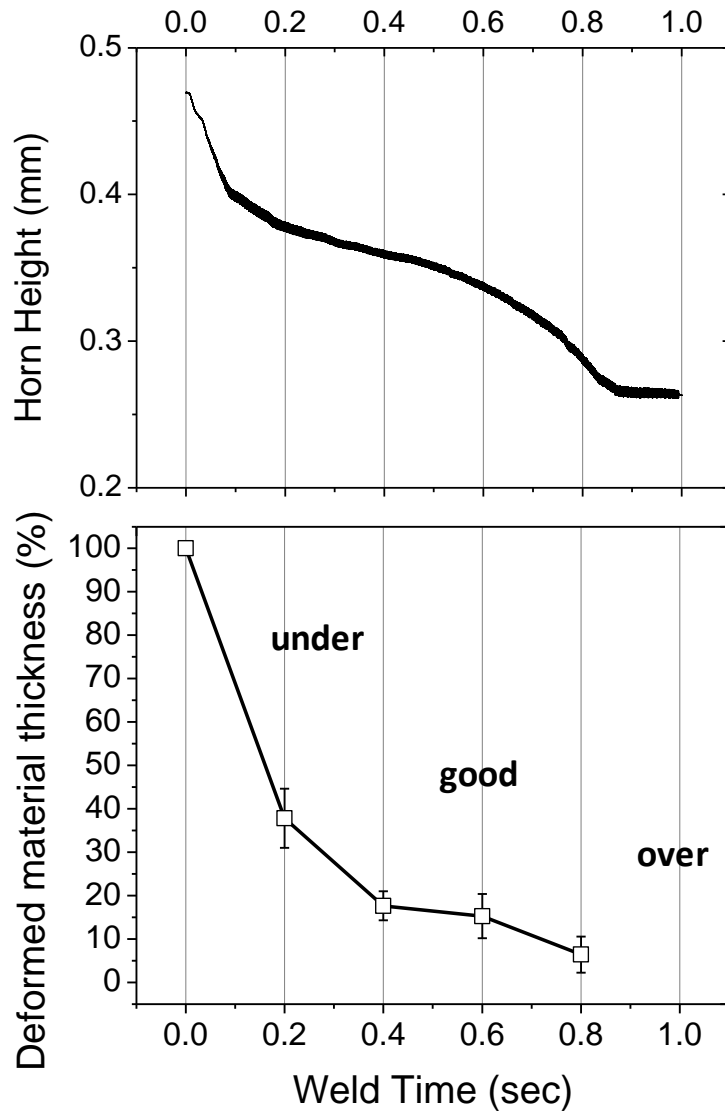


Figure 2.14 Horn height obtained from LVDT sensor (upper); percentile ratio of indentation measured from optical cross-section images (lower)

As welding time increases the upper workpiece is deformed more and more until its thickness becomes less than 10% of the original thickness. It is also noted that a similar trend of indentation is observed from both the LVDT signal and the measured thickness in optical cross-section images. More than 60% of the original thickness is deformed by the indentation during the first 0.2 second, and then the deformation rate slows down as welding proceeds. This fast indentation rate in the initial stage of the welding process is mainly because there is a plenty of room for the material to flow in between each valley area of the horn tip. As referred to the weld performance, under weld quality is resulted during the initial fast deformation stage, and gradually changed into good quality of weld with high tensile strength as the deformation rate becomes stable. The indented thickness for the over weld case (1.0s) was not able to measure because of the vague bonding line due to the complete breakage of the nickel layer and the blending into copper.

2.4.3 Thermo-mechanically affected zone (TMAZ) and weld nugget

The microstructures and mechanical properties of metal weldment are difficult to measure due to locality sensitivity [Zhou *et al.* 1999]. In addition, the preparation of microscopic mechanical testing specimens for ultrasonic metal welds is not easy. Therefore, the material properties of the welds such as yield strength can be obtained by empirical relationships between material strength and hardness [Zhou *et al.* 1999]. As a linear relationship (i.e., $Hardness = c\sigma_y$) [Cáceres *et al.* 2005], the relative change in yield strength can be estimated by the relative change of hardness, which can be expressed as

$$\frac{\sigma_y}{\sigma_{y,as-received}} = \frac{HV_{measured}}{HV_{as-received}} \quad (2)$$

where σ_y is the yield strength and HV is the hardness value. From this relationship and the hardness profiles of the weld specimens, the plastic behavior of the material for each different zone can be indirectly estimated.

Hardness distribution:

Hardness profiles over the entire weld region for different weld times (0.2, 0.6, and 1.0s) were collected and presented in Figure 2.15. Figure 2.15(b) shows the hardness variation along the weld interface (inside the weld zone), and the hardness profile along the center line of the top material (outside the weld zone) is in Figure 2.15(c). The test locations selected for those hardness measurements are shown in the schematic drawing of weld cross-sections (Figure 2.15(a)). To compare the hardness profiles at two different scales, it should be noted that the interval of each peak and valley in Figure 2.15(b) is 1.45mm for the selected design of the horn tip, and the hardness for Figure 2.15(c) was measured in every 0.1mm.

The hardness profile on the weld interface for under weld case in Figure 2.15(b) shows a large variation from peak to valley, whereas the hardness profile gradually levels off as shifted to good and over weld case. In addition, an overall degradation in absolute hardness value over time is shown at the same time. These simultaneous variations in hardness profile, in terms not only of the regional difference within the bonding line but of the weld process time, are resulted from the work hardening due to severe plastic

deformation and the softening from intense ultrasonic energy input, as discussed in the prior section (2.3.2).

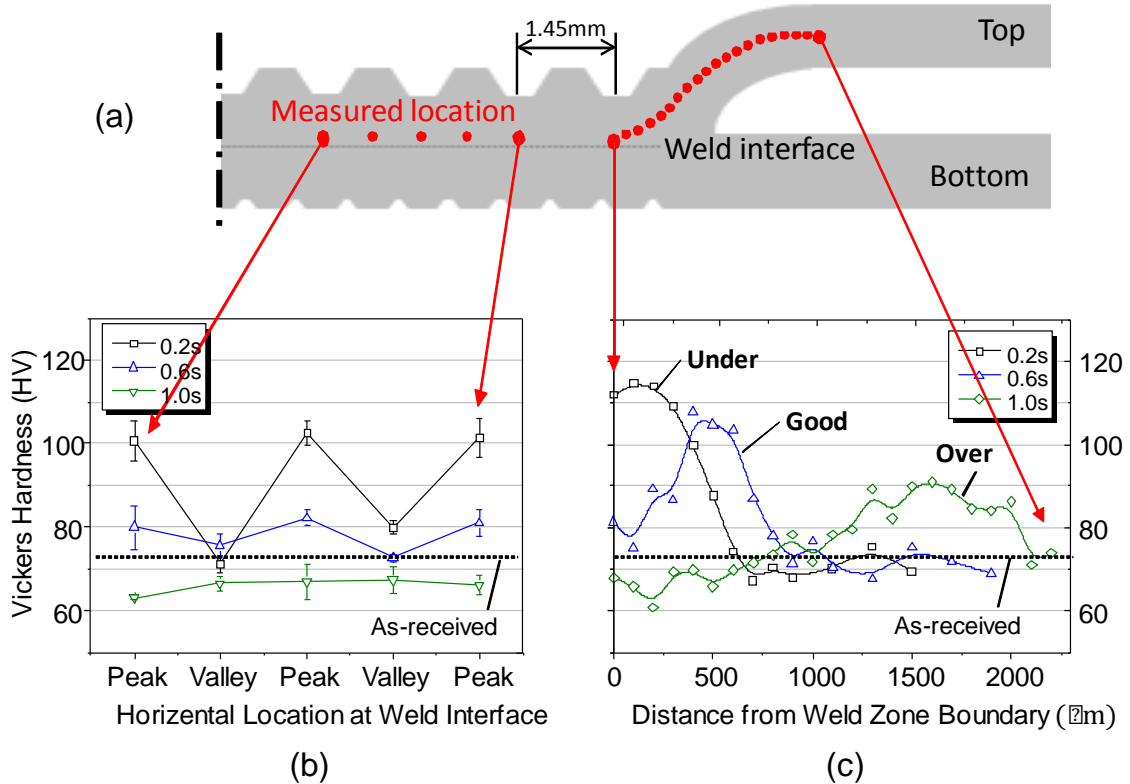


Figure 2.15 Hardness distribution of the weld samples for different weld time: (a) a schematic diagram of ultrasonically welded joint; (b) hardness profile of the weld interface; (c) hardness profile outside of weld zone

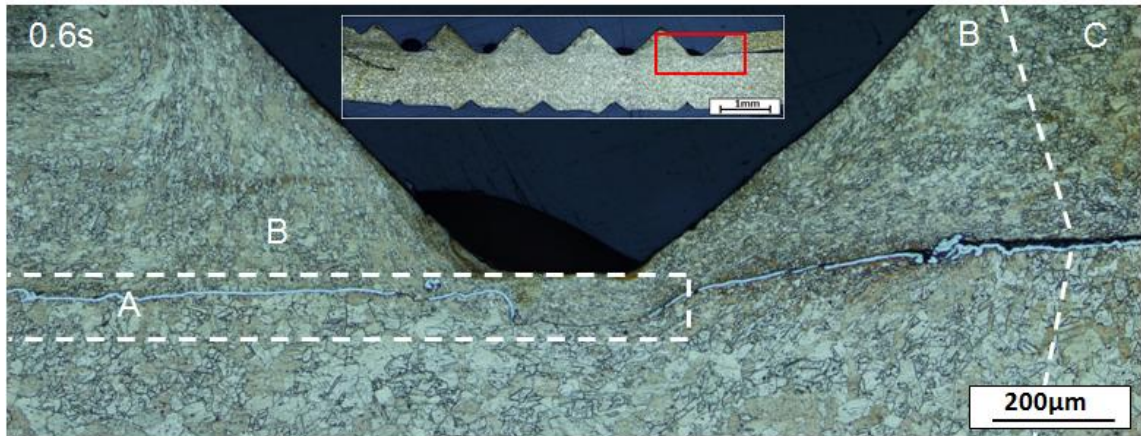
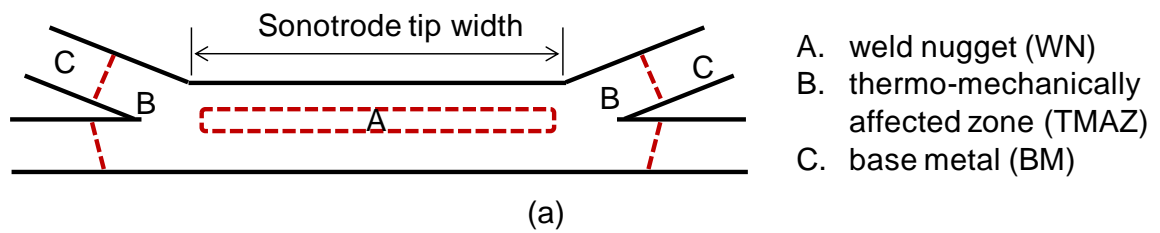
The hardness profile on the weld interface for under weld case in Figure 2.15(b) shows a large variation from peak to valley, whereas the hardness profile gradually levels off as shifted to good and over weld case. In addition, an overall degradation in absolute hardness value over time is shown at the same time. These simultaneous variations in hardness profile, in terms not only of the regional difference within the bonding line but of the weld process time, are resulted from the work hardening due to severe plastic

deformation and the softening from intense ultrasonic energy input, as discussed in the prior section (2.3.2).

Figure 2.15(c) shows a result on the hardness variation of the region outside the weld zone. It can be seen as an extension of the horizontal hardness profile at the weld interface of Figure 2.15(b). Each weld sample produced in different welding time experiences a different pattern of work hardening and softening. For shorter weld time (0.2s) the increased hardness can be read at the region very close to the boundary of weld zone, and then lowers its value back to the original hardness of as-received materials. However, as welding time becomes longer, the region where the highest hardness value is found to move outwards away from the boundary. In an 'over' weld, high hardness value outside the weld region exists because of the work hardening in the metal sheets due to the plastic deformation. At the same time, the absolute value of the peak hardness is slowly decreasing, but still higher than any of hardness inside the weld zone. The hardness increase in this area is resulted from the cold working due to the cyclic stresses exerted both horizontally (ultrasonic vibration) and vertically (clamping force). However, the hardness decreases at the boundary due to the softening with the temperature rise. The hardness in this region for over weld case falls even below the original hardness value because the material experiences higher stress right under the horn tip. Therefore, the regions outside the weld zone are also thermally and mechanically affected by the ultrasonically oscillating tools.

Weld region classification:

Various zones in an ultrasonic metal weld were distinguished by their mechanical properties and micrographs. As depicted in a schematic diagram of an ultrasonically welded joint (Figure 2.16(a)), the weld is divided into three primary regions. Area 'A' is called 'weld nugget (WN)' where an actual interfacial bonding between the metals occurs. It is found that an extensive amount of plastic deformation due to friction between surfaces creates a metal-to-metal bonding, and recrystallized grain structures due to increased temperature are also observed in this area. Area 'B' is affected by both heat and plastic deformation and named as the 'thermo-mechanically affected zone (TMAZ)'. This terminology, normally used in other solid state welding process especially in friction stir welding (FSW) [Prangnell and Heason 2005; Geuser *et al.* 2010; Steuwer *et al.* 2011], is selected here because the basic material behaviors under the influence of the welding tools (e.g., a horn tip or an anvil) are similar in ultrasonic metal welding, although the intensity of deformation in FSW is much higher due to the direct stirring motion of the tool. From the hardness distribution previously shown in Figure 2.15, evidence of thermo-mechanical effects is found in this area, and the degree of affection in the area is also identified. The microstructure of the TMAZ on the upper sheet of workpiece as in Figure 2.16(b) shows an elongated grain structure parallel to the vibration direction. Area 'C' is base metal (BM) which is affected neither by heat nor by deformation in terms of microstructure or mechanical properties (e.g., hardness).



(b)

Figure 2.16 Weld region classification: (a) a schematic diagram of weld region classification; (b) optical micrograph of an ultrasonic weld produced in 0.6s welding time, giving an overview of classified weld regions

Figure 2.17 shows an optical image of the microstructure of the weld cross-section, which was ultrasonically welded for 1.0s (over weld case). The same weld region classification can be applied to this figure: WN, TMAZ and BM. However, the micrograph is slightly different from that of Figure 2.16(b) which is a typical microstructure of the good weld case. The area of the TMAZ of over weld case has been much enlarged than that of good weld case, and so has the WN.

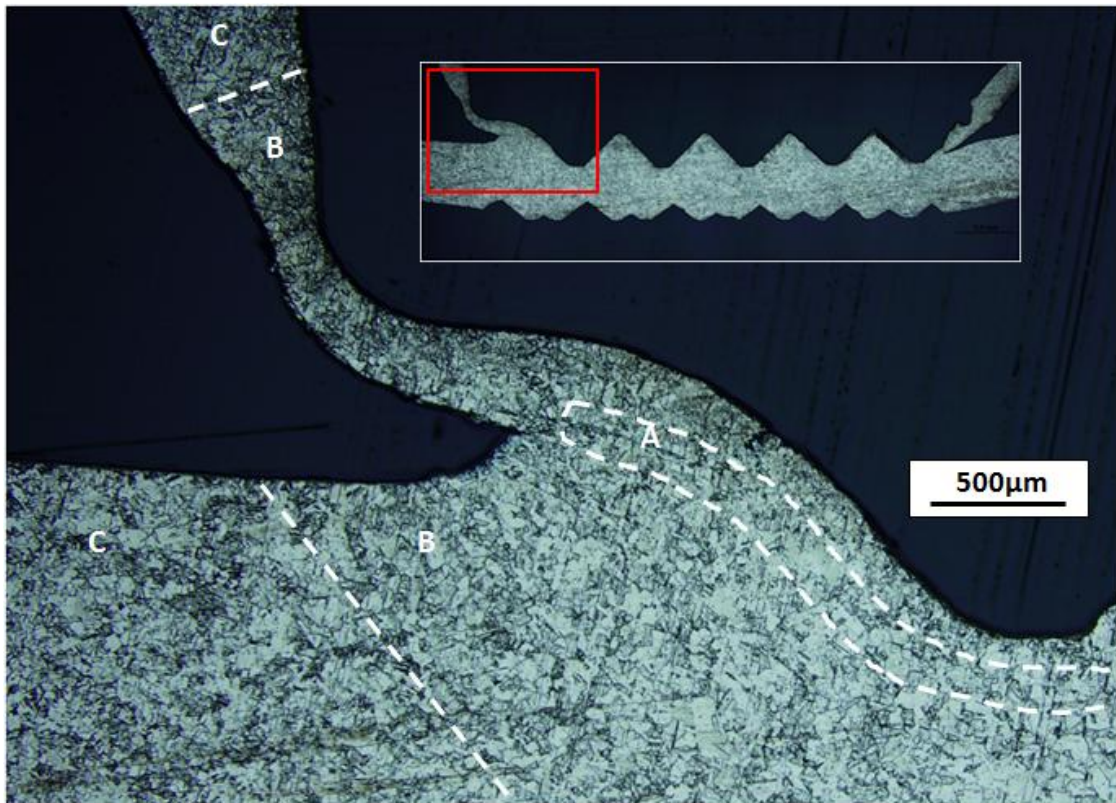


Figure 2.17 Optical micrograph of an ultrasonic weld produced in 1.0s welding time with classified weld regions

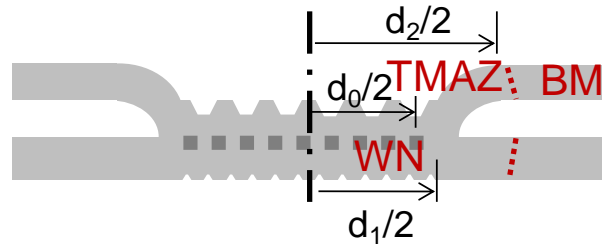
Relationship between size of TMAZ or WN and weld performance:

High performance of an ultrasonic weld tends to be associated with the failure type when performing destructive tests for their joint strengths [Bakavos and Prangnell 2010]. The previous U-tensile test showed a good quality weld failed near the outermost horn teeth while a under or an over quality weld experienced different failure types. The failure type variation can be related to the changes in microstructure and mechanical properties with space and time, so the location for stress concentration will vary with the different weld quality. Therefore, a relationship between weld performance and the size

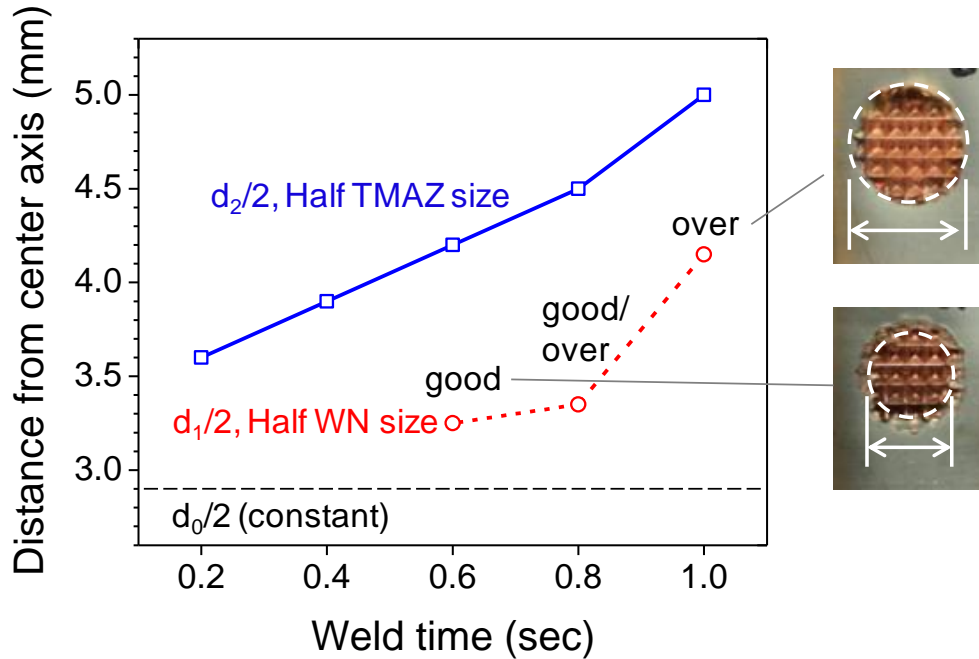
variation of each classified weld region (i.e., WN, TMAZ, and BM) within the weldment can be qualitatively established.

The boundaries between each zone (e.g., WN/TMAZ or TMAZ/BM) are determined by the areas where the hardness profile changes its value in a relative gradient as shown in Figure 2.15(c). For example, the hardness for the weld specimen of 0.6s weld time shows a sudden increase at the location slightly off the outermost teeth ($\sim 350\mu\text{m}$). The hardness passes its peak point and then decreases back to the hardness of as-received condition at the location away from the horn ($\sim 1300\mu\text{m}$). The first transition zone is regarded as the boundary of the WN, and the latter one as the boundary between the TMAZ and the BM.

Figure 2.18(b) shows the approximate half sizes of these zones, which is schematically indicated in Figure 2.18(a), measured from the hardness profile plotted against the welding time. It should be noted that the half WN size for 0.2s and 0.4s was not applicable since the weld specimens in this condition showed interfacial separation during the performance testing. This is because the WN zone has not been grown well. As shown in Figure 2.18(b), the half TMAZ size increased proportionally to the weld process time and the half WN size also grew with time. Of these two, the half WN size is more related to the stress concentration area which plays a role in the failure type of the weld specimen during the performance test. The failure type of circumferential fracture may be resulted from the crack initiation along the boundary of WN. The photo images of the failed parts showing their weldments adhered to the bottom sheets have a good agreement with the measured sizes of half WNs.



(a)



(b)

Figure 2.18 Classified weld regions associated with failure types: (a) a schematic diagram indicating dimension of each weld region (TMAZ and WN); (b) half TMAZ size and half WN size over weld time, with failed weldment images after U-tensile test

2.4.4 Surface cracks

As discussed in the previous section, a good quality weld was not always achieved as the WN size grew. Instead, the excessive welding time or energy input caused extra thinning around the TMAZ area, and eventually led to lower weld strength

during the performance testing. In addition to material thinning, various sizes of cracks can be generated on the surface of the material, especially on the outer TMAZ area, due to the high strain rate caused by an intense forming action from the horn. These surface cracks are referred as one of the defects that an ultrasonic metal weld with excessive condition may have.

Figure 2.19 shows a series of SEM images of an ultrasonic weld produced in an over weld condition (1.0s weld time), focusing on the outer TMAZ area. The images were collected right after weld completion with the weld samples being cut in half by a diamond wheel saw and placed in the sample chamber of a FEG-SEM. The fatigue damages shown in the figure were found on the stretched metal surface, which had been in direct contact with the horn. Figure 2.19(a) is a macroscopic view of the weld spot (cut in half) where various surface characteristics exist. It should be noted that the vibration is of out-and-in-of-plane direction and the clamping direction is downward. An ‘island’ feature shown in Figure 2.19(b) is formed from severely twisted interfacial waves, which is exposed to the surface due to an extensive amount of thinning in the upper sheet. Figure 2.19(c) shows direct evidence of fatigue failure undergone high frequency of cyclic loading, having evenly spaced, clear fatigue striation marks all over the deformed surface. Figure 2.19(d) is another macroscopic view of the weld as a continuous image from Figure 2.19(a). Visible cracks from large size (50~100 μm) to micro-size (less than 5 μm) are seen in Figure 2.19(e-f). These surface defects may be the reason for leading to fractures during the tensile test due to the stress concentration, and sometimes to perforations within the given weld time.

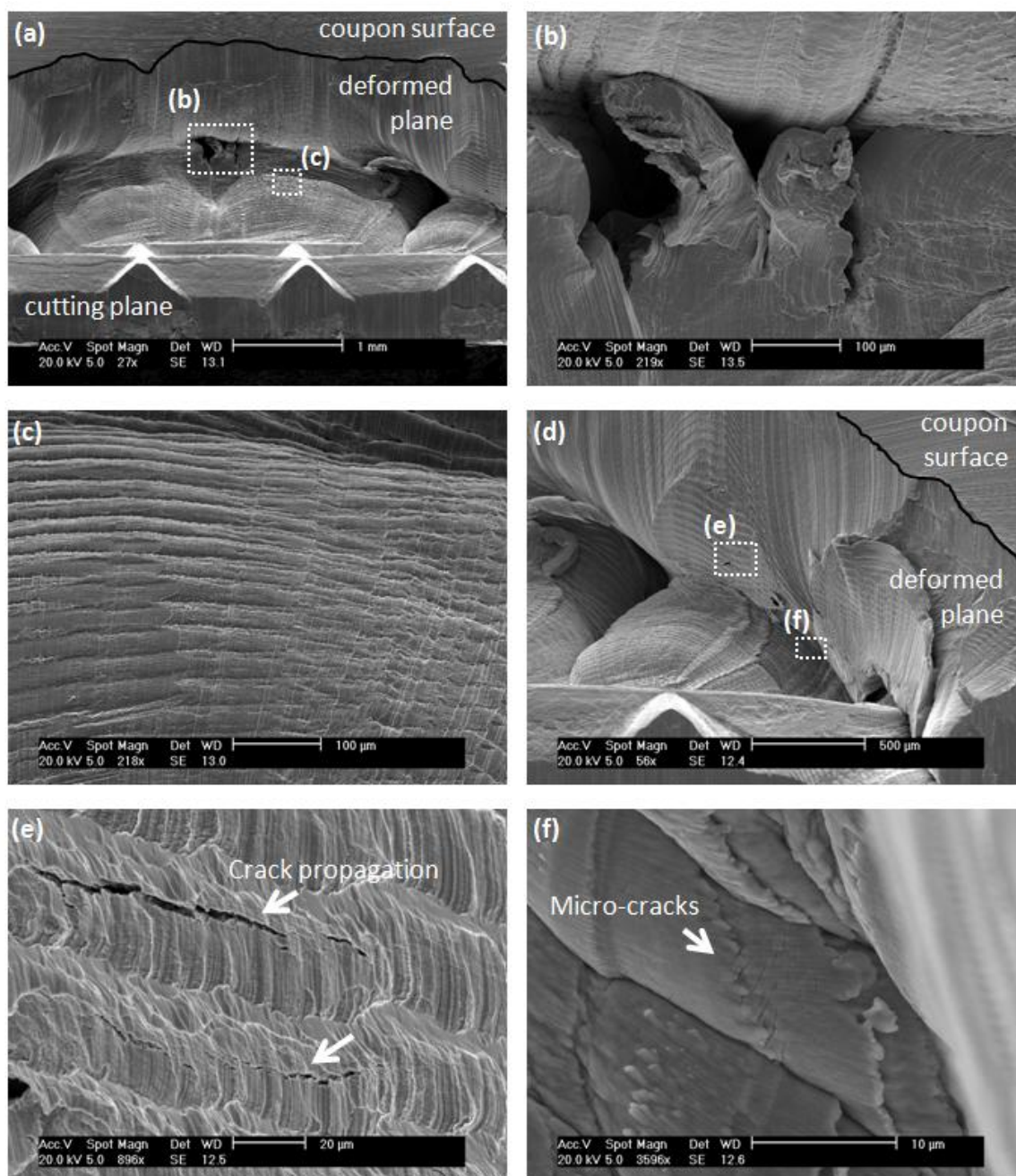


Figure 2.19 SEM images of deformed surfaces around the weld zone from the ‘over’ weld: (a) a front view image (vibration direction: out-and-in-plane); (b) ‘island’ features; (c) fatigue striation marks; (d) another front view image of the right hand side of image-(a); (e) crack propagations; (f) micro-cracks

2.4.5 Summary of correlation between weld attributes and quality

The relationship between the weld performance and two attributes (i.e., bond density and post-weld thickness) is summarized in Figure 2.20, plotted against weld time. The bond density is increasing over weld time due to an expansion of the micro-bonds at the weld interface, and the post-weld thickness is decreasing due to material thinning. The highest joint strength is shown in the middle at a weld time of about 0.6 sec. This shows that a good quality weld in ultrasonic welding is achieved when the interfacial bond reaches a level of enough metallurgical adhesion and mechanical interlocking, but the material thinning has not progressed to the extent to severely reduce the mechanical strength.

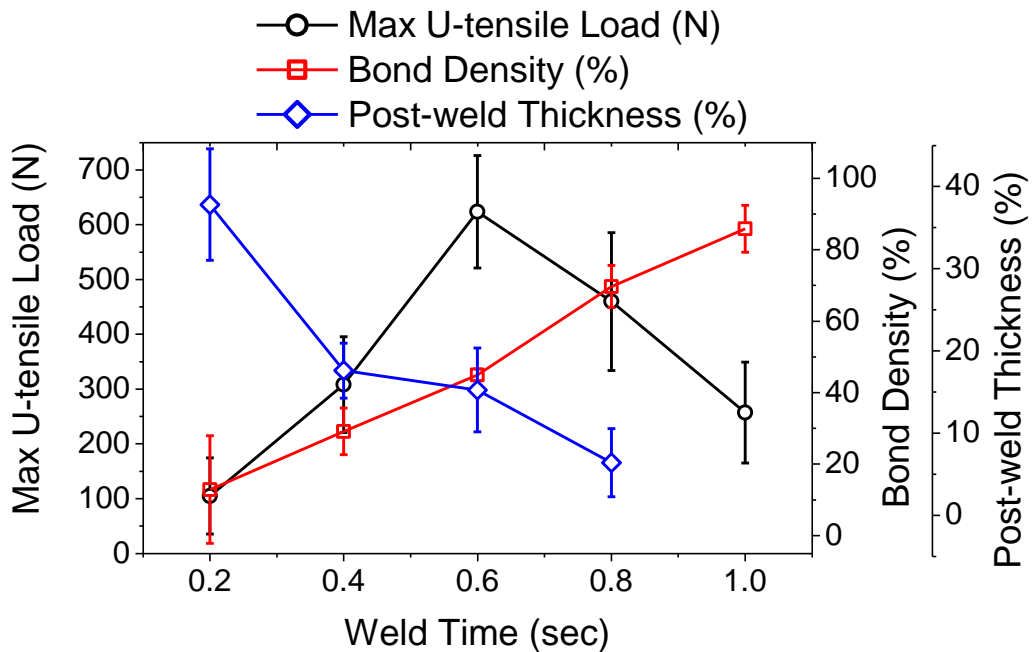


Figure 2.20 Correlation of weld performance with bond density and post-weld thickness

2.5 CONCLUSIONS

A set of measurable weld attributes have been proposed to characterize ultrasonically welded joints of copper and nickel plated copper. The joint characteristics of different quality welds were investigated using those attributes and the relationship between attributes and performance was quantitatively identified.

The main conclusions of this chapter are as follows:

- 1) The bonding strength of ultrasonically welded joints for copper and nickel-plated copper is due to the combined effect of metallurgical adhesion (micro-bonds) and mechanical interlocking.
- 2) Different levels of weld quality (i.e., under, good, or over weld) are correlated to the combination effect of the bonded area density and the post-weld thickness, which show opposite tendencies.
- 3) Material flow with extensive plastic deformation occurs at the metal surface in contact with each horn tooth, and causes material thinning or indentation. Indentation of the metal surface intensifies as welding proceeds, and its rate also differs in different quality regions: fast indentation rate in under weld samples, slowing down in good weld and regaining the indentation rate in over weld.
- 4) Material that has received high ultrasonic energy input show instant work hardening due to the cold working and then softening with continuous

temperature increase, which resembles an annealing process (i.e., recovery, recrystallization, and grain growth).

- 5) Various zones in an ultrasonic metal weld are distinguished by their mechanical properties and micrographs: Weld Nugget (WN), Thermo-Mechanically Affected Zone (TMAZ), and Base Material (BM). The sizes of TMAZ and WN affect the failure type during performance testing and, eventually, weld quality.

A set of well-defined weld attributes help to link welding process variables with weld quality based on an understanding of the characteristics of the weldment. The scientific understanding obtained from this chapter can guide manufacturers in establishing robust process parameter regions to achieve consistent quality. The methodology on identifying these weld attributes will be extended to multi-layer welding in our future work.

ACKNOWLEDGEMENT

The work presented here is sponsored by the General Motors Collaborative Research Lab in Advanced Vehicle Manufacturing at the University of Michigan. The authors appreciate the support provided by Dr. Kai Sun at the University of Michigan Electron Microbeam Analysis Laboratory (EMAL).

REFERENCES

- Bakavos, D. and Prangnell, P. B. (2010). "Mechanisms of Joint and Microstructure Formation in High Power Ultrasonic Spot Welding 6111 Aluminium Automotive Sheet." *Materials Science and Engineering: A* 527(23): 6320-6334.
- Cáceres, C. H., Griffiths, J. R., Pakdel, A. R. and Davidson, C. J. (2005). "Microhardness Mapping and the Hardness-Yield Strength Relationship in High-Pressure Diecast Magnesium Alloy Az91." *Materials Science and Engineering: A* 402(1-2): 258-268.
- Cheng, X. and Li, X. (2007). "Investigation of Heat Generation in Ultrasonic Metal Welding Using Micro Sensor Arrays." *Journal of Micromechanics and Microengineering* 17: 273.
- Geuser, F. D., Bley, F., Denquin, A. and Deschamps, A. (2010). Mapping the Microstructure of a Friction-Stir Welded (Fsw) Al-Li-Cu Alloy. *Journal of Physics*, IOP Publishing.
- Gunduz, I. E., Ando, T., Shattuck, E., Wong, P. Y. and Doumanidis, C. C. (2005). "Enhanced Diffusion and Phase Transformations During Ultrasonic Welding of Zinc and Aluminum." *Scripta materialia* 52(9): 939-943.
- Hetrick, E., Baer, J., Zhu, W., Reatherford, L., Grima, A., Scholl, D., Wilkosz, D., Fatima, S. and Ward, S. (2009). "Ultrasonic Metal Welding Process Robustness in Aluminum Automotive Body Construction Applications." *Welding Journal* 88(7).
- Hu, S. J., Senkara, J. and Zhang, H. (1996). "Performance Characteristics of Resistance Spot Welds in the Automotive Industry: A Structural Point of View." *Proceedings of IBEC' 96 Body & Engineering*: 91-98.
- Ji, H., Li, M., Kung, A. T., Wang, C. and Li, D. (2005). The Diffusion of Ni into Al Wire at the Interface of Ultrasonic Wire Bond During High Temperature Storage. *Electronic Packaging Technology*, 2005 6th International Conference on.
- Joshi, K. C. (1971). "The Formation of Ultrasonic Bonds between Metals." *Welding Journal* 50(12): 840-848.
- Kim, T. H., Yum, J., Hu, S. J., Spicer, J. P. and Abell, J. A. (2011). "Process Robustness of Single Lap Ultrasonic Welding of Thin, Dissimilar Materials." *CIRP Annals - Manufacturing Technology* 60(1): 17-20.

- Kong, C., Soar, R. and Dickens, P. (2003). "Characterisation of Aluminium Alloy 6061 for the Ultrasonic Consolidation Process." *Materials Science and Engineering A* 363(1-2): 99-106.
- Kong, C., Soar, R. and Dickens, P. (2004). "Optimum Process Parameters for Ultrasonic Consolidation of 3003 Aluminium." *Journal of Materials Processing Technology* 146(2): 181-187.
- Kreye, H. (1977). "Melting Phenomena in Solid State Welding Processes." *Welding Journal* 56(5): 154-158.
- Lee, S. S., Kim, T. H., Hu, S. J., Cai, W. and Abell, J. A. (2010). "Joining Technologies for Automotive Lithium-Ion Battery Manufacturing: A Review." *ASME Conference Proceedings* 2010(49460): 541-549.
- Li, J., Han, L. and Zhong, J. (2008). "Short Circuit Diffusion of Ultrasonic Bonding Interfaces in Microelectronic Packaging." *Surface and Interface Analysis* 40(5): 953-957.
- Prangnell, P. B. and Heason, C. P. (2005). "Grain Structure Formation During Friction Stir Welding Observed by the 'Stop Action Technique'." *Acta Materialia* 53(11): 3179-3192.
- Ram, G. D. J., Robinson, C., Yang, Y. and Stucker, B. (2007). "Use of Ultrasonic Consolidation for Fabrication of Multi-Material Structures." *Rapid Prototyping Journal* 13(4): 226-235.
- Steuwer, A., Dumont, M., Altenkirch, J., Biroasca, S., Deschamps, A., Prangnell, P. and Withers, P. (2011). "A Combined Approach to Microstructure Mapping of an Al-Li Aa2199 Friction Stir Weld." *Acta Materialia*.
- Yang, Y., Ram, G. D. J. and Stucker, B. E. (2010). "An Analytical Energy Model for Metal Foil Deposition in Ultrasonic Consolidation." *Rapid Prototyping Journal* 16(1): 20-28.
- Zhang, C. and Li, L. (2009). "A Coupled Thermal-Mechanical Analysis of Ultrasonic Bonding Mechanism." *Metallurgical and Materials Transactions B* 40(2): 196-207.
- Zhou, B., Thouless, M. and Ward, S. (2006). "Predicting the Failure of Ultrasonic Spot Welds by Pull-out from Sheet Metal." *International journal of solids and structures* 43(25-26): 7482-7500.

Zhou, B., Thouless, M. D. and Ward, S. (2005). "Determining Mode-I Cohesive Parameters for Nugget Fracture in Ultrasonic Spot Welds." *International Journal of Fracture* 136(1): 309-326.

Zhou, M., Hu, S. J. and Zhang, H. (1999). "Critical Specimen Sizes for Tensile-Shear Testing of Steel Sheets." *Welding Journal (Miami, Fla)* 78(9).

Zhou, M., Zhang, H. and Hu, S. J. (2003). "Relationships between Quality and Attributes of Spot Welds." *Welding Journal (Miami, Fla)* 82(Compendex): 72S-77S.

CHAPTER 3

CHARACTERIZATION OF ULTRASONIC METAL WELDING BY CORRELATING ONLINE SENSOR SIGNALS WITH WELD ATTRIBUTES*

ABSTRACT

Online process monitoring using sensors in ultrasonic welding of lithium-ion batteries for automotive applications is essential for a robust and reliable battery pack assembly. Although monitoring algorithms can be developed by systematic feature extraction and selection without expert knowledge of the process, the selected online features may not be repeatable when facing untrained data sets. The purpose of this study is to establish an in-depth understanding of sensor signals and their relationship to the ultrasonic welding process and joint quality. The fundamental physics behind the ultrasonic welding process is investigated using two sensor signals, weld power and horn displacement. Several online features are identified by examining those sensor signals and their variations under abnormal process conditions. The joint quality is predicted by correlating such online features to weld attributes such as bond density and post-weld thickness that directly impact the weld performance. This study provides a guideline for feature selection to achieve a reliable online monitoring system in ultrasonic metal welding.

* The contents of this chapter are ready to be submitted to *ASME Journal of Manufacturing Science and Engineering*.

3.1 INTRODUCTION

Ultrasonic metal welding is one of the major processes used to join automotive lithium-ion batteries [Lee *et al.* 2010; Kim *et al.* 2011; Lee *et al.* 2013]. In ultrasonic metal welding, a high frequency shear oscillation generated by a piezoelectric system, as described in Figure 3.1, removes surface oxides or contamination by friction [Zhang and Li 2009]. The continuous scrubbing action under pressure yields an increase in contact area, resulting in metallurgical adhesion [Kong *et al.* 2003; 2005; Siddiq and Ghassemieh 2009] or diffusion [Gunduz *et al.* 2005; Li *et al.* 2008] at the exposed metal interfaces. These solid-state bonding characteristics are advantageous for joining dissimilar metals such as copper, aluminum and nickel, which are commonly used materials for battery tabs. In addition, the temperature in this process does not exceed the melting point of the metal workpiece, eliminating undesirable compounds, phase, and metallurgical defects that can result from most fusion welding processes [Annoni and Carboni 2011]. Therefore, the ultrasonic welding process is well suited for battery tab joining.

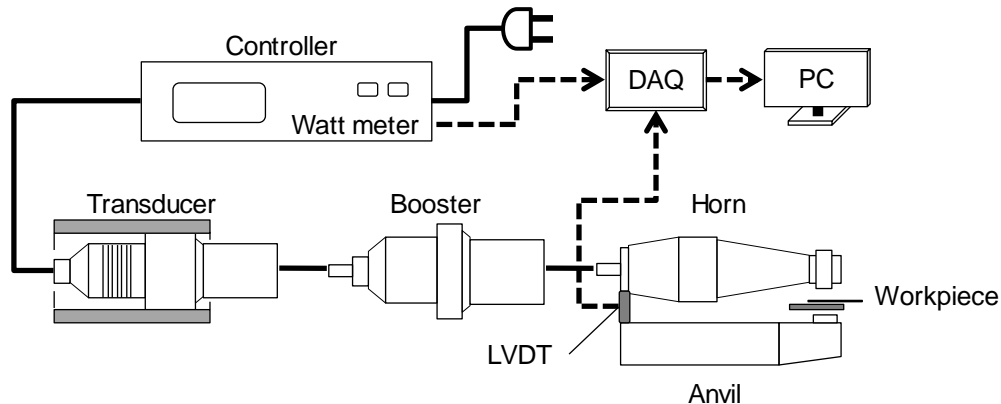


Figure 3.1 Ultrasonic metal welding system and sensor signal acquisition

In a typical battery pack for hybrid and electric vehicles, several hundred battery cells are joined together through tabs and bus-bars to meet the desired power and energy capacity requirements. The battery joints should possess reliable electrical connections as well as robust mechanical strength because failure of a single weld can result in degradation, even failure, of battery pack performance. Therefore, quality inspection is essential to ensure acceptable quality on every battery joint. As a quality assurance method, online process monitoring is widely used in manufacturing to ensure joint quality and process stability [Chu *et al.* 2004; Hu *et al.* 2011]. Although monitoring algorithms can be developed by systematic feature selection from various sensor signals utilizing appropriate statistical methods without expert knowledge of the process [Shao *et al.* 2013], selected features may not perform well when new abnormal process conditions are encountered. Thus, in order to develop a robust and reliable monitoring system, an in-depth understanding of sensor signals and their relationship to the welding process and eventually to weld quality should be established.

A significant amount of research has been done on the relationship between sensor signals and weld quality for various welding technologies. For example, Ling *et al.* [2010] predicted the quality of resistance spot welds by analyzing input voltage and current signals during the welding process. Li *et al.* [2000] estimated the resistance spot weld quality by correlating online signal features such as dynamic resistance with nugget size. Tseng and Chuang [2012] showed the influence of maximum electrode displacement on the nugget diameter and thickness in predicting spot weld quality. Park and Kim [2012] indicated that the plasma light intensity obtained by optical sensors could express the plasma/keyhole behavior, which directly impacts laser weld quality. A

comprehensive review was performed by Sun *et al.* [1999] on the usage of multiple sensors in real-time monitoring of laser weld quality and incorporation of sensor fusion with a neural network approach. In gas metal arc welding, the welding voltage and current signals were correlated to the weld quality using a statistical process control method by Wu *et al.* [2007]. Nevertheless, only limited research has been carried out on the sensor signals and their relationship to weld quality in ultrasonic metal welding. Or *et al.* [1998] utilized a piezoelectric sensor to evaluate the weld quality during the ultrasonic wire-bonding process, which was different from ultrasonic welding for sheet metals. They monitored the changes in resonant frequency or vibration amplitude caused by mechanical impedance change in the bonding zone. Zhao *et al.* [2013] developed a measurement system for monitoring transient temperature during the ultrasonic welding process using thin-film thermocouples fabricated on silicon substrates and inserted in a pre-machined slot in the weld tool. Their study showed that the heat flux and its rate change during the welding process provides good physical understanding of ultrasonic bonding at the weld interface [Li *et al.* 2013]. The methodology provided in their study showed some feasibility for process monitoring and control. However, no further examination was conducted on how the temperature would vary when abnormal situations occurred during the process.

In the previous study on ultrasonic welding of battery tabs [Lee *et al.* 2013], several weld attributes such as bond density (BD) and post-weld thickness (PWT) were identified from optical micrographs and correlated to weld quality. According to this study, the performance of an ultrasonic metal weld, such as mechanical strength, can be indirectly linked to process parameters through such attributes. However, there are

limitations of using weld attributes for process monitoring since they are only available through off-line post weld measurement. Therefore, this chapter attempts to investigate the fundamental physics behind the weld formation in ultrasonic welding using sensor signals and relating them to weld attributes, which in turn determine the weld quality.

The remainder of this chapter is organized as follows. Section 3.2 summarizes weld formation mechanism in ultrasonic metal welding. Section 3.3 describes the experimental procedure and sensor signals and analyzes signal variation under abnormal process conditions. Section 3.4 identifies the relationship between signal features and weld attributes, which provides direct information of weld quality. Section 3.5 summarizes and concludes the chapter.

3.2 WELD FORMATION MECHANISM IN ULTRASONIC METAL WELDING

Ultrasonic metal welding is a solid-state welding process. The frictional work between the workpiece generated from the high frequency shear scrubbing in combination with the normal force breaks and disperses the surface films (oxides, contaminants, etc.), and increases the actual contact area at the weld interface. This, in turn, leads to a local intimate contact between exposed metal surfaces to form metallurgical bonds, which are atomic bonds between the metal lattices [Gao and Doumanidis 2002]. These locally created bonds (i.e., micro-welds) increase in density over the region affected by the weld tip as a result of the rise in temperature caused by extensive plastic deformation. In addition to the metallurgical adhesion, the continuous shear motion and static force from the horn result in bonding lines that curl around the

micro-welds, and they play a role in mechanical interlocking. Thus, a weld in ultrasonic metal welding of similar materials, nickel-plated copper in this chapter, is formed mainly by metallurgical adhesion with partial aid of mechanical interlocking. Ultrasonic metal welding does not create any fusion zone where the temperature of the mating metals reaches the melting point.

Figure 3.2 shows the microstructure of cross-sectioned weld samples of 1.0mm nickel plated copper and 0.4mm copper (C11000). After the nickel layer (less than $2\mu\text{m}$) is broken by the oscillating shear force, a unified grain structure between the two bare copper sheets is formed as shown in Figure 3.2(a). The nickel layer broken as pieces and curled along the weld line, as shown in Figure 3.2(b), provides additional mechanical strength.

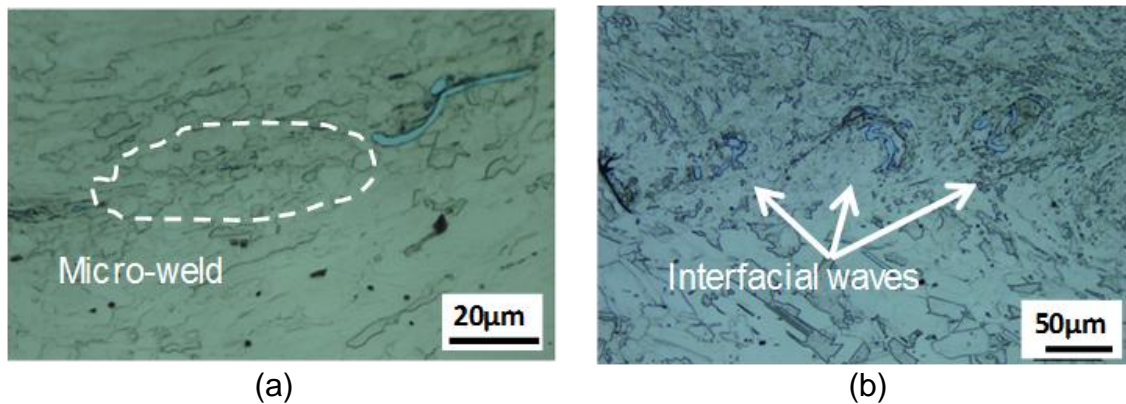


Figure 3.2 Optical micrographs with two main bonding mechanisms for ultrasonic metal welds: (a) metallurgical adhesion; and (b) mechanical interlocking [Lee *et al.* 2013]

In this chapter, two key weld attributes which have a direct impact on the final weld performance, BD and PWT, are measured and correlated with signal features. BD is the proportion of bonded region to the entire weld width while PWT is the proportion of

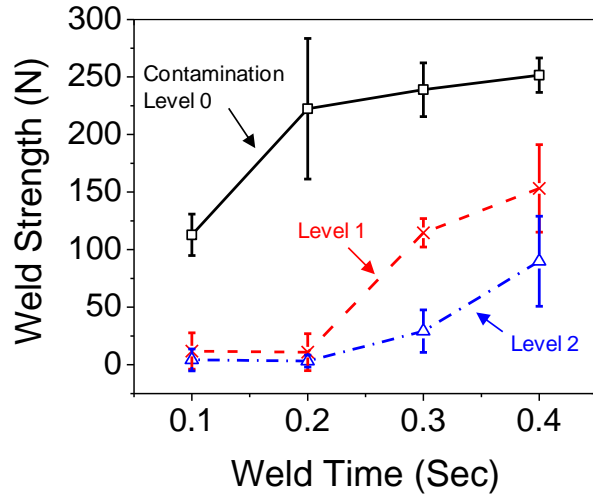
the indented thickness of the upper sheet to the original thickness. These non-dimensional parameters were defined in a previous study of joint quality characterization in ultrasonic metal welding by Lee *et al* [Lee *et al.* 2013]. Figure 3.3 shows the effect of a key process variable, weld time, on joint performance, BD and PWT. As shown in Figure 3.3(a), the weld strength increases dramatically in a short welding time. Then it shows a slow increase as welding time keeps increasing despite a steady increase of BD as described in Figure 3.3(b). This is caused by the decrease of PWT over time as shown in Figure 3.3(c), which may lead to excessive thinning of the material. Based on these results, the performance of an ultrasonic metal weld is in positive relation with BD while in negative relation with PWT. The process variation with contaminated surface in Figure 3.3 is detailed in the next section.

3.3 SENSOR SIGNALS FROM THE ULTRASONIC WELDING PROCESS

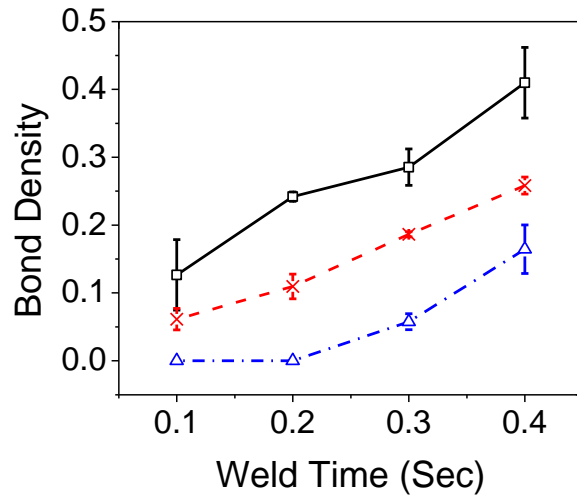
In this section, the signals collected by the sensors equipped in an AmTech Ultraweld® L-20 high power welder are analyzed to describe the mechanism of weld formation during the ultrasonic welding process. The experimental procedure is described in Section 3.3.1. Two sensor signals, power and displacement, are introduced in Section 3.3.2, and their variations under surface contamination are examined in Section 3.3.3.

3.3.1 Experiment

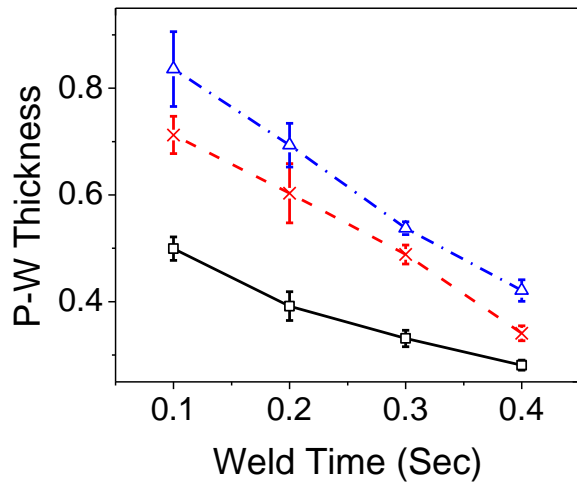
Prepared coupons of nickel plated copper sheets of dimensions 20 mm by 50 mm



(a)



(b)



(c)

Figure 3.3 Influence of weld time on (a) weld strength obtained from U-tensile test; (b) bond density; and (c) post-weld thickness

were welded for different welding times using the AmTech ultrasonic welder. The pressure and the vibration amplitude were fixed at 35 psi and 40 μm , respectively. The lap joint of two copper sheets of different thicknesses, 0.2 mm and 1.0 mm, was designed for simulating joints between battery tabs and bus-bars. Table 3.1 summarizes the factors, levels and corresponding replications for this experiment. During the welding experiment, the power and displacement signals from the sensors built into the welder, as illustrated in Figure 3.1, were collected and processed to analyze the relation between signal features and product or process quality. Three weld samples produced were then subjected to a U-tensile test for obtaining their mechanical properties. Another three weld samples were cross-sectioned, mounted, and polished using 0.03 μm colloidal silica suspension followed by etching [Lee *et al.* 2013] in order to conduct further microscopy and weld attribute measurement. More replications for 0.4s weld time (twelve for tensile test; three for cross-sectioning) were made in order to have enough data to analyze the trend of sensor signals with fixed weld time.

An abnormal process condition was simulated by applying oil-based stamping fluid (Daphne vanishing oil with kinematic viscosity of 1.3 at 40 $^{\circ}\text{C}$) at the interface between the workpieces as surface contaminant. This has been reported in the assembly line of battery packs as a possible source of contamination. The level of contamination was controlled by a transfer pipette providing 0.05mL per drop. Three different levels of contamination were applied in this experiment: level 0 (cleaned with isopropyl alcohol), level 1 (one drop of vanishing oil), and level 2 (two drops of vanishing oil). After the drops were applied, the welding took place immediately to minimize the effect of oil's evaporation on the result.

Table 3.1 Factors and levels for experimental design

Welding time (sec)	Surface contamination	Replications	
		U-tensile test	Post-weld measurement
0.1	Level 0	3	3
0.1	Level 1	3	3
0.1	Level 2	3	3
0.2	Level 0	3	3
0.2	Level 1	3	3
0.2	Level 2	3	3
0.3	Level 0	3	3
0.3	Level 1	3	3
0.3	Level 2	3	3
0.4	Level 0	12	3
0.4	Level 1	12	3
0.4	Level 2	12	3

3.3.2 Sensor signals

Two sensor signals are analyzed: (1) the electric power required for maintaining the mechanical vibration of the weld tool (i.e., horn) and (2) the linear displacement of the horn in the clamping direction.

Power

The ultrasonic vibration is provided by a piezoelectric system and transmitted to a booster/horn stack assembly with designated amplitude. To maintain this mechanical vibration at a constant level of amplitude, the amount of electrical power is controlled throughout the welding process depending upon the mechanical loading conditions on the weld joint, which may vary during the process. The power can be defined as:

$$Power = F \cdot \frac{dS(t)}{dt} \quad (1)$$

where F is the force exerted on the weld tip as a function of friction coefficient (μ) and clamping force (F_N), and $dS(t)/dt$ is the velocity profile of the weld tip function.

Figure 3.4 shows (a) the power required to initiate and maintain the vibration motion of the horn during the weld cycle and (b) the cross-section images of the weld interface over welding time. As shown in Figure 3.4(a), the power rapidly ramps up for the initial 0.1 second of welding time and stays at a constant level to maintain the vibration. As ultrasonic energy is transmitted to the weld interface, the shear force generated from the high frequency lateral movement results in yielding of the material. Extensive plastic deformation or cold work is observed in the elongated grains along the bonding line as seen in the initial stage of weld process (Figure 3.4(b)). As welding proceeds, severely deformed grains and the migration of high angle grain boundaries lead to the formation of a new grain structure (i.e., recrystallization) [Bakavos and Prangnell 2010; Patel *et al.* 2011; Prangnell *et al.* 2011], and a continuous welding action with increased temperature results in growth of the recrystallized grains [Lee *et al.* 2013]. Those recrystallized grain structures are seen in most normal quality welds, which have already been described in many previous studies [Bakavos and Prangnell 2010; Patel *et al.* 2011; Prangnell *et al.* 2011; Lee *et al.* 2013]. This is mainly due to the temperature rise at the weld interface with the aid of severe cold working of the material, which is caused from the dissipation of mechanical energy (i.e., vibration) by friction. Therefore, such power signals that are influenced by the surface condition of the mating metal sheets can provide useful information on the weld formation process.

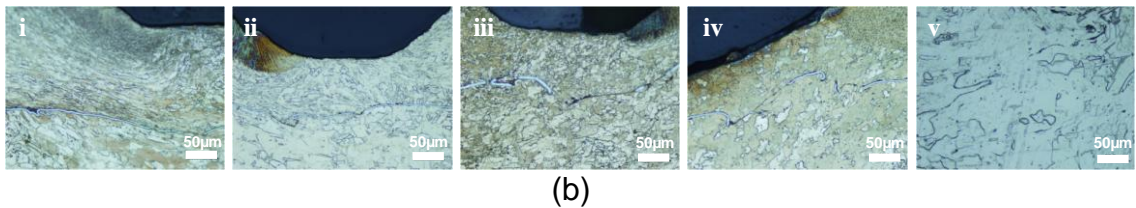
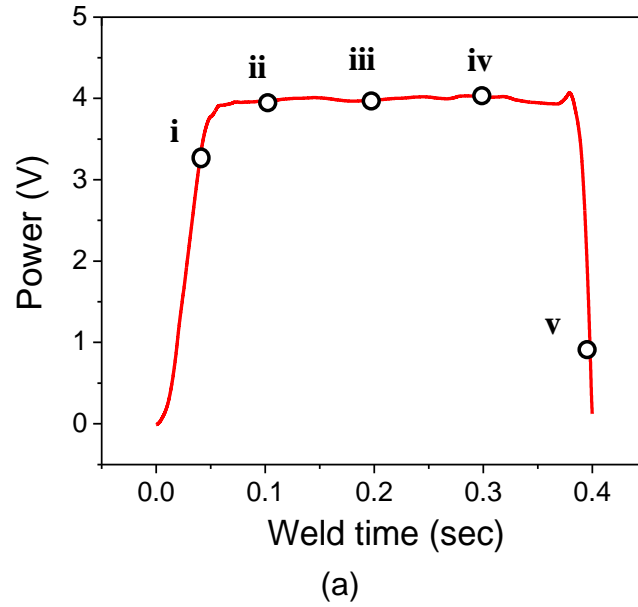


Figure 3.4 Power signal variation over time: (a) power profile for a single welding cycle; and (b) continuous cross-section images at the weld interface during welding cycle

Displacement

A Linear variable differential transformer (LVDT) was used to measure the horn displacement in the clamping direction. This signal data provides information on mechanical deformation, or indentation, made by the teeth of the horn.

The displacement profile as shown in Figure 3.5(a) shows the trend typically seen in normal quality welds. In the initial stage of the welding process (< 0.05 sec), the indentation of the material occurs at relatively high speed, but at a lower speed after that (> 0.05 sec). Figure 3.5(b) describes a series of cross-section images that impose a material filling phenomenon into the space between knurl teeth. Based on the findings

from the previous study [Lee *et al.* 2013], the quality of ultrasonic welds has a close relationship with an indented thickness of the material. Thus, the linear displacement profile of the horn can be utilized as valuable data for process monitoring.

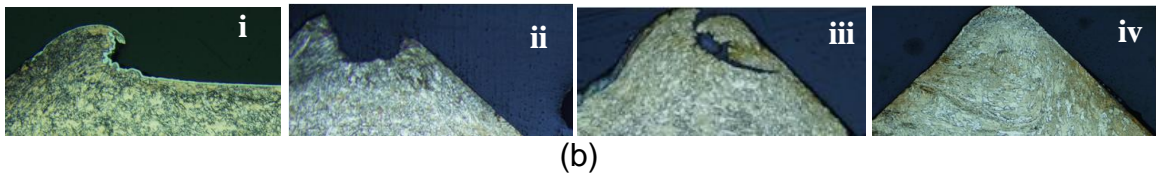
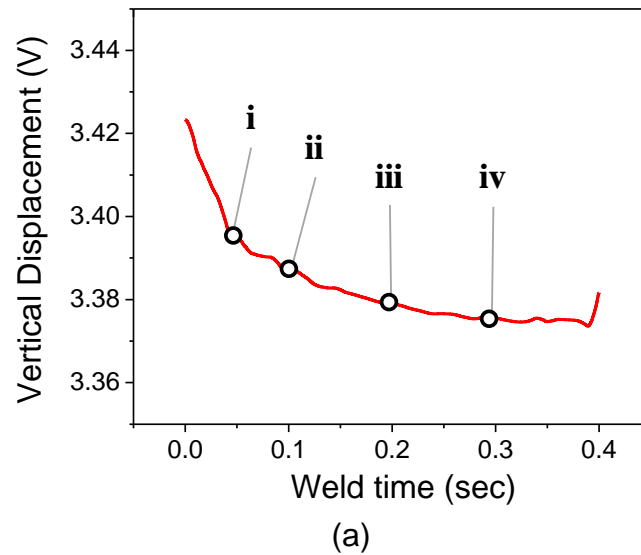


Figure 3.5 LVDT signal: (a) profile of horn displacement; (b) cross-section images at the top of metal surface illustrating material filling behavior that corresponds to the displacements shown in (a)

3.3.3 Signal variation under process disturbance

As discussed in Section 3.1, process disturbance during the ultrasonic welding process for battery tab joining was simulated by contaminating the workpiece surface with stamping fluid. The weld samples produced with three different levels of contamination – level 0, level 1 and level 2 – are examined by microscopy.

Figure 3.6(a) illustrates the typical trend of power signals for the three contamination levels during the welding process. 15 replicated signals were collected from the welding experiment, and all showed similar patterns. The power for welding of materials with clean surface shows a fast increase up to about 2300W, followed by a steady power level until welding is over, whereas the power for both contaminated cases does not reach the same power requirement as the clean surface case but only 70% to 75% of that (stage I in Figure 3.6). Instead, the power decreases over a period of time (stage II) and gradually increases again (stage III) before settling as the end of the weld cycle is reached (stage IV). The lack of power ramp-up in stage I and continuous reduction in stage II for the contaminated surface cases mainly come from the low frictional resistance to the relative motion of metal sheets due to the slippery surface, so the welder does not require such high power to maintain the vibration with the designated amplitude. However, once the contaminants of the surface have been dispersed or removed by the scrubbing action, the welder regains its power in stage III as the friction resistance recovers back to the normal condition. The time duration for stage II depends on the amount of contamination at the interface as shown in Figure 3.6(a).

Figure 3.6(b) shows the variation of the horn's absolute position during welding of copper sheets of different contamination levels. The same stage division as the power signal can be applied to this LVDT signal. At stage I, the horn abruptly decreases its position as the weld tool penetrates the metal surface even though the depth of indentation with contaminated surface differs from one with clean surface. For surface contamination cases, the low power level in stage I causes less heat generation, which results in less softening of the material and, therefore, less indentation. This penetration

helps the weld tool fully engaged in the metal surface. After the initial indentation, the horn slows down its descent in stage II while very little descent is made for the contaminated surface case due to the decrease in power. Then, as the welder increases power again in stage III, the speed at which the horn is descending is regained whereas the horn slows down for clean surface case.

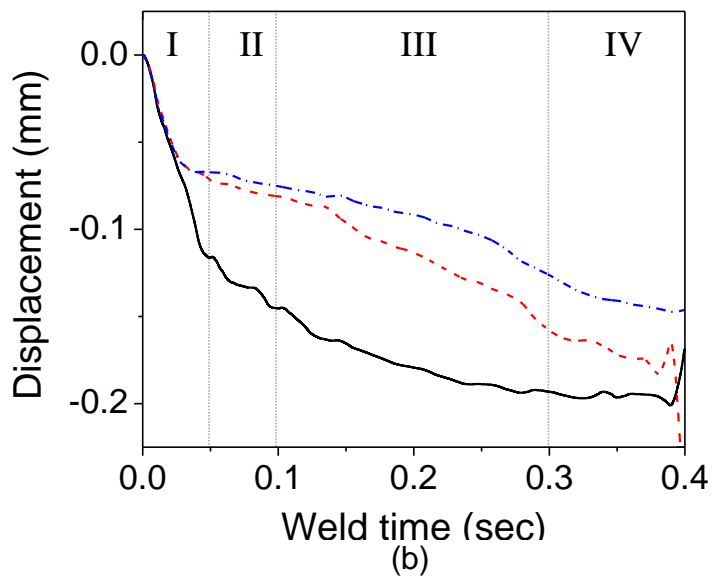
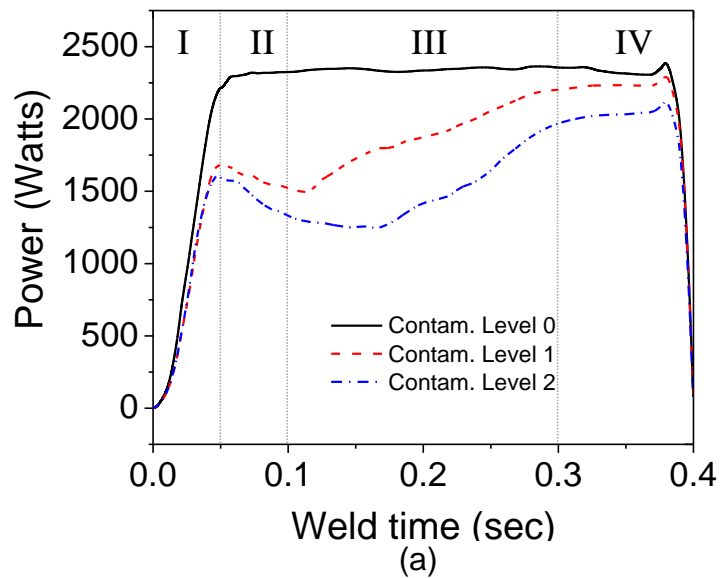


Figure 3.6 Variation of (a) power signal and (b) displacement signal for different levels of surface contamination

Figure 3.7 is a series of microscopic images focused at the weld interface of a weld sample with clean surface. It shows that, as power increases and the horn lowers its altitude, the nickel layer is dispersed or broken apart by a shear force exerted on the interface. Micro-welds are developed along the weld line, which becomes curled as welding proceeds. The micrographs shown in Figure 3.8 indicate that the contaminants are trapped in the weld interface and formed as a swirl, which makes the joint weaker. This is because the remaining oil layer in the early stages of the welding process hinders the adhesion of two metal surfaces and delays the weld development.

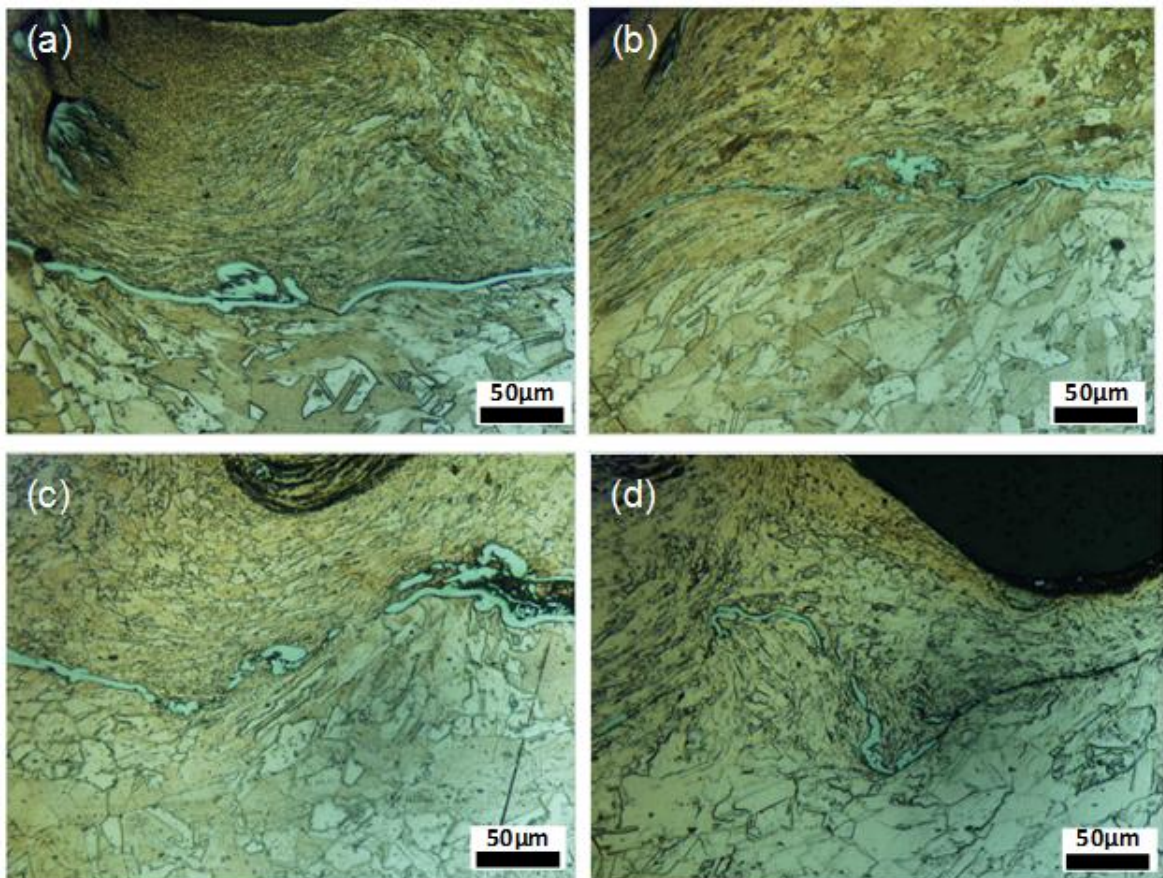


Figure 3.7 Optical micrographs showing weld line formation with welding time of (a) 0.1s, (b) 0.2s, (c) 0.3s, and (d) 0.4s

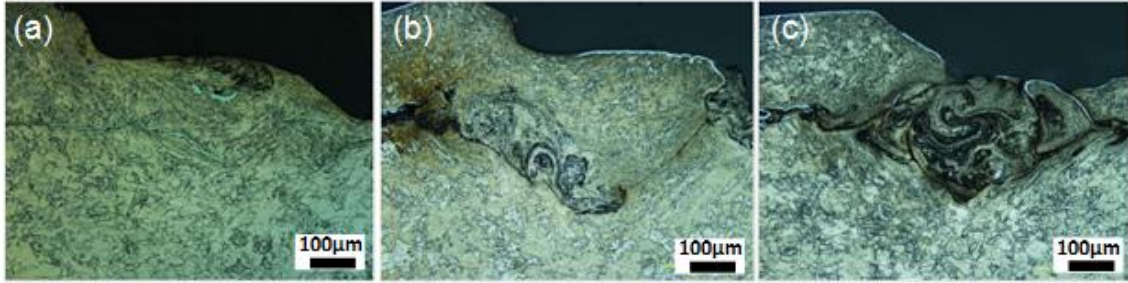


Figure 3.8 Optical micrographs at the weld interface for three levels of surface contamination: (a) level 0 (clean); (b) level 1; and (c) level 2

3.4 RELATIONSHIP BETWEEN WELD ATTRIBUTES AND SIGNAL FEATURES

In this section, signal features are correlated to weld attributes to identify the relationship between sensor signals and product quality. First, Section 3.4.1 introduces several features in power and displacement profiles. Then feature variations during the welding process are presented in Section 3.4.2, and finally the relationship between those features and weld attributes is presented in Section 3.4.3.

3.4.1 Features in sensor signals

Based on our understanding of the physics behind the signal variation under process disturbance as discussed in Section 3.3, the early stages of the welding process is crucial for sensing some abnormal process conditions. For example, the power required in this period changes depending on the level of surface contamination due to different friction conditions. These different power levels lead to different amounts of material deformation, resulting in changes in horn displacement. Thus, the energy used and the indentation depth in this early stages are two important features in both power and

displacement signals. For the simplicity of calculation, the energy is obtained from the beginning to the mid-point of the welding process. In the same manner, the indentation depth of the mid-point of the welding process is chosen as one feature of the displacement signal. Those two features are named E_{mid} and D_{mid} , respectively.

As discussed previously, an ultrasonic metal weld is formed through continuous rubbing action that yields an increase of bonded areas between clean metal surfaces. The curved weld line is found in typical weld samples with normal weld quality. The welding experiments performed in this chapter show that the weld samples produced in 0.4s welding time have the strongest joint performance owing to high bond density and reasonable indentation depth, as described in Figure 3.3. Therefore, the normal quality weld requires a certain level of welding time or energy input. In that sense, total energy used and total indentation depth during the entire welding process are also important features in the power and displacement curves. They are named E_{total} and D_{total} , respectively. Figure 3.9 illustrates the main features measured in the power and displacement signals.

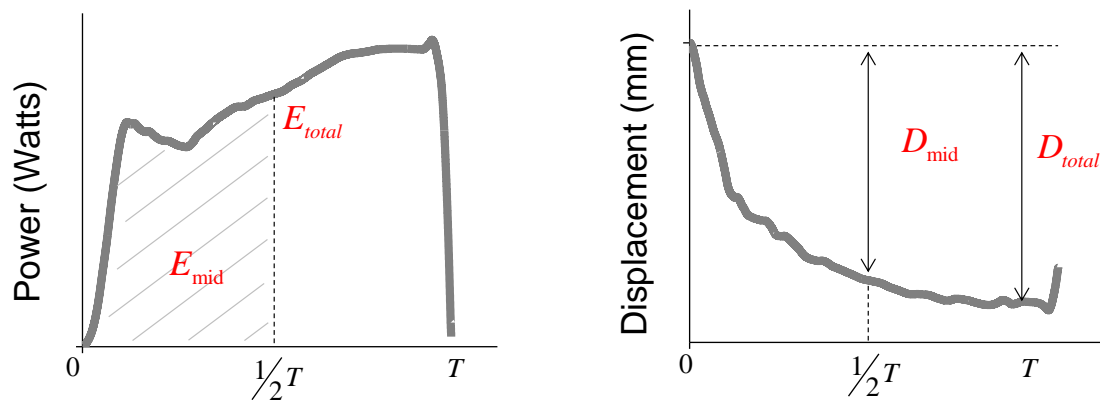


Figure 3.9 Features in power and displacement signals

Figure 3.10 shows the relationship between weld strength and each signal feature. As shown in Figure 3.10(a) and (b), E_{total} and E_{mid} of the power signal for normal weld samples is clearly distinguished from those for problematic welds caused by surface contamination. D_{mid} , as a displacement signal feature, also shows the capability of separating normal and defective weld groups as described in Figure 3.10(d) while D_{total} in Figure 3.10(c) shows some capability to distinguish two weld groups but not as much as D_{mid} does. All these four features show a linear relationship with joint performance, indicating that the welds with higher strength possess higher E_{total} , E_{mid} , D_{total} or D_{mid} . As indicated in all four plots, the amount of contaminants on the metal surface also affects the level of weld energy or indentation depth.

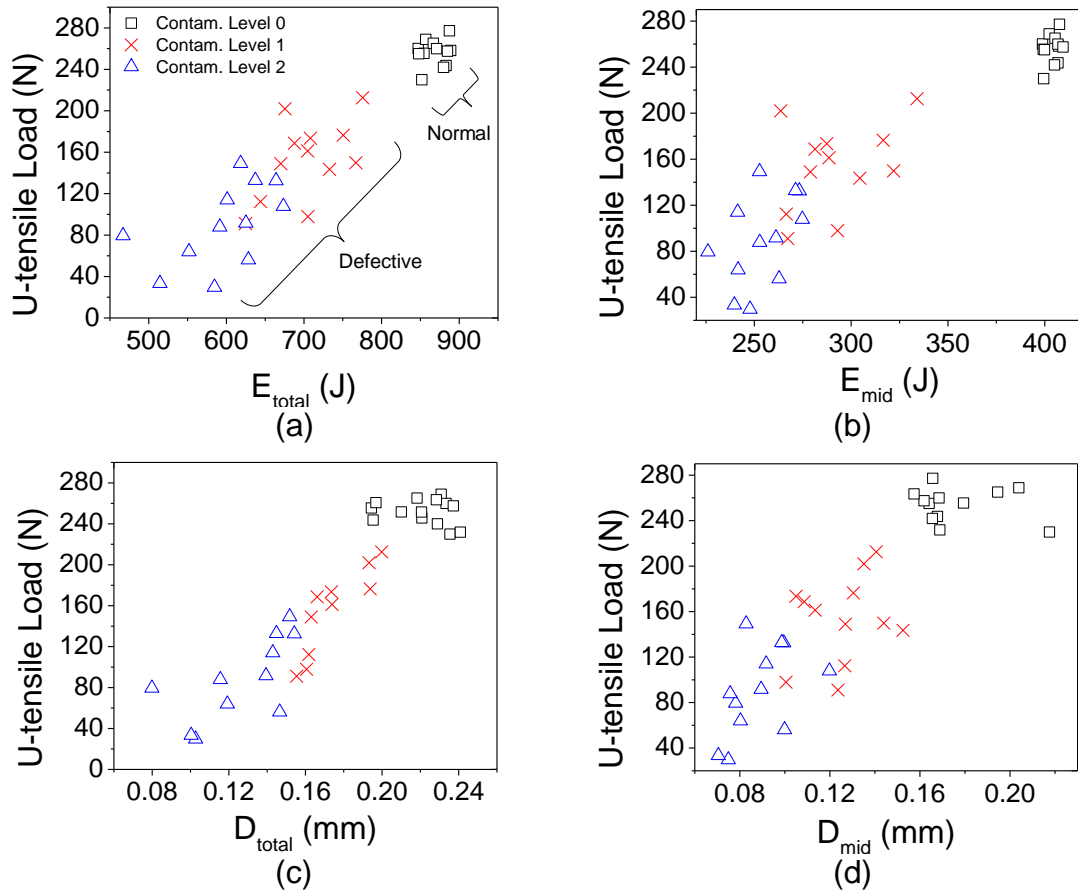


Figure 3.10 Relationship between weld performance and signal features: (a) E_{total} ; (b) E_{mid} ; (c) D_{total} ; and (d) D_{mid}

3.4.2 Effect of welding parameters on signal features

For the signal features that have been identified, their relationship to a key process variable, welding time, is established in this sub-section. E_{total} and D_{total} are plotted against welding time, as illustrated in Figure 3.11, which shows that E_{total} and D_{total} increase linearly over time regardless of the level of surface contamination. As welding time increases, more ultrasonic energy is consumed for frictional heating, plastic deformation and bond formation at the interface. Consequently, more heat generated by increased weld energy yields softening of the material, resulting in deeper indentation by the weld tool. However, only a fraction of the energy is used for welding a surface contaminated workpiece. In the very early stages of the process (0.1s), approximately 160 J is consumed for welding clean metals whereas only 60% of this energy is used for both contamination level 1 and 2, as indicated in Figure 3.11(a). As welding proceeds, the energy consumption for contamination level 1 and level 2 increases at different rates. At the very end of the welding process (0.4s), approximately 82% energy of the clean surface case is used for level 1 contamination, and only 65% for level 2. This is because the larger amount of contaminants the workpiece possesses, the longer time is taken for removing the remaining contaminants by oscillating shears. D_{total} has a similar increasing trend with increasing weld time as E_{total} , as shown in Figure 3.11(b), but the increasing rate depends on the level of contamination. For example, the difference in post indentation depth from 0.1s to 0.4s for level 0 is 0.19 mm whereas that for level 1 and level 2 is only 30% and 50% of level 0, respectively. In a similar manner to that for weld energy, indentation for contaminated surface cases is slower than that for clean surface.

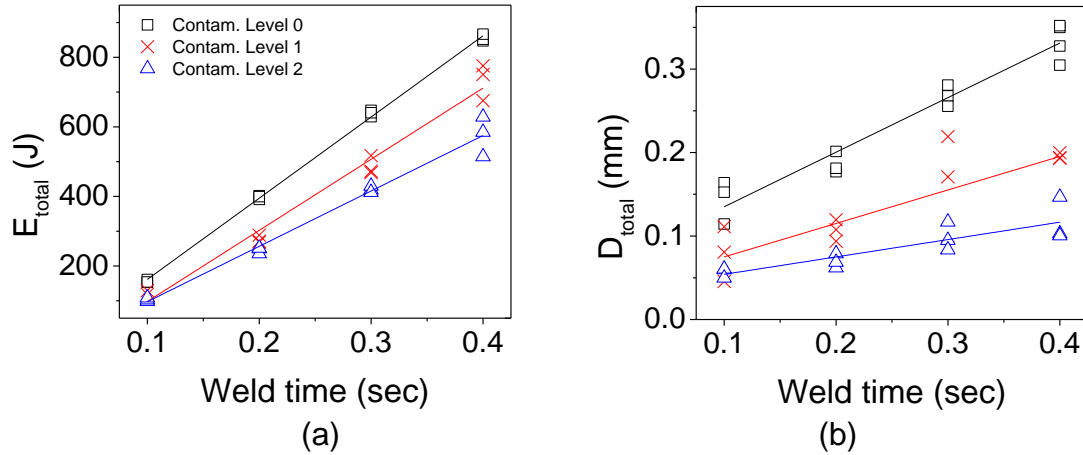


Figure 3.11 Effect of welding time on: (a) E_{total} ; and (b) D_{total}

3.4.3 Relationship between weld attributes and signal features

Weld attributes such as BD and PWT were defined as the physical criteria for weld quality in the previous study [Lee et al. 2013]. Correlating these attributes with signal features ensures good understanding of the weld formation during the welding process so that the weld quality can be predicted by sensor signals.

Figure 3.12 illustrates the relationship between weld attributes and the signal feature extracted from the power signal. As seen in Figure 3.12(a), BD and E_{total} are in a positive linear relation for both clean and surface contaminated case while a negative linear relation exists between PWT and E_{total} as described in Figure 3.12(b). Given the fact that normal quality welds that provide the highest joint performance in the preliminary U-tensile test (Figure 3.3) have BD around 40% and PWT around 28%, the minimum required value for E_{total} can be set to around 800 J. Figure 3.12(c) and (d) describe the scatter plots of BD and PWT against another signal feature extracted from the power signal, E_{mid} . As seen in the figure, E_{mid} of clean surface case is clearly

distinguished from that of contaminated surface case. This ability of separating normal and problematic weld quality makes E_{mid} a valuable feature for online monitoring. The required energy level at the mid-point of welding process can be set to around 400 J in order to achieve 40% BD and 28% PWT.

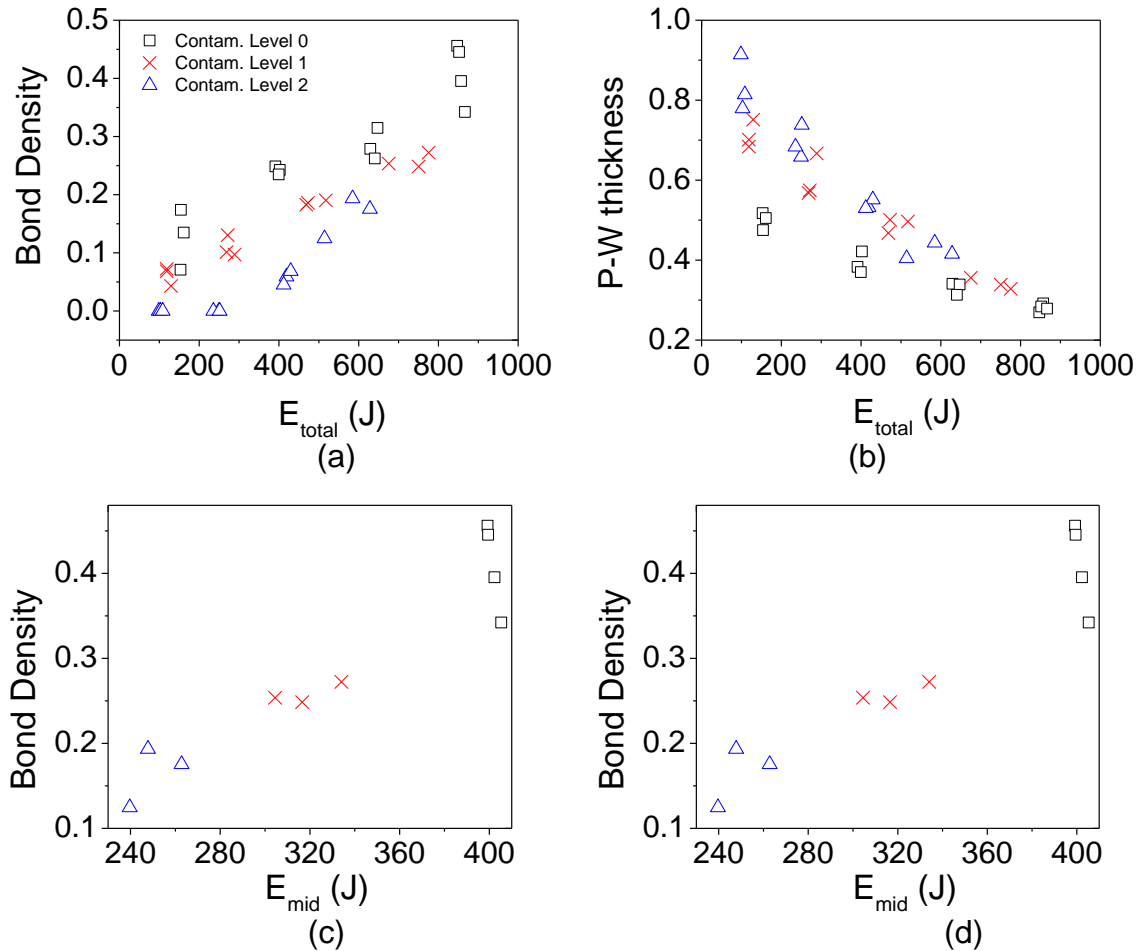


Figure 3.12 Relationship between weld attributes and power signal features: (a) BD vs. E_{total} ; (b) PWT vs. E_{total} ; (c) BD vs. E_{mid} ; and (d) PWT vs. E_{mid}

In addition to E_{total} and E_{mid} , D_{total} and D_{mid} also shows strong relationships to BD or PWT as illustrated in Figure 3.13. Of those two features, D_{mid} , as shown in Figure 3.13(c) and (d) has ability in discriminating between normal and defective weld groups that result

from surface contamination. Process variation due to such abnormal condition mostly occurs during the early welding stages. It should be noted that both E_{mid} and D_{mid} are the extracted features from the first half of the process. D_{total} of 0.25 mm or D_{mid} of 0.18 mm can be set as desired values for required PWT of normal quality welds, as indicated in Figure 3.13(a) and (b).

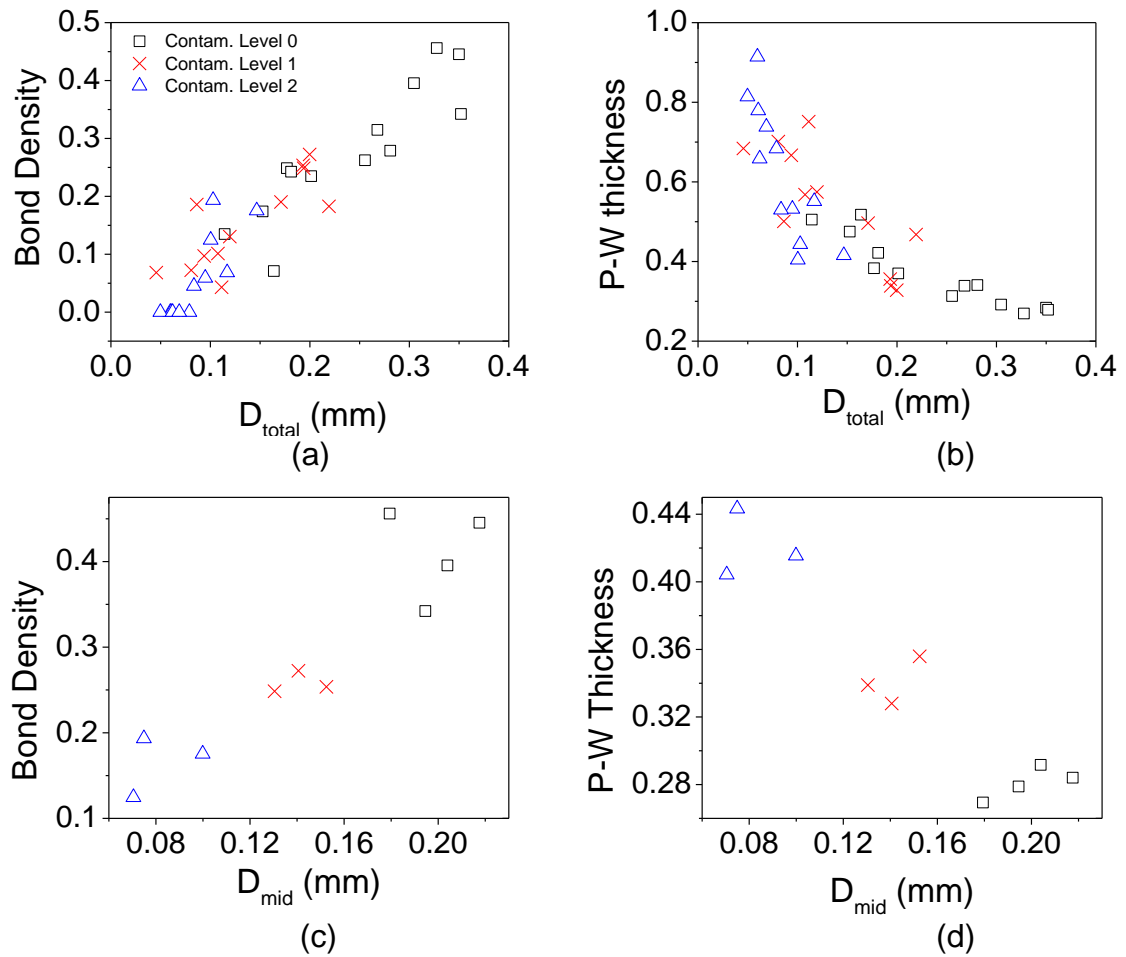


Figure 3.13 Relationship between weld attributes and displacement signal features:
(a) BD vs. D_{total} ; (b) PWT vs. D_{total} ; (c) BD vs. D_{mid} ; and (c) PWT vs. D_{mid}

By correlating online features to weld attributes, the physics behind the signal feature's change under process variation are understood: for example, one can learn how

the feature variations are related to the change in geometric and mechanical attributes of an ultrasonic weld. Figure 3.14 shows the scatter plots of four online features, which enable the feasibility for online process monitoring to be ascertained.

Figure 3.14(a) shows the direct relationship between two signal features, E_{mid} and D_{mid} , halfway through the welding process, while Figure 3.14(b) shows the relationship between two features, E_{total} and D_{total} , collected after the process is over. Both E_{mid} and E_{total} clearly distinguish problematic weld group (contamination level 1 and 2) from normal quality group (level 0). D_{mid} and D_{total} also show this discriminative capability, but not as clearly as E_{mid} and E_{total} in terms of the distance generated between two data groups (normal vs. defective). E_{mid} and D_{mid} , can be used as in-line monitoring signatures since they capture the process variations in the early welding stages. A proper control action can then be taken, based on the characteristics shown in those signatures. On the other hand, E_{total} and D_{total} can be used as post-weld monitoring signatures so that the product quality after welding can be determined.

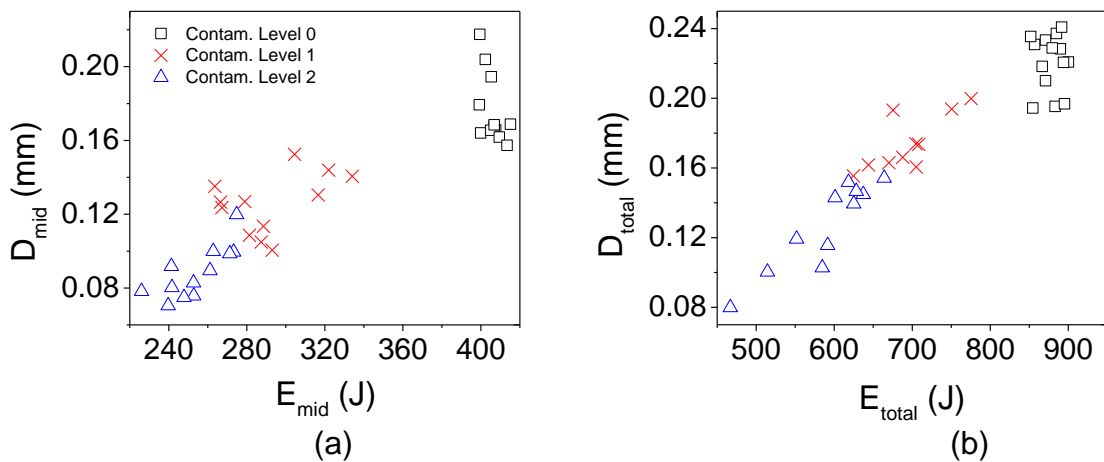


Figure 3.14 Relationship between signal features: (a) E_{mid} vs. D_{mid} ; (b) E_{total} vs. D_{total}

3.5 CONCLUSIONS

In this study, two sensor signals, weld power and horn displacement, are thoroughly examined to understand the physics behind the ultrasonic welding process. Several signal features are identified, based on the physical understanding of signal variations under abnormal process conditions such as surface contamination. These signal features are then correlated to weld attributes measured from micrographs of cross-sectioned weld samples. By achieving the relationship between those signal features and weld attributes, the joint quality can be successfully predicted. In-depth characterization of the ultrasonic metal welding process using sensor signals will help to understand the impact of internal or external process variation on the weld quality. This study will also provide a guideline for feature extraction/selection and setting criteria on selected features in process monitoring of ultrasonic metal welding.

Specific conclusions are as follows:

- 1) Power signal provides useful information on the change of mechanical resistance at the weld interface during the ultrasonic welding process whereas displacement signal reflects the pattern for material deformation.
- 2) The power signal for the first half of the welding process provides critical information on the mechanical loading on the weld tool. Low level of weld power is shown in the early welding stages under process disturbance such as low frictional surface due to stamping fluid. Similarly, the indentation at the mid-point of the process as measured by LVDT also shows clear distinction between normal and abnormal process conditions.

- 3) The energy used and the total indentation depth for the whole welding process indicate whether the weld formation at the interface is completed.
- 4) The relationships between weld attributes and several signal features such as E_{total} , E_{mid} , D_{total} , and D_{mid} provide physical understanding on the impact of process conditions on the weld quality. They can be used to establish criteria for weld quality monitoring.

REFERENCES

- Annoni, M. and Carboni, M. (2011). "Ultrasonic Metal Welding of AA 6022-T4 Lap Joints: Part I-Technological Characterisation and Static Mechanical Behaviour." *Science and Technology of Welding & Joining* 16(2): 107-115.
- Bakavos, D. and Prangnell, P. B. (2010). "Mechanisms of Joint and Microstructure Formation in High Power Ultrasonic Spot Welding 6111 Aluminium Automotive Sheet." *Materials Science and Engineering: A* 527(23): 6320-6334.
- Chu, Y., Hu, S.J, Hou, W., Wang, P. and Marin, S. (2004). "Signature Analysis for Quality Monitoring in Short-Circuit Gmaw." *Welding journal* 83(12): 336S-343S.
- Gao, Y. and Doumanidis, C. (2002). "Mechanical Analysis of Ultrasonic Bonding for Rapid Prototyping." *Journal of Manufacturing Science and Engineering* 124(2): 426-434.
- Gunduz, I. E., Ando, T., Shattuck, E., Wong, P. Y. and Doumanidis, C. C. (2005). "Enhanced Diffusion and Phase Transformations During Ultrasonic Welding of Zinc and Aluminum." *Scripta materialia* 52(9): 939-943.
- Hu, S.J, Hou, W., Du, H., Wang, P.-C. and Menassa, R. J. (2011). Method for Controlling the Consistency of an Arc Welding Process by Monitoring Welding Voltage to Determine Weld Droplet Detachment, Google Patents.
- Kim, T. H., Yum, J., Hu, S. J., Spicer, J. P. and Abell, J. A. (2011). "Process Robustness of Single Lap Ultrasonic Welding of Thin, Dissimilar Materials." *CIRP Annals - Manufacturing Technology* 60(1): 17-20.
- Kong, C., Soar, R. and Dickens, P. (2003). "Characterisation of Aluminium Alloy 6061 for the Ultrasonic Consolidation Process." *Materials Science and Engineering A* 363(1-2): 99-106.
- Kong, C., Soar, R. and Dickens, P. M. (2005). "A Model for Weld Strength in Ultrasonically Consolidated Components." *Proceedings of the Institution of Mechanical Engineers, Part C: Journal of Mechanical Engineering Science* 219(1): 83-91.
- Lee, S. S., Kim, T. H., Hu, S. J., Cai, W. and Abell, J. A. (2010). "Joining Technologies for Automotive Lithium-Ion Battery Manufacturing: A Review." *ASME Conference Proceedings* 2010(49460): 541-549.

- Lee, S. S., Kim, T. H., Hu, S. J., Cai, W., Abell, J. A. and Li, J. (2013). "Characterization of Joint Quality in Ultrasonic Welding of Battery Tabs." *Journal of Manufacturing Science and Engineering* 135(2): 021004.
- Li, H., Choi, H., Zhao, J., Li, X. C., Cai, W. and Abell, J. A. (2013). "Transient Temperature and Heat Flux Measurement in Ultrasonic Joining of Battery Tabs Using Thin-Film Micro Sensors." *accepted by Journal of Manufacturing Science and Engineering*.
- Li, J., Han, L. and Zhong, J. (2008). "Short Circuit Diffusion of Ultrasonic Bonding Interfaces in Microelectronic Packaging." *Surface and Interface Analysis* 40(5): 953-957.
- Li, W., Hu, S. J. and Ni, J. (2000). "On-Line Quality Estimation in Resistance Spot Welding." *Journal of manufacturing science and engineering* 122(3): 511-512.
- Ling, S.-F., Wan, L.-X., Wong, Y.-R. and Li, D.-N. (2010). "Input Electrical Impedance as Quality Monitoring Signature for Characterizing Resistance Spot Welding." *NDT & E International* 43(3): 200-205.
- Or, S., Chan, H., Lo, V. and Yuen, C. (1998). "Ultrasonic Wire-Bond Quality Monitoring Using Piezoelectric Sensor." *Sensors and Actuators A: Physical* 65(1): 69-75.
- Park, Y. W. and Kim, D. (2012). "Optimization of Laser Welding Parameters in Aluminum Alloy Welding and Development of Quality Monitoring System for Light Weight Vehicle." *Materials Science Forum* 706-709: 2998-3003.
- Patel, V. K., Bhole, S. D. and Chen, D. L. (2011). "Influence of Ultrasonic Spot Welding on Microstructure in a Magnesium Alloy." *Scripta Materialia* 65(10): 911-914.
- Prangnell, P., Haddadi, F. and Chen, Y. (2011). "Ultrasonic Spot Welding of Aluminium to Steel for Automotive Applications: Microstructure and Optimisation." *Materials Science and Technology* 27(3): 617-624.
- Shao, C., Paynabar, K., Kim, T. H., Jin, J. J., Hu, S. J., Spicer, J. P., Wang, H. and Abell, J. A. (2013). "Feature Selection for Manufacturing Process Monitoring Using Cross-Validation." *submitted to Journal of Manufacturing Systems*.
- Siddiq, A. and Ghassemieh, E. (2009). "Theoretical and Fe Analysis of Ultrasonic Welding of Aluminum Alloy 3003." *Journal of manufacturing science and engineering* 131(4): 041007.

- Sun, A., Kannatey-Asibu Jr, E. and Gartner, M. (1999). "Sensor Systems for Real-Time Monitoring of Laser Weld Quality." *Journal of Laser Applications* 11: 153.
- Tseng, K. H. and Chuang, K. J. (2012). "Monitoring Nugget Size of Micro Resistance Spot Welding (Micro Rsw) Using Electrode Displacement-Time Curve." *Advanced Materials Research* 463: 107-111.
- Wu, C., Gao, J. and Hu, J. (2007). "Real-Time Sensing and Monitoring in Robotic Gas Metal Arc Welding." *Measurement science and technology* 18(1): 303.
- Zhang, C. and Li, L. (2009). "A Coupled Thermal-Mechanical Analysis of Ultrasonic Bonding Mechanism." *Metallurgical and Materials Transactions B* 40(2): 196-207.
- Zhao, J., Li, H., Choi, H., Cai, W., Abell, J. A. and Li, X. (2013). "Insertable Thin Film Thermocouples for in Situ Transient Temperature Monitoring in Ultrasonic Metal Welding of Battery Tabs." *Journal of Manufacturing Processes* 15(1): 136-140.

CHAPTER 4

ANALYSIS OF WELD FORMATION IN MULTILAYER ULTRASONIC METAL WELDING USING HIGH-SPEED IMAGES*

ABSTRACT

One of the biggest challenges in manufacturing automotive lithium-ion batteries is to achieve consistent weld quality in joining multiple layers of dissimilar materials. While most fusion welding processes face difficulties in such joining, ultrasonic welding overcomes those difficulties due to its solid-state process characteristics. However, inconsistency of weld quality still exists because of limited knowledge on the weld formation through the multiple interfaces. This chapter aims to establish real-time phenomenological observation on the multilayer ultrasonic welding process by analyzing the vibration behavior of metal layers. Such behavior is characterized by a direct measurement of the lateral displacement of each metal layer using high-speed images. Two different weld tools are used in order to investigate the effect of tool geometry on the weld formation mechanism and the overall joint quality. A series of microscopies and bond density measurements is carried out to validate the observations and hypotheses of those phenomena in multilayer ultrasonic welding. The results of this research enhance the understanding of the ultrasonic welding process of multiple metal sheets and provide insights for optimum tool design to improve the quality of multilayer joints.

* The contents of this chapter are ready to be submitted to *ASME Journal of Manufacturing Science and Engineering*.

4.1 INTRODUCTION

Ultrasonic metal welding creates a solid-state bond between metals using oscillating shears generated by a high frequency ultrasonic energy. It has recently been applied to joining lithium-ion batteries for hybrid and electric vehicles. This process is well suited for such applications because of its ability in joining multiple layers of dissimilar materials [Lee *et al.* 2013].

In the battery assembly, a large number of battery cells are connected through bus-bars to meet the desired power and capacity requirement [Lee *et al.* 2010]. In such configuration, multiple layers of dissimilar metals, mostly of copper, nickel or aluminum as typical materials of anodes, cathodes, and bus-bars, are welded together. Achieving consistent weld quality in those multiple weld interfaces is critical for good battery performances.

While extensive research has been done on the weld formation of two metal sheets in ultrasonic welding [Joshi 1971; Harthoorn 1973; Kreye 1977; Tucker 2002; De Vries 2004; Zhang and Li 2009], only limited research has been carried out on multilayer welding. Ram *et al.* [2006] presented layer-by-layer fabrication between multiple foils of Al 3000 series using ultrasonic consolidation process in additive manufacturing. They described the effects of process parameters on product quality in fabricating multiple layers of similar materials and further investigated the weldability between multiple, dissimilar materials, especially of Al alloys to brass or to stainless steel [Ram *et al.* 2007]. Obielodan *et al.* [2010] examined ultrasonic welding of several other multi-material combinations, such as silver/copper/nickel, molybdenum/aluminum/copper, aluminum/titanium, and nickel/stainless steel. However, most of these studies were

limited to demonstrating the ability of ultrasonic welding in joining multilayer dissimilar materials. Recently, some research has been carried out on the ultrasonic welding of multi-stacked batteries. Kang *et al.* [2012; 2013] presented the effect of structural vibration that is generated from the ultrasonic welding process on weld quality in the multilayer battery tab configuration. Lee *et al.* [2012] conducted research on the ultrasonic welding of multiple, dissimilar metals by developing a mechanical-thermal coupled finite element model. In their study, the temperature distribution within the multi-material stack-up was obtained for a considerable amount of weld time (500 ms) by the numerical simulation model. Nonetheless, there is still a lack of understanding on the oscillating behavior of each metal sheet in multi-stacked configurations during the ultrasonic welding process. Little effort has been made to identify how and in what order the weld is created through multiple interfaces.

Several researchers investigated how the weld is developed at the interface during the ultrasonic welding process by experiments and numerical simulations. Ji *et al.* [2005] examined the cross section of Al+1%Si wire-bonded on the Au/Ni/Cu pad using scanning electron microscopy with energy dispersive X-ray spectroscopy, and observed a large number of vacancies and dislocations that can be fast diffusion paths across the weld interface. Zhang and Li [2009] developed a dynamic temperature-displacement finite element model to correlate process parameters with the weld development, whereas Elangovan *et al.* [2009] introduced friction as a heat source to the workpiece in their numerical model. Siddiq and Ghassemieh developed a theoretical [2009] as well as a numerical model [2008] to investigate the effect of friction and material softening

behaviors on the temperature change at the interface. However, most of these studies lack real-time phenomenological observation on weld development during the process.

In this chapter, the weld formation mechanism through the multiple interfaces is investigated experimentally using high-speed images. High-speed imaging has been widely used by many researchers for analyzing various welding techniques, for example, laser welding [Eriksson *et al.* 2010; Eriksson *et al.* 2010] or arc welding [Zaal *et al.* 2008; Ogawa 2011; Wen *et al.* 2011; 2012], but never been attempted for ultrasonic metal welding due to its high speed process characteristics. However, recent developments in high-speed imaging technology [AmeTek 2013] enable the observation of high frequency oscillations of the metal sheets in ultrasonic welding.

The goal of this study is to characterize weld development in multilayer ultrasonic welding through in-depth understanding of the vibration behavior of the metals. Such behavior is analyzed by processing high-speed images obtained during the welding process and measuring the lateral displacement of the workpiece. Different weld tools are introduced to investigate their impact on the vibration behaviors, and ultimately on the weld propagation mechanism. Furthermore, microscopic analyses and bond density measurements provide additional information on weld development in multilayer ultrasonic welding.

The remainder of this chapter is organized as follows: Section 4.2 describes experimental setups and procedures; Section 4.3 discusses the results from high-speed imaging and post-weld experiments; and Section 4.4 summarizes and concludes the chapter.

4.2 EXPERIMENT

4.2.1 Ultrasonic welding process

Figure 4.1 describes a typical ultrasonic metal welding system. A piezoelectric transducer converts a low frequency electrical signal to a high frequency, 20 kHz or above, mechanical vibration. This mechanical vibration is amplified by a booster and then transferred to a horn. The metal sheets to be joined are placed and clamped under pressure between the horn and anvil. As welding begins, oscillating shears generated by the welder breaks the oxide layers or contaminants and finally creates a solid-state bond between the exposed metals. Because of such bonding characteristics, a wide range of multiple, dissimilar metal sheets or thin foils can be joined by ultrasonic welding despite the thickness limitation of workpiece to 3 mm [Lee *et al.* 2010].

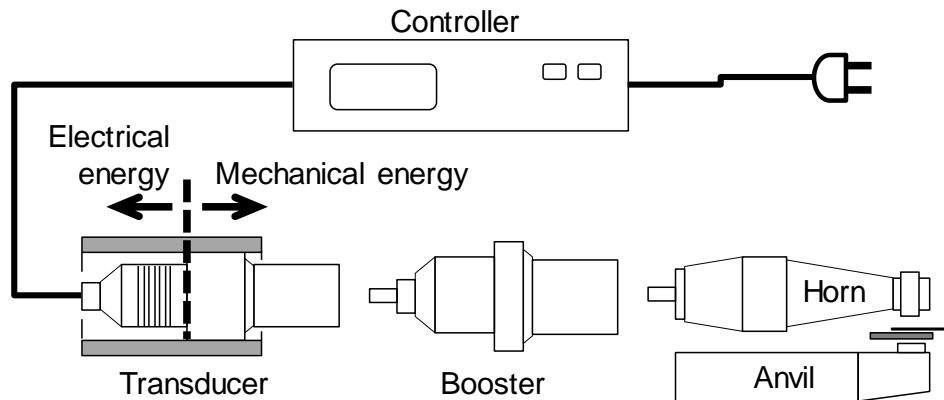


Figure 4.1 Ultrasonic metal welding system

4.2.2 High speed imaging

In this study, the Phantom v1610 digital high-speed camera with a telescope lens was used to record the dynamics of the metal workpiece during ultrasonic welding, as

described in Figure 4.2(a). Three layers of 0.2 mm nickel-plated C11000 copper (top) and one layer of the same material but 1.0 mm (bottom) were placed on an anvil, as seen in Figure 4.2(b). Figure 4.2(c) shows the front view of the workpiece as shown in the camera screen. To measure displacement, the group of metal layers was marked with a straight line. Figure 4.3(a) illustrates the side view of the camera setup showing the workpiece aligned with the horn. This alignment was intended for observing the vibration behavior of the horn and workpiece together.

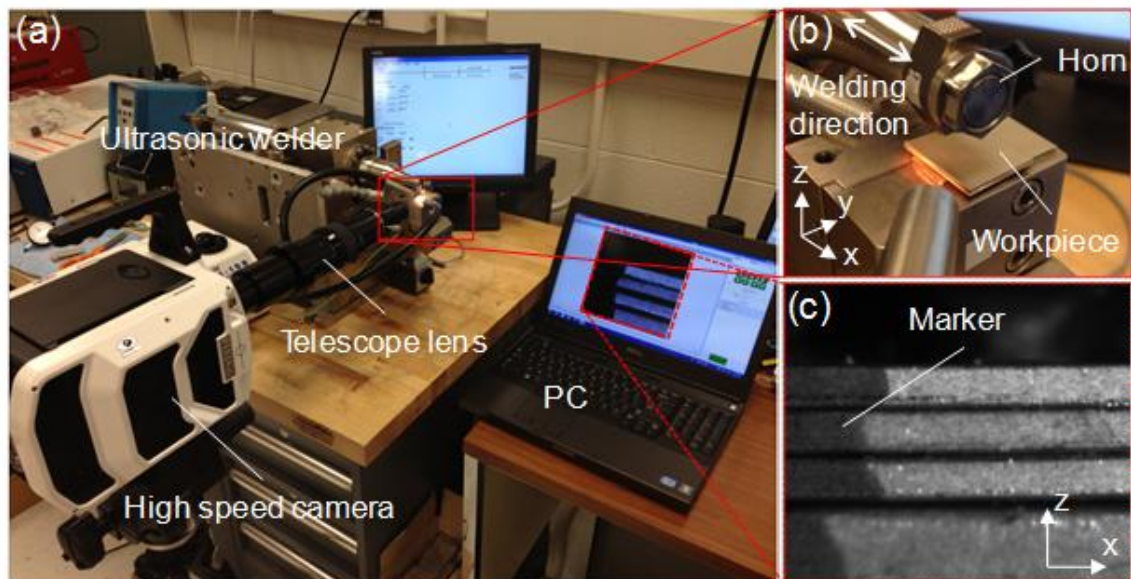


Figure 4.2 High-speed camera setup: (a) entire view of setup; (b) focused view on welding part; and (c) workpiece in PC screen view

The images were taken at 100,000 frames per second with an exposure time of 9 μ s, which provides five images per one vibration cycle. The size of the image was 256×256 pixels. The small vibration motion of a metal layer, tens of microns, was able to be recorded owing to a 35 times zoom capability of the telescope lens together with the CCD. Light was provided by a 150W Dolan-Jenner illuminator through fiber optic light-

guides for high-speed imaging. Finally, the images were digitally obtained and processed by Phantom camera control application software. The lateral displacement of each metal layer was measured in the consecutive high-speed images as illustrated in Figure 4.3(b).

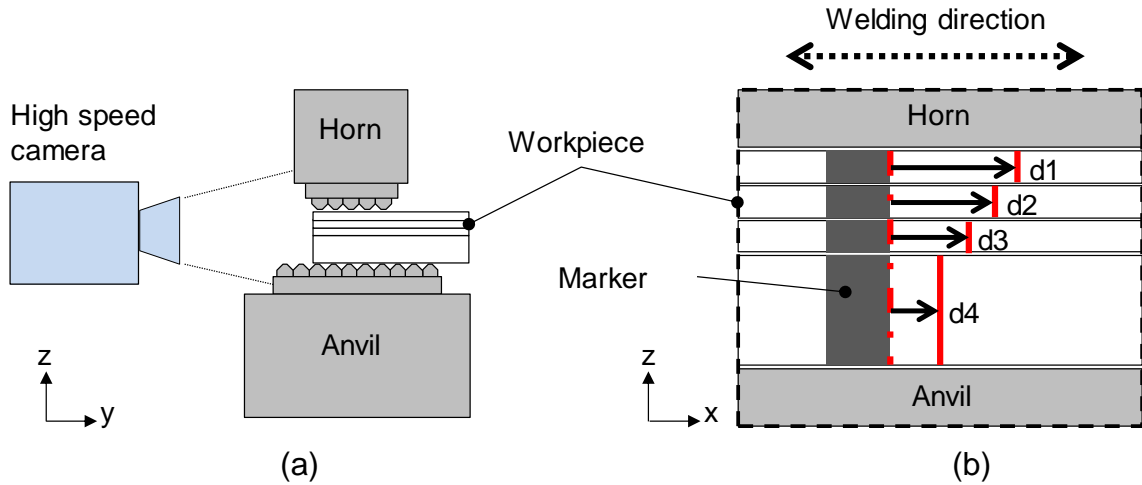


Figure 4.3 Schematic of high-speed camera setup: (a) workpiece stack-up aligned with horn (side view); and (b) displacement measurement of metal layer (front view)

4.2.3 Multilayer welding experiment

The multiple layers of nickel plated copper with different thicknesses were welded by a 20 kHz, 3.6 kW, *AmTech* lateral-drive ultrasonic spot welder. Table 4.1 shows the input parameters and their levels. The clamping pressure and the horn vibration amplitude were fixed at 50 psi and 60 μm , respectively. The weld time was varied to analyze the weld formation through multiple interfaces during the welding process. The input range of weld time was pre-determined by a screening test. Replication of each parameter was ten: nine for T-peel testing and one for cross-sectioning. Two anvil types with different knurl patterns (“fine” and “coarse”) were used to study the effect of the anvil roughness on the weld formation in multilayer ultrasonic welding. Figure 4.4

describes the knurl patterns and their dimensions. It is expected that the difference in anvil teeth geometry will cause different levels of material deformation, which eventually affect the weld development at the bottom interface.

Table 4.1 Factors and levels for experimental design

Factor	Level
Weld time (sec), T	0.1, 0.2, 0.3, 0.4, 0.5, 0.6
Anvil type	Fine, coarse

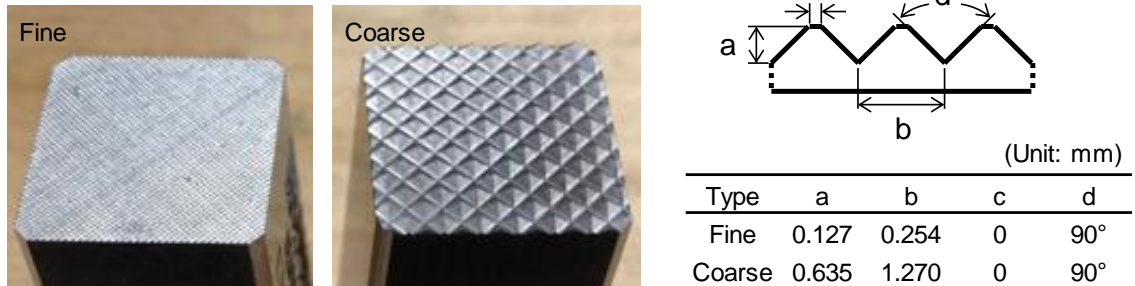


Figure 4.4 Two anvil types and their knurl dimensions

4.2.4 Post-weld performance testing/ microscopy/ bond density measurement

As a multi-joint configuration, each weld sample has three interfaces: 1st, 2nd and 3rd. To evaluate the mechanical strength of multilayer joints, a T-peel test [Kim *et al.* 2011] per sample, as illustrated in Figure 4.5, was performed by an *Instron* testing machine with a pulling speed of 10 mm/min. Of the nine T-peel samples, three are tested for each interface. The maximum tensile load during the T-peel test was recorded. The remaining one weld sample was cross-sectioned, mounted, polished, and applied to light surface etching for further optical micrographs and bond density measurement. The

details of sample preparation and post-weld measurement for ultrasonic metal welds were fully described in the previous study [Lee *et al.* 2013].

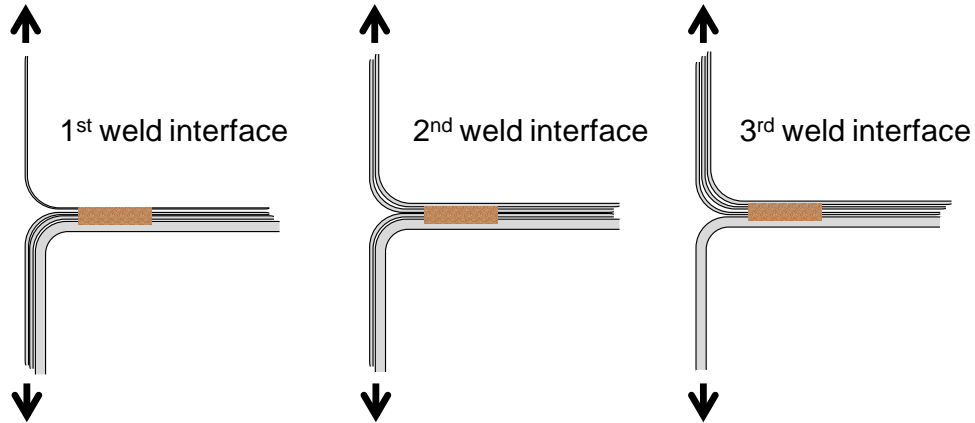


Figure 4.5 T-peel test for multi-joint welds

4.3 RESULTS AND DISCUSSION

This section presents the results from high-speed imaging and post-weld experiments. Based on these results, we discuss the weld formation mechanism in multilayer welding as well as the effect of anvil geometry on the vibration behaviors of the metal sheets and the weld development.

4.3.1 Observation of vibration development in multiple layers

Figure 4.6 shows an example of how the lateral displacement of one metal layer varies in a single weld cycle of 5×10^{-5} second. As the horn vibrates with constant amplitude, the workpiece also vibrates with it. The displacement of each layer is measured from the high-speed images as seen in Figure 4.6(a), which shows six

consecutive images taken at 0.00001 second intervals. These six images constitute a vibration cycle as described in Figure 4.6(b).

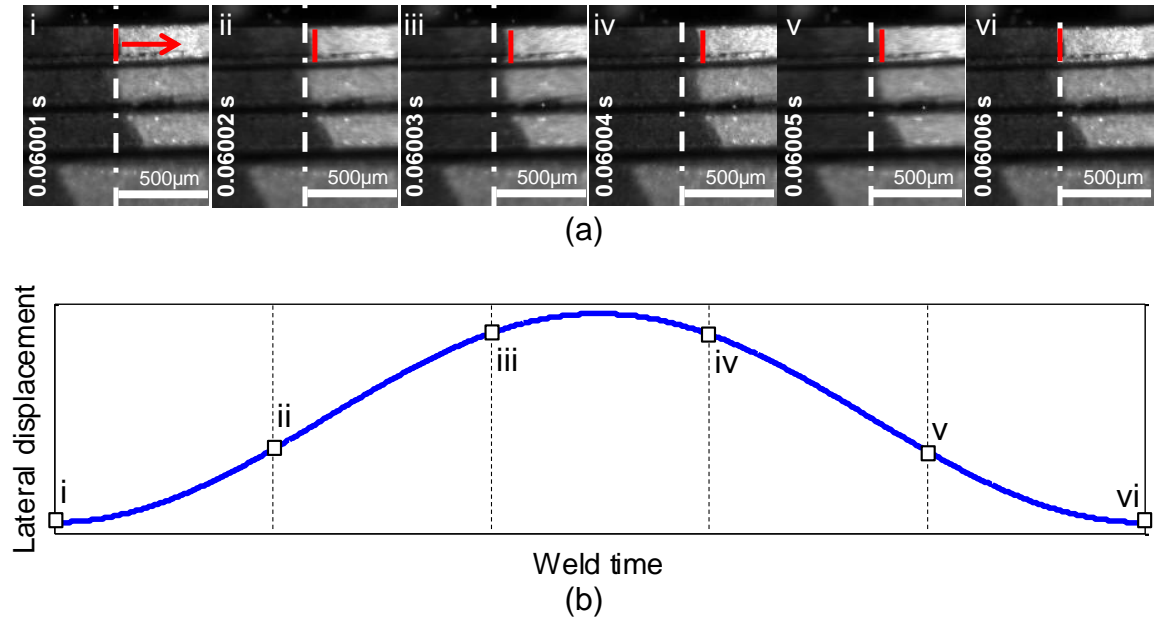


Figure 4.6 Example of displacement variation in one weld cycle (5×10^{-5} second): (a) consecutive high-speed images showing single vibration cycle of a metal layer; (b) an illustration of displacement curve measured from (a)

Figure 4.7 describes the development of vibration cycles for each metal layer during the initial 0.1s weld time. Each plot in Figure 4.7 shows two vibration cycles of four metal layers at a weld time of 0.005s, 0.02s, 0.04s, 0.06s, 0.08s, and 0.1s. Each data point in the plots is obtained by using the image processing algorithm in the Phantom application software. The resolution of this measurement is approximately 3 μm. Despite the limitation of focal length of the telescope lens used in this experiment, the variation cycles and their developing trends are clearly shown. The weld time 0.005s in Figure 4.7 (a) represents the vibration cycles at the very beginning of the welding process, and the

rest of the figures (Figure 4.7(b)-(f)) show the progress of the vibrations with increment of 0.02s weld time. The following observations can be made from the figure.

- In two consecutive cycles, very little difference in the vibration magnitude exists.
- When the observations are made sufficiently apart from each other, then a clear increase in the vibration magnitude can be seen. Each layer experiences an increase in vibration amplitude during the initial 0.1s of weld time, which can be called “growth” of the vibration of the layers.
- The vibration magnitude is highest in the top layer, but the vibration of the other layers increases over time and finally reaches that of the top layer.

We confirmed that the results in Figure 4.7 were repeatable based on multiple measurements from the same images, and were not subject to operator reproducibility.

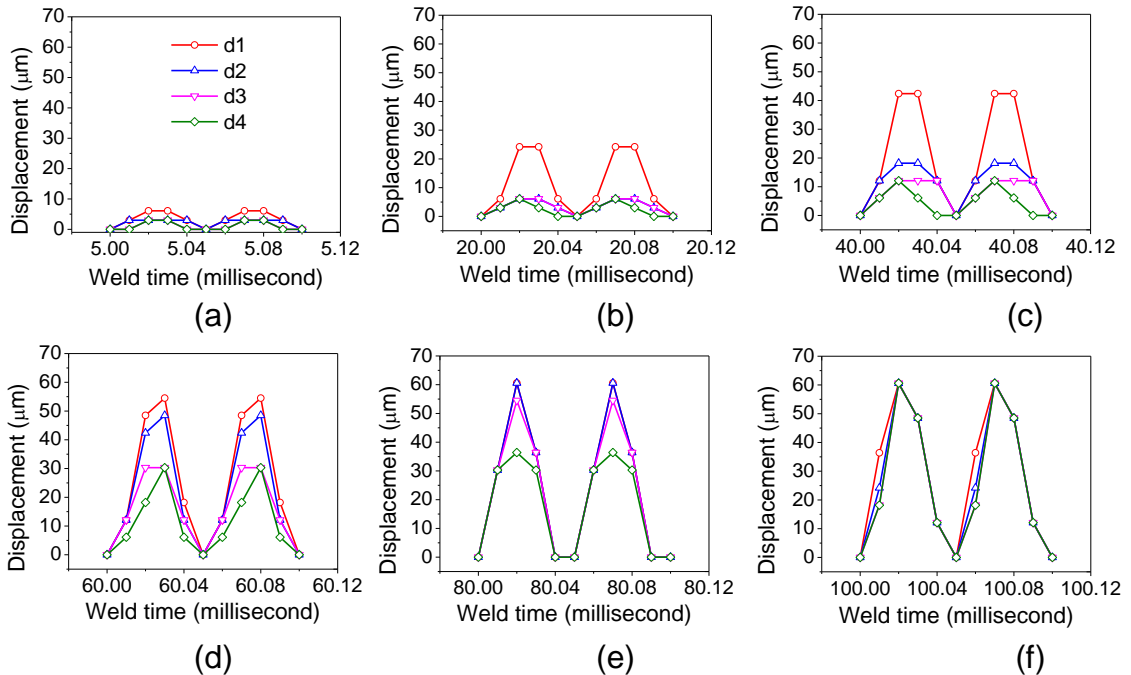


Figure 4.7 Development of vibration cycles of multiple layers with fine anvil: (a) 0.005s; (b) 0.020s; (c) 0.040s; (d) 0.060s; (e) 0.080s; and (f) 0.100s weld time

4.3.2 Weld formation mechanism in multilayer welding

Many previous studies agreed that an intensive frictional behavior between the metals is crucial for forming a pure metallurgical bond at the interface [Zhang *et al.* 2006; 2007; 2008; Yang *et al.* 2010]. Gao and Doumanidis [2002] introduced, a slippage and stick (i.e., bonding) phenomenon, which is accompanied by a frictional coefficient that varies throughout the welding process. Gilbert *et al.* [2010] further confirmed this. They argued that the friction force induced by the shear motion of the horn led to a slippage between workpiece resulting in plastic deformation thorough dislocations and finally a weld at the joint. Therefore, the slippage or rubbing action also plays a key role in weld formation in multilayer configuration.

To characterize the variations of lateral movements of the metal layers during the initial stages of the welding process, the vibration magnitudes at different weld times are extracted from Figure 4.7 and plotted against time as described in Figure 4.8. The following observations can be made from the figure.

- The top metal layer (d1) increases its vibration amplitude exactly with the vibration amplitude of the horn. Then, the vibration of the rest of the layers is developed sequentially, i.e., in the order of d2, d3 and d4.
- The amplitude of the vibration for the fine anvil converges to 60 μm while that for the course anvil converges to 30 μm .
- The third and fourth layer (d3 and d4) for the course anvil show less vibration than those for the fine anvil.

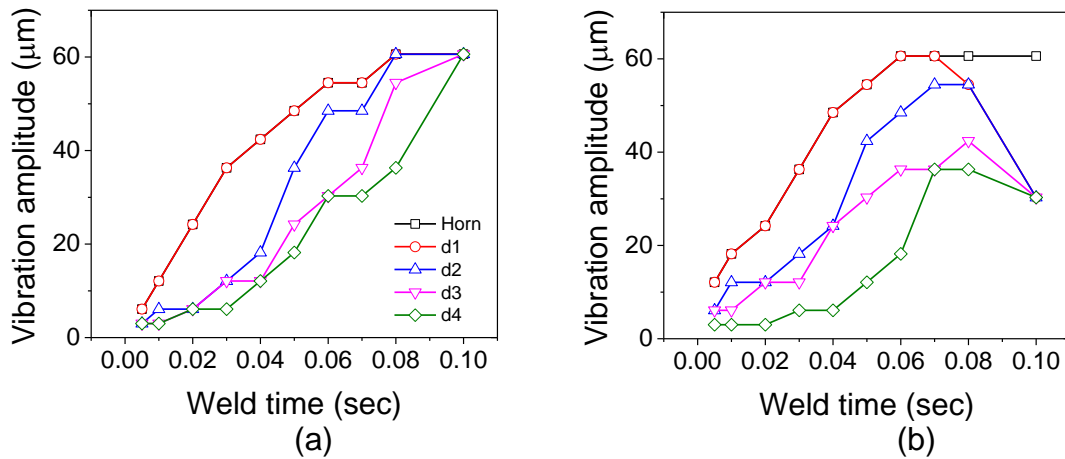


Figure 4.8 Progress of vibration amplitude of horn and four metal layers during initial stages (0 ~ 0.1s) of welding process when using (a) fine anvil; and (b) coarse anvil

To understand the trend of amplitude change of the multiple layers for the entire welding process, Figure 4.8 is extended further to 0.4s weld time, as seen in Figure 4.9. Figure 4.9(a) shows the variation of vibration amplitude for the horn and four nickel-plated copper sheets when using the fine type anvil whereas Figure 4.9(b) is the result from the coarse type anvil. The following observations can be made from the figure.

- Both results in Figure 4.9 show that the vibration amplitude of each metal layer initially changes over time and then merges into uniform amplitude for the rest of the welding process.
- As weld time reaches 0.1s, the vibration amplitudes of all four layers when using the fine type anvil converge at approximately 60 μm , the same magnitude as the horn, and decrease to 30 μm , while those with the coarse type converge at 30 μm and stay until the end of the process.
- After 0.1s weld time, slippage is observed between the tool (both horn and anvil) and workpiece.

These indicate that the average vibration in multilayer welding is bigger with the fine type anvil than with the coarse type. This is mainly because the lower layers in the stack-up experience more slippage during the initial welding process ($< 0.1s$) due to the smaller engagement between the material and the tool when using the fine knurl. In contrast, the bigger teeth of the coarse knurl allows the tool to penetrate the material more and provides a tighter engagement, which leads to less vibration in the lower metal layers. In addition, the extra slippage between the tool and metal workpiece imply possible tool wear.

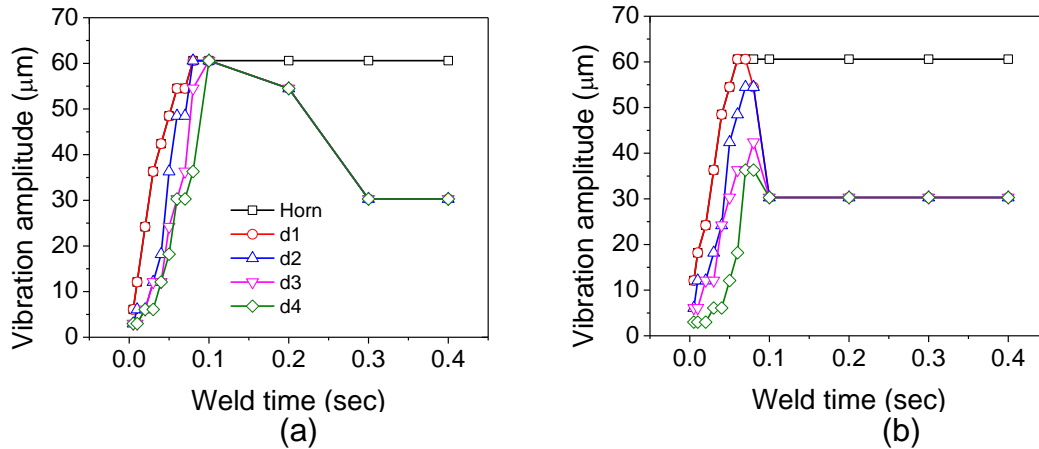


Figure 4.9 Progress of vibration amplitude of horn and four metal layers during the entire welding process when using (a) fine anvil; and (b) coarse anvil

Figure 4.10 shows the relative displacement between the two metal layers that face each other, which represents the amplitude difference between two adjacent layers in Figure 4.8. The following observations can be made from the figure.

- As described in Figure 4.10(a), the maximum difference in vibration amplitude between d1 and d2 occurs at around 0.03s ~ 0.04s whereas those maximum points for the 2nd and 3rd weld interface were at 0.06s and 0.08s,

respectively. Therefore, the relative motion between layers is maximal first at the 1st weld interface, and then followed by the 2nd and 3rd interface.

- The relative motion between layers in Figure 4.10(b) is developed in the order of the 1st (~ 0.04s), 3rd (~ 0.05s) and 2nd weld interface (~ 0.07s).

These different trends indicate that, when the fine anvil is used, a larger amount of slippage occurs between the bottom layer and the anvil so that the rubbing action between the 3rd and 4th layer is relatively low compared to that of the coarse anvil case. This difference in mobility of the bottom layer between those anvils may result in the different sequence of weld formation in multi-interfaces.

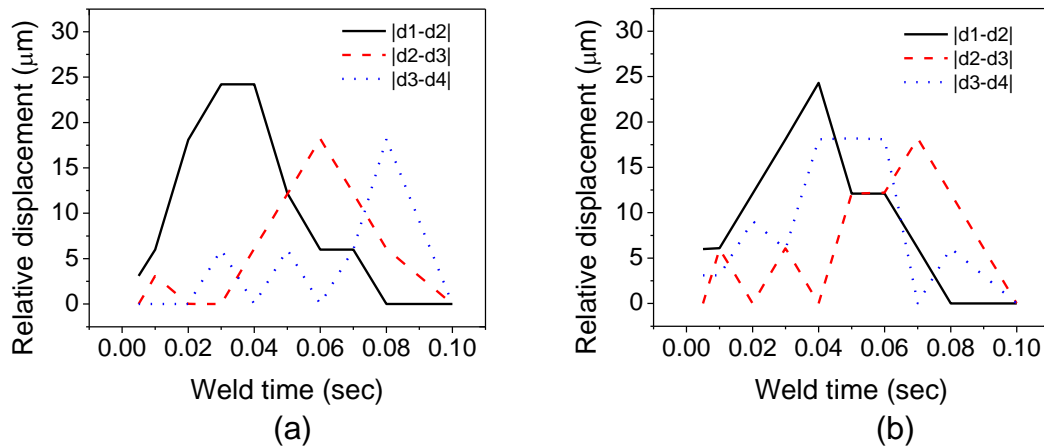


Figure 4.10 Progress of relative displacement between metal layers during initial stages (0 ~ 0.1s) of welding process when using (a) fine anvil; and (b) coarse anvil

Figure 4.11 shows the progression of the vibration amplitude of the 4th layer which interfaces with the anvil during the welding process. A clear distinction in mobility between the fine and coarse anvil is shown due to the different frictional conditions induced by different knurl patterns. The difference in relative movement between the 4th layer and the anvil is also evidenced by the difference in the amount of tool wear between fine and coarse anvils.

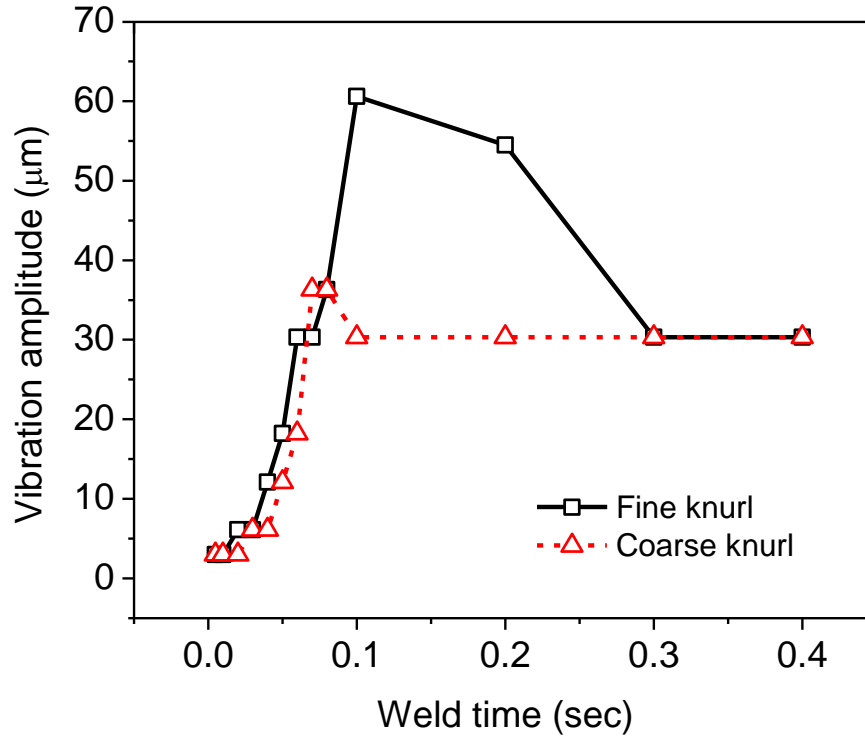


Figure 4.11 Progress of vibration amplitude of the 4th layer (anvil side) during the entire welding process with different anvil types

4.3.3 Post-weld microscopy

To validate the observations and hypotheses of the different weld propagation phenomena between the fine and coarse anvils, post-weld micrographs of the cross-sectioned weld samples made at different weld times are analyzed in this section.

Figure 4.12 shows optical microscopic images of the weld samples produced at different weld times when the fine anvil is used. As discussed in the previous study [Lee et al. 2013], the bonded region in an ultrasonic weld sample of nickel-plated copper sheets can be determined by the micrograph in which an intimate contact or adhesion is seen between the bare materials with unified grain structures. In addition, the weld line (i.e., nickel layer) is severely curled around the local bond, providing a mechanical interlock. Those bonded regions are easily recognizable in the microscopic images in

Figure 4.12. At 0.2s weld time, the curvy weld line and the pure bond between the bare copper surfaces are developed in the first weld interface as shown in Figure 4.12(a). Some regions in which the bonding just begins are also seen in the second interface, but none is seen in the third interface. In Figure 4.12(b), those bonded regions enlarge their areas with the continuing ultrasonic energy input, and a local bonding is just initiated in the third interface in Figure 4.12(c). As welding continues, the bonded regions are found in most weld interfaces in Figure 4.12(d). Based on the observations in the microscopic images of consecutive weld times, the weld propagates from top to bottom when using the fine anvil.

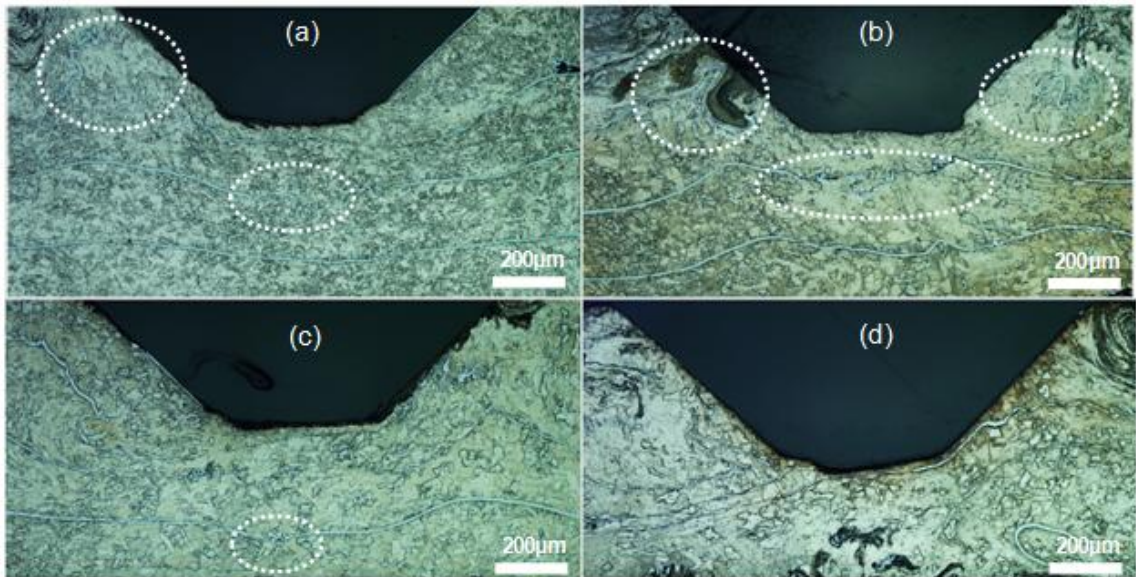


Figure 4.12 Micrographs of cross-sectioned weld samples produced with a fine anvil type for: (a) 0.2s, (b) 0.3s, (c) 0.4s, and (d) 0.5s

Figure 4.13 shows the micrographs of the weld samples produced with the coarse anvil. As seen in Figure 4.13(a), the local bonds are developed in the first and third weld interface while no distinct regions of adhesion or distorted interface are found in the

middle. Then, the weld is formed in the second interface as shown in Figure 4.13(b). In Figure 4.13(c), the bonded regions are extended in most weld interfaces as the oscillating shear force is continuously applied to the workpiece with an intense deformation by the weld tool. Finally, most nickel layers are dispersed, and a high density of bonding line is established in Figure 4.13(d). The weld formation sequence in Figure 4.13 displays that the weld propagates from both horn and anvil to the middle interface.

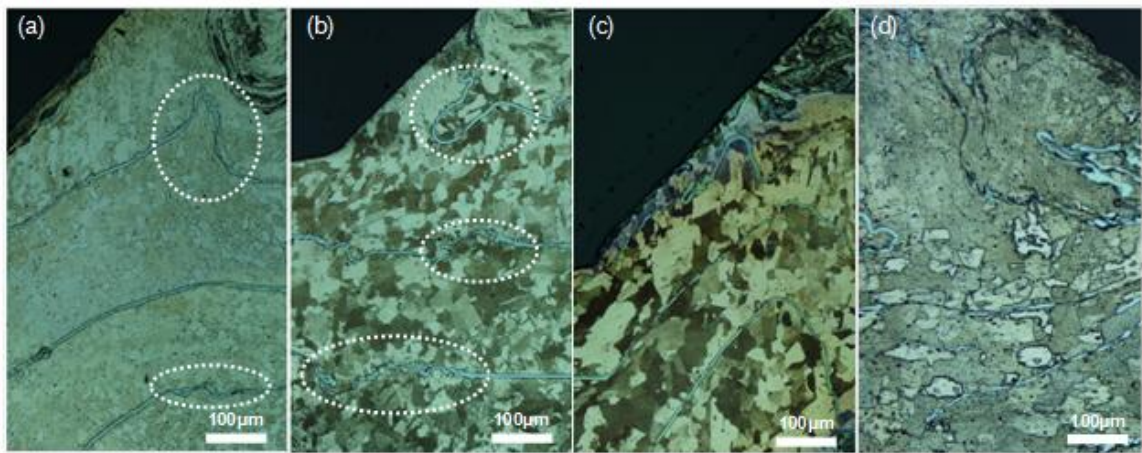


Figure 4.13 Micrographs of cross-sectioned weld samples produced with a coarse anvil for: (a) 0.2s, (b) 0.3s, (c) 0.4s, and (d) 0.5s

4.3.4 Effect of weld tool geometry on bond density and joint strength

The bond density is one of the key weld attributes that defines quality in an ultrasonic metal weld in a quantitative way [Lee *et al.* 2013]. Figure 4.14 shows how the bond densities in multiple weld interfaces are developed throughout the welding process. For the fine anvil case, the bond densities in second and third interface are very low (less than 10%) in the beginning of the welding process (~ 0.2s). As welding proceeds, the bond density in the second interface remarkably increases up to almost the same level as

the first interface, 80%, whereas that in the third interface increases only up to 40%. This slow development of bond density in the third interface is mainly caused by a large amount of slippage between the bottom metal layer and the anvil, especially during the middle stage of the welding process, as discussed in Section 4.3.2. However, when using the coarse anvil, the bond densities in the second and third interface begin with relatively higher levels than the fine anvil case (approximately 25% and 15%, respectively), and increase rapidly with time: both are over 70%. This faster growing trend of weld formation in the third interface results from the higher relative motion between the last two sheets due to reduced slippage of the bottom sheet against the anvil, which is caused by the tighter engagement between them.

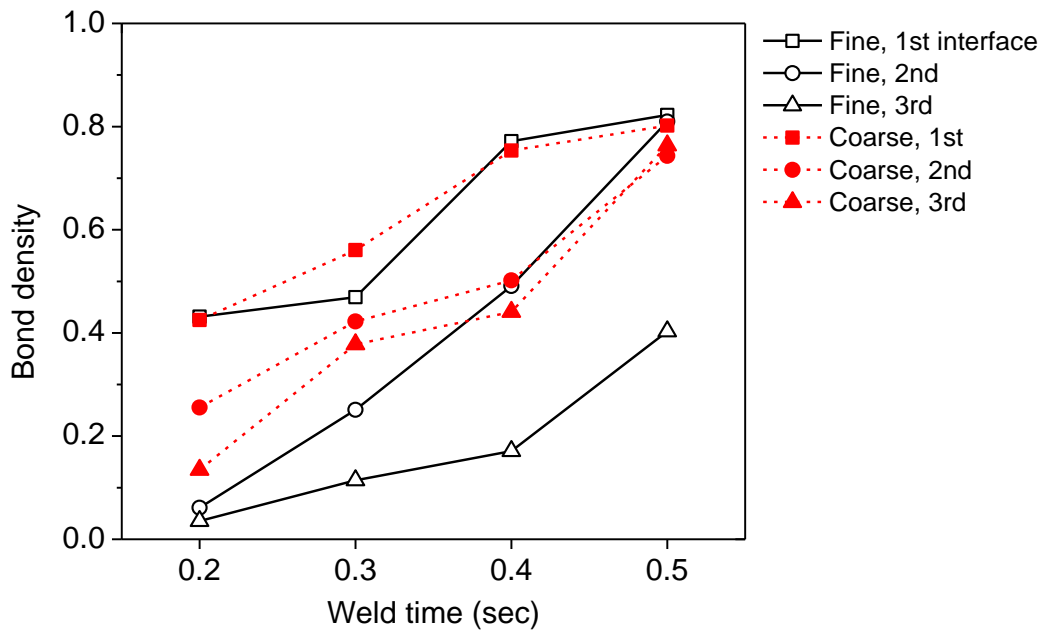
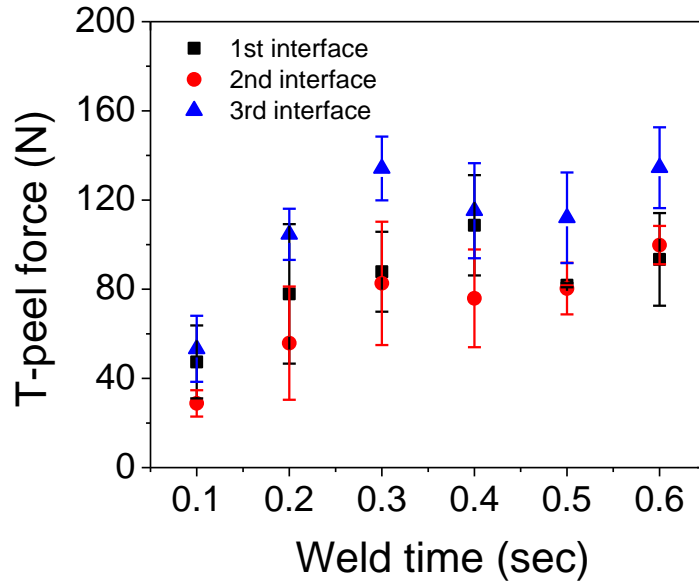


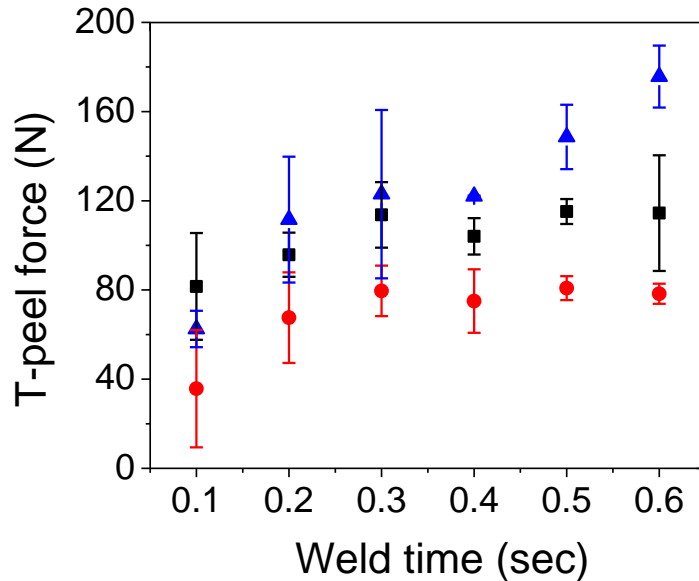
Figure 4.14 Bond density development at multiple weld interfaces for different anvil types

This high bond density development is supported by the T-peel test result in which the joint of the third interface with course anvil is stronger than the joint with fine anvil, as shown in the later welding process in Figure 4.15. It should be noted that the

reason of higher performance of the third interface in most regions is a bigger weld thickness or diffusion layer that may be formed between the thicker materials (total 1.2 mm) than other interfaces (total 0.4 mm). The effect of the ultrasonic weld thickness on the ultrasonic weld strength can be further investigated.



(a)



(b)

Figure 4.15 Mechanical performance of multiple joints (three weld interfaces) obtained by T-peel test for: (a) fine anvil type; and (b) coarse anvil type

4.4 CONCLUSIONS

This chapter proposes a new methodology of high-speed imaging for characterizing the ultrasonic metal welding process and reveals insights for optimum tool design to improve the quality of multilayer joints. To analyze the weld formation in multilayer ultrasonic welding, a high-speed camera is used to record the vibration of the metal sheets. The vibrating profiles of the multiple layers and their relative motions are obtained by high-speed images. The results from this high-speed imaging and the subsequent microscopic analyses provide in-depth understanding of the propagation mechanism in multilayer ultrasonic welding. Two anvil types are used to investigate the impact of tool geometry on the weld formation in the multiple interfaces. This study provides valuable insights on tool wear that can result from the extensive amount of slippage during the ultrasonic welding process.

Notable findings are summarized as follows:

- 1) The vibration cycles of the multiple layers develop with increasing magnitude in the initial period of the welding process. Each layer oscillates with different amplitude but in phase, meaning that there are relative differences in amplitude but no out-of-phase motions between the layers.
- 2) The maximum difference in vibration magnitude between the interfacing layers occurs in the order of 1st, 2nd, and 3rd weld interface when using the fine anvil, whereas the order is 1st, 3rd, and 2nd when using the coarse anvil.
- 3) The weld with the fine anvil propagates from top to bottom interface, i.e., “uni-directional”, while the weld with the coarse anvil is developed from both

ends, i.e., “bi-directional”. These different propagation mechanisms between two anvil types are mainly caused by different amounts of slippage between the bottom layer and the anvil due to the distinction in tool engagement with materials.

- 4) The coarse anvil design performs better than the fine anvil in terms of higher bond density and higher mechanical strength over the multiple weld interfaces.
- 5) The coarse anvil provides longer tool life since relative movement between the 4th layer and the tool is smaller compared with the anvil with fine geometry.

REFERENCES

- AmeTek (2013). Phantom V1610 Digital High-Speed Camera Data Sheet.
- De Vries, E. (2004). Mechanics and Mechanisms of Ultrasonic Metal Welding.
- Elangovan, S., Semeer, S. and Prakasan, K. (2009). "Temperature and Stress Distribution in Ultrasonic Metal Welding—an Fea-Based Study." *journal of materials processing technology* 209(3): 1143-1150.
- Eriksson, I., Gren, P., Powell, J. and Kaplan, A. F. (2010). "New High-Speed Photography Technique for Observation of Fluid Flow in Laser Welding." *Optical Engineering* 49(10): 100503-100503-100503.
- Eriksson, I., Powell, J. and Kaplan, A. F. (2010). Ultra High Speed Camera Investigations of Laser Beam Welding. *International Congress on Applications of Lasers & Electro-Optics (ICALEO), Anaheim (CA), USA.*
- Gao, Y. and Doumanidis, C. (2002). "Mechanical Analysis of Ultrasonic Bonding for Rapid Prototyping." *Journal of Manufacturing Science and Engineering* 124(2): 426-434.
- Gibert, J. M., McCullough, D. T., Fadel, G. M., Martin, G. K. M. and Austin, E. M. (2010). Stick-Slip Dynamics in Ultrasonic Consolidation. *2009 ASME International Design Engineering Technical Conferences and Computers and Information in Engineering Conference, DETC2009, August 30, 2009 - September 2, 2009, San Diego, CA, United states, American Society of Mechanical Engineers.*
- Harthoorn, J. (1973). "Joint Formation in Ultrasonic Welding Compared with Fretting Phenomena for Aluminium." *Ultrasonics international* 1973: 43-51.
- Ji, H., Li, M., Kung, A. T., Wang, C. and Li, D. (2005). The Diffusion of Ni into Al Wire at the Interface of Ultrasonic Wire Bond During High Temperature Storage. *Electronic Packaging Technology, 2005 6th International Conference on.*
- Joshi, K. C. (1971). "The Formation of Ultrasonic Bonds between Metals." *Welding Journal* 50(12): 840-848.
- Kang, B. S., Cai, W. and Tan, C. A. (2012). "Vibrational Energy Loss Analysis of Battery Bus-Bar in Ultrasonic Welding." *submitted to International Journal of Mechanical Sciences.*

- Kang, B. S., Cai, W. and Tan, C. A. (2013). "Dynamic Response of Battery Tabs under Ultrasonic Welding." *accepted by Journal of Manufacturing Science & Engineering*.
- Kim, T. H., Yum, J., Hu, S. J., Spicer, J. P. and Abell, J. A. (2011). "Process Robustness of Single Lap Ultrasonic Welding of Thin, Dissimilar Materials." *CIRP Annals - Manufacturing Technology* 60(1): 17-20.
- Kreye, H. (1977). "Melting Phenomena in Solid State Welding Processes." *Welding Journal* 56(5): 154-158.
- Lee, D., Kannatey-Asibu, E. and Cai, W. (2012). "Ultrasonic Welding Simulations for Multiple, Thin and Dissimilar Metals." *submitted to ASME International Symposium on Flexible Automation*.
- Lee, S. S., Kim, T. H., Hu, S. J., Cai, W. and Abell, J. A. (2010). "Joining Technologies for Automotive Lithium-Ion Battery Manufacturing: A Review." *ASME Conference Proceedings* 2010(49460): 541-549.
- Lee, S. S., Kim, T. H., Hu, S. J., Cai, W., Abell, J. A. and Li, J. (2013). "Characterization of Joint Quality in Ultrasonic Welding of Battery Tabs." *Journal of Manufacturing Science and Engineering* 135(2): 021004.
- Obielodan, J., Ceylan, A., Murr, L. and Stucker, B. (2010). "Multi-Material Bonding in Ultrasonic Consolidation." *Rapid Prototyping Journal* 16(3): 180-188.
- Ogawa, Y. (2011). "High Speed Imaging Technique Part 1 ‐ High Speed Imaging of Arc Welding Phenomena." *Science and Technology of Welding & Joining* 16(1): 33-43.
- Ram, G. D. J., Robinson, C., Yang, Y. and Stucker, B. (2007). "Use of Ultrasonic Consolidation for Fabrication of Multi-Material Structures." *Rapid Prototyping Journal* 13(4): 226-235.
- Ram, G. D. J., Yang, Y. and Stucker, B. (2006). "Effect of Process Parameters on Bond Formation During Ultrasonic Consolidation of Aluminum Alloy 3003." *Journal of Manufacturing Systems* 25(3): 221-238.
- Siddiq, A. and Ghassemieh, E. (2008). "Thermomechanical Analyses of Ultrasonic Welding Process Using Thermal and Acoustic Softening Effects." *Mechanics of Materials* 40(12): 982-1000.

- Siddiq, A. and Ghassemieh, E. (2009). "Theoretical and Fe Analysis of Ultrasonic Welding of Aluminum Alloy 3003." *Journal of manufacturing science and engineering* 131(4): 041007.
- Tucker, J. C. (2002). Ultrasonic Welding of Copper to Laminate Circuit Board.
- Wen, Y. M., Huang, S. S. and Liu, G. X. (2011). "Testing and Analysis of High-Speed Camera for Droplet Transition." *Advanced Materials Research* 271: 79-83.
- Wen, Y. M., Huang, S. S. and Liu, G. X. (2012). "Testing and Analysis of High-Speed Camera for Pulse Mig/Mag Welding Droplet Transition." *Applied Mechanics and Materials* 103: 134-137.
- Yang, Y., Ram, G. D. J. and Stucker, B. E. (2010). "An Analytical Energy Model for Metal Foil Deposition in Ultrasonic Consolidation." *Rapid Prototyping Journal* 16(1): 20-28.
- Zaal, J., van Driel, W., Kessels, F. and Zhang, G. (2008). Correlating Drop Impact Simulations with Drop Impact Testing Using High-Speed Camera Measurements. *Thermal, Mechanical and Multi-Physics Simulation and Experiments in Microelectronics and Micro-Systems, 2008. EuroSimE 2008. International Conference on, IEEE.*
- Zhang, C. and Li, L. (2007). "Effect of Friction on Ultrasonic Consolidation." *ASME Conference Proceedings* 2007(42908): 61-70.
- Zhang, C. and Li, L. (2008). "A Friction-Based Finite Element Analysis of Ultrasonic Consolidation." *WELDING JOURNAL-NEW YORK-* 87(7): 187.
- Zhang, C. and Li, L. (2009). "A Coupled Thermal-Mechanical Analysis of Ultrasonic Bonding Mechanism." *Metallurgical and Materials Transactions B* 40(2): 196-207.
- Zhang, C., Zhu, X. and Li, L. (2006). "A Study of Friction Behavior in Ultrasonic Welding (Consolidation) of Aluminum." *87th FABTECH International and AWS Welding Show Professional Program.*

CHAPTER 5

CONCLUSIONS AND FUTURE WORK

5.1 CONCLUSIONS

Ultrasonic metal welding is believed to be most suitable for battery joining because of its advantages on joining multiple thin layers of highly conductive and dissimilar materials due to its solid-state characteristics. Since this joining technology is newly adopted for battery pack manufacturing, there is a lack of widely accepted standards on weld quality. In addition, limited understanding of the process hinders achieving consistent product quality, which is critical for ensuring high power battery packs. Thus, the goal of this thesis was to develop a methodology that can define the ultrasonic weld quality using physical weld attributes, and to establish in-depth understanding of the weld formation mechanisms in ultrasonic metal welding utilizing sensor signals and high-speed images. This research has provided a comprehensive characterization on the ultrasonic metal welding process and guidelines for systematic quality definitions. Moreover, the scientific understanding obtained from this dissertation will guide manufacturers in establishing a robust and reliable ultrasonic welding process to achieve consistent quality.

The major findings of this dissertation can be summarized in three parts.

1) *Characterization of joint quality in ultrasonic welding of battery tabs*

A set of measurable weld attributes have been proposed to characterize ultrasonically welded joints of copper and nickel plated copper. The joint characteristics of different quality welds were investigated using those attributes and the relationship between attributes and performance was quantitatively identified. The main conclusions are summarized as follows:

- The bonding strength of ultrasonically welded joints for copper and nickel-plated copper results from the combined effect of metallurgical adhesion and mechanical interlocking.
- Different levels of weld quality (i.e., under, good, or over weld) are correlated to the bond density and the post-weld thickness. The bond density increases as the quality level changes from under, good to over weld whereas the post-weld thickness decreases.
- Material flow with extensive plastic deformation occurs at the metal surface in contact with each horn tooth, and causes material thinning.
- Material that has received high ultrasonic energy input show instant work hardening due to the plastic deformation and then softening with continuous temperature increase.
- Various zones in an ultrasonic metal weld are distinguished by their mechanical properties and micrographs. The sizes of these zones impact the failure type during tensile testing and, eventually, weld quality.

2) *Characterization of ultrasonic metal welding by correlating online sensor signals with weld attributes*

Power signal and horn displacements are thoroughly examined to understand the physics behind the ultrasonic welding process. Several features from these two signals are identified based on the physical understanding of signal variations under abnormal process conditions such as surface contamination. These signal features are then correlated to weld attributes measured from micrographs of cross-sectioned weld samples. By relating those signal features to weld attributes, the joint quality can be successfully predicted. The main conclusions are summarized as follows.

- Power signal provides useful information on the change of mechanical resistance at the weld interface whereas displacement signal reflects the pattern for material deformation.
- The power and displacement signals halfway through the process provide critical information on the abnormal process conditions.
- The energy used and the indentation depth for the whole welding process indicate whether weld formation at the interface is completed.
- The relationships between weld attributes and several signal features such as E_{total} , E_{mid} , D_{total} , and D_{mid} provide physical understanding on the impact of process conditions on the weld quality.

3) *Analysis of weld formation in multilayer ultrasonic metal welding using high-speed images*

A new methodology of high-speed imaging is developed for characterizing the ultrasonic metal welding process and reveals insights for optimum tool design to improve the quality of multilayer joints. The vibrating profiles of the multiple layers and their relative motions are obtained from high-speed images. Two anvil types are used to investigate the impact of tool geometry on weld formation in the multiple interfaces. The results from this high-speed imaging and the subsequent microscopic analyses provide in-depth understanding on the propagation mechanism in multilayer ultrasonic welding. The main conclusions are summarized as follows.

- The vibration cycles of the multiple layers are developed with increasing amplitudes in the initial period of the welding process.
- The maximum difference in vibration magnitude between the interfacing layers occurs in the order of 1st, 2nd, and 3rd weld interface when using the fine anvil, whereas the order is 1st, 3rd, and 2nd when using the coarse anvil.
- The weld with the fine anvil propagates from top to bottom interface, i.e., “uni-directional”, while the weld with the coarse anvil is developed from both ends, i.e., “bi-directional”.
- The coarse anvil design performs better than the fine anvil in terms of higher bond density and higher mechanical strength over the multiple weld interfaces.
- The coarse anvil provides longer tool life since relative movements between the 4th layer and the tool is smaller compared with the anvil with fine geometry.

5.2 FUTURE WORK

Based upon the findings of this dissertation, the future work may include the following directions:

1) *Performance modeling of ultrasonic metal welds*

A sophisticated finite element model of joint performance can be developed by incorporating weld attributes that determine the weld quality. A design of experiment for the simulations can be performed to identify critical weld attributes affecting the joint performance. This will establish complete relationships between weld process, attributes, and performances.

2) *Ultrasonic welding of copper and aluminum*

Dissimilar welding of copper and aluminum is another challenging task in battery manufacturing, due to different material properties including surface hardness (pure aluminum: 23~28 HV of Vickers [Murr *et al.* 1997]; pure copper: 55~60 HV [Kaneko *et al.* 2005]) . In addition, pure aluminum is very prone to sticking on the weld tool [Bloss 2007]. By using the same methodology provided in this dissertation, a comprehensive characterization on the ultrasonic welding of copper and aluminum will maximize the robustness and reliability of the process.

3) *Development of real-time process control*

In-depth understanding of the ultrasonic welding of multiple metal sheets is established by phenomenological observation on the process. From this observation, possible tool wear is seen due to extensive slippage between the tool and workpiece.

A real-time control of process variables, such as pressure and vibration amplitude, may reduce the slippage and provide longer tool life, resulting in cost saving.

REFERENCES

- Bloss, M. C. (2007). *Ultrasonic Metal Welding: The Weldability of Stainless Steel, Titanium, and Nickel-Based Superalloys*, Ohio State University.
- Kaneko, Y., Mizuta, Y., Nishijima, Y. and Hashimoto, S. (2005). "Vickers Hardness and Deformation of Ni/Cu Nano-Multilayers Electrodeposited on Copper Substrates." *Journal of Materials Science* 40(12): 3231-3236.
- Murr, L., Liu, G. and McClure, J. (1997). "Dynamic Recrystallization in Friction-Stir Welding of Aluminium Alloy 1100." *Journal of materials science letters* 16(22): 1801-1803.